Université de Montréal

Cellular mechanisms underlying the regulation of calcium signaling in brain pericytes

Par

Braxton Phillips

Département de Neurosciences

Faculté de Médecine

Mémoire présenté à la faculté des études supérieures en vue de l'obtention du grade de Maîtrise ès sciences (M.Sc.) en Neurosciences

Juin 2023

Université de Montréal

Département de Neurosciences
Faculté de Médecine

Ce mémoire intitule

Cellular mechanisms underlying the regulation of calcium signaling in brain pericytes

Présenté par

Braxton Phillips

A été évalué par un jury compose des personnes suivantes

Dr. Arlette Kolta
Président-rapporteur

Dr. Ravi Rungta
Directeur de recherche

Dr. Jannic Boehm
Membre du jury

Summary

Brain mural cells are a grouping of neurovascular cells that display exceptional molecular, morphological, and functional heterogeneity. Mid-capillary pericytes, the mural cells which contact the smallest vessels of the brain, are known to be critical to brain homeostasis, and their contractile ability has long been debated. However, many of their physiological properties, such as their Ca^{2+} signaling mechanisms, have not been elucidated. This thesis aims to uncover the cellular mechanisms of brain mid-capillary pericyte Ca^{2+} signaling. In chapter 2, we harness pharmacology and imaging of brain pericytes expressing the calcium indicator GCaMP6f (from transgenic PDGFRβ-Cre::GCaMP6f mice) to uncover these mechanisms. In contrast to ensheathing pericytes whose Ca^{2+} signaling is dependent on voltage-gated Ca^{2+} channels (VGCCs), we find that mid-capillary pericyte Ca^{2+} signals are independent of VGCCs. Instead, we find that mid-capillary pericyte Ca^{2+} transients are inhibited by removal of extracellular Ca^{2+}, inhibition of store-operated Orai channels, blockade of endoplasmic reticulum store filling, as well as inhibition of ryanodine receptors (RyRs) and inositol triphosphate receptors (IP_3Rs). We further find that store-operated Ca^{2+} entry can be induced by endoplasmic reticulum store depletion and inhibited by Orai blockers in mid-capillary pericytes, and that basal Ca^{2+} influx is largely dependent on store depletion. Finally, we show that Orai store-operated Ca^{2+} entry amplifies cytosolic Ca^{2+} elevations in response to the vasoconstrictor endothelin-1. We conclude that both spontaneous and G_q-coupled protein receptor agonist-induced Ca^{2+} signaling in mid-capillary pericytes is regulated by coupling between endoplasmic reticulum store release and store-operated influx pathways.

Keywords: Pericytes, calcium, capillaries, orai, ryanodine receptor, IP3 receptor, live cell imaging, confocal microscopy

Résumé

Les cellules murales du cerveau sont un groupe de cellules neurovasculaires qui présentent une hétérogénéité moléculaire, morphologique et fonctionnelle exceptionnelle. Celles en contact avec les plus petis vaisseaux du cerveau, les péricytes du lit capillaire moyen sont connues pour être essentielles à l'homéostasie cérébrale, bien que leur capacité contractile ait longtemps été débattue. Cependant, nombre de leurs propriétés physiologiques, telles que leurs mécanismes de signalisation calcique, n'ont pas encore été élucidées. Cette thèse vise donc à identifier les mécanismes cellulaires de la signalisation calcique des péricytes des capillaires cérébraux. Dans le chapitre 2, nous utilisons la pharmacologie et l'imagerie des péricytes cérébraux exprimant l'indicateur de calcium GCaMP6f (provenant de souris transgéniques PDGFRβ-Cre::GCaMP6f) pour découvrir ces mécanismes. Contrairement aux péricytes engainants dont la signalisation du calcique dépend des canaux calcique voltage-dépendants, nous constatons que les signaux calcique des péricytes capillaire moyen sont indépendants des canaux calcique voltage-dépendants. Au contraire, nous constatons que les signaux calciques transitoires des pericytes du lit capillaire moyen sont inhibés par l'élimination du Ca^{2+} extracellulaire, l'inhibition des canaux Orai opérés par les réserves, le blocage du remplissage des réserves du réticulum endoplasmique, ainsi que l'inhibition des récepteurs de la ryanodine (RyRs) et des récepteurs de l'inositol trisphosphate (IP_3Rs). Nous constatons également que l'entrée de Ca^{2+} opérée par les réserves peut être induite par la déplétion des réserves du réticulum endoplasmique et inhibée par les bloqueurs d'Orai dans les pericytes du lit capillaire moyen, et que l'influx basal de Ca^{2+} est largement dépendant de la déplétion des réserves. Enfin, nous montrons que l'entrée de Ca^{2+} opérée par les réserves d'Orai amplifie les élévations de Ca^{2+} cytosolique en réponse au vasoconstricteur endothéline-1. Nous concluons que la signalisation calcique dans les pericytes du lit capillaire moyen, qu'elle soit

spontanée ou induite de façon agoniste, est régulée par le couplage entre la libération des réserves du réticulum endoplasmique et les voies d'influx opérées par les réserves.

Mots-clés : Péricytes, calcium, capillaires, orai, récepteur de la ryanodine, récepteur IP3, imagerie cellulaire en direct, microscopie confocale

Preface

Chapter 2 is based on a published manuscript:

Phillips, B., Clark, J., Martineau, É., Rungta, RL. (2023). Orai, RyR, and IP_3R channels cooperatively regulate Ca^{2+} signaling in brain mid-capillary pericytes. *Communications Biology* **6**, 493

I designed the study with R.L.R. and E.M. I performed most of the *ex vivo* Ca^{2+} imaging experiments with important contributions from J.C. I analyzed the data and interpreted results with R.L.R. and J.C. Figure 2.S2 was completed by J.C. J.C. additionally contributed data and analyses to Figures 2.1, 2.2, 2.5, and 2.S1. I collected and analyzed the data for all other figures. R.L.R. and I wrote the manuscript with feedback from E.M. E.M. developed analysis procedures, and R.L.R. supervised the work. All authors agreed to the final version of the manuscript.

Table of Contents

Summary……I
Résumé……II
Preface……IV
Table of Contents……V
List of Figures……VI
List of Tables……VII
List of Abbreviations……VIII
Chapter 1: General Introduction……1
1.1 Introduction to Brain Mural Cells and their Heterogeneity……1
1.2 Non-Contractile Pericyte Functions at the Neurovascular Unit……9
1.2.1 Blood-Brain Barrier Regulation……9
1.2.2 Neuroimmune Regulation……11
1.2.3 Scar Formation and Stem Cell Properties……11
1.3 Ca^{2+} Signaling……13
1.3.1 A Brief Introduction to Ca^{2+} Signaling……13
1.3.2 Voltage-Gated Ca^{2+} Channels……14
1.3.3 Transient Receptor Potential Channels……17
1.3.4 Intracellular Ca^{2+} Channels……18
1.3.5 Store-Operated Ca^{2+} Entry (SOCE)……20
1.4 Ca^{2+} Signaling and Functions in Brain Pericytes……23
1.5 G Protein-Coupled Receptor Signaling in Brain Pericytes……27
1.5.1 A Brief Overview of G Protein-Coupled Receptor Signaling……27
1.5.2 The Phosphatidylinositol Pathway in Brain Pericytes……28
1.5.3 The cAMP Pathway in Brain Pericytes……30
1.6 Research Objectives and Experimental Design……33
Chapter 2: Orai, RyR, and IP_3R channels cooperatively regulate Ca^{2+} signaling in brain mid-capillary pericytes……32
2.1 Abstract……33
2.2 Introduction……34
2.3 Methods……36
2.3.1 Ethics Statement and Animals……36
2.3.2 Acute Brain Slice Preparation……37
2.3.3 Pharmacology and Ion Substitution……37
2.3.4 Confocal Imaging……38
2.3.5 Data Collection and Analysis……39
2.3.6 Statistics……40
2.4 Results……41
2.5 Discussion……61
2.5.1 Study Limitations……66
2.6 Appendix……68
Chapter 3: General Discussion……77
3.1 Summary of Research Findings……77
3.2 Expanded Discussion of Research Findings……78
3.3 Future Directions……83
References……85

List of Figures

Figure 1.1 Morphological heterogeneity of mural cells across vascular zones……..3
Figure 1.2 Molecular heterogeneity of mural cells……8
Figure 1.3 An overview of Ca^{2+}-permeable channels……..14
Figure 2.1 Imaging of mid-capillary pericyte Ca^{2+} transients and their dependence on extracellular Ca^{2+} ……...43
Figure 2.2 Mid-capillary pericyte Ca^{2+} transients are not potentiated by depolarization or mediated by VGCCs……...47
Figure 2.3 Mid-capillary pericyte Ca^{2+} transients signals are dependent on Orai Ca^{2+} channels……..51
Figure 2.4 Mid-capillary pericyte Ca^{2+} transients are mediated by RyR and IP_3R store release pathways……55
Figure 2.5 Mid-capillary pericytes express functional SOCE that is blocked with Orai inhibitors……58
Figure 2.6 Ca^{2+} influx via Orai SOCE influx is required to sustain and amplify endothelin-1 $[Ca^{2+}]_i$ elevations……60
Figure 2.S1 Imaging of mid-capillary pericyte microdomain Ca^{2+} signals and their dependence on extracellular Ca^{2+} ……..68
Figure 2.S2 Effect of ET-1 at different time points following extracellular Ca^{2+} removal…….70
Figure 2.S3 Analysis of Ca^{2+} transient frequency in response to DMSO and 500 nM TTX……72
Figure 2.S4 Effects of pharmacological compounds on resting Ca^{2+}…….73

List of Tables

Table 2.1 Summarized data and statistics for all pharmacological treatments on pericyte processes……..74
Table 2.2 Summarized data and statistics for all pharmacological treatments on pericyte somas……...75
Table 2.3 Information on pharmacological agents and vehicles used……76

List of Abbreviations

2-APB	2-aminoethoxydiphenyl borate
α-SMA	Alpha smooth muscle actin
ACSF	Artificial cerebral spinal fluid
ATP	Adenosine triphosphate
BBB	Blood-brain barrier
BK_{Ca}	Large-conductance calcium-activated potassium channel
Ca^{2+}	Calcium ions
$[Ca^{2+}]_{ex}$	Extracellular calcium
$[Ca^{2+}]_{ER}$	Endoplasmic reticulum calcium
$[Ca^{2+}]_{i}$	Cytosolic calcium
cAMP	Cyclic adenosine monophosphate
CBF	Cerebral blood flow
CICR	Calcium-induced-calcium-release
Cl^{-}	Chloride ions
Cl_{Ca}	Calcium-activated chloride channel
CNS	Central nervous system
CPA	Cyclopiazonic acid
CREB	cAMP response element-binding protein
DAG	Diacylglycerol
EGTA	Ethylene glycol-bis(β-aminoethyl ether)-N,N,N′,N′-tetraacetic acid
ET-1	Endothelin-1
ER	Endoplasmic reticulum
HVA	High voltage activation
GECI	Genetically encoded calcium indicator
GPCR	G protein-coupled receptor
I_{CRAC}	Calcium-release activated current
IP_3	Inositol triphosphate
IP_3R	Inositol triphosphate receptor
IP-TNT	Inter-pericyte tunneling nanotube
K^{+}	Potassium ions
K_{ATP}	ATP-sensitive potassium channel
LPS	Lipopolysaccharides
LVA	Low voltage activation
MSC	Mesenchymal stem cells
Na^{+}	Sodium ions
NFAT	Nuclear factor of activated T cells
NMDG	N-methyl-D-glucamine
NVC	Neurovascular coupling
NVU	Neurovascular unit
PDGFRβ	Platelet derived growth factor beta receptor
PKA	Protein kinase A
PKC	Protein kinase C
PLC	Phospholipase C
PMCA	Plasma membrane calcium ATPase

ROI	Region of interest
RyR	Ryanodine receptor
TRP	Transient receptor potential
TRPC	Transient receptor potential canonical
TTX	Tetrodotoxin
SERCA	Sarcoendoplasmic reticulum ATPase
SOCE	Store-operated calcium entry
SMC	Smooth muscle cell
UTP	Uridine triphosphate
VGCC	Voltage-gated calcium channel

Chapter 1: General Introduction

1.1 Introduction to Brain Mural Cells and their Heterogeneity

Mural cells are a grouping of cells that includes smooth muscle cells (SMCs) and pericytes of diverse morphologies (Grant et al., 2019). These cells are grouped together owing to their shared protein markers (e.g., PDGFRβ, NG2, CD13, RGS5) (Krueger and Bechmann, 2010), origin (Armulik et al., 2011), and presence at the abluminal surface of the vasculature. Mural cells are found throughout the body but are especially numerous in the central nervous system (CNS) (Armulik et al., 2011). Indeed, mural cells are central players of the neurovascular unit (NVU), which also includes neurons, astrocytes, endothelial cells, and perivascular microglia (Sweeney et al., 2016). Despite the similarities that define their grouping, mural cells display substantial morphological, transcriptomic, and functional heterogeneity along the arteriovenous axis.

There is a wide range of mural cell morphologies, and the morphology of any individual mural cell is dictated by the blood vessel it contacts (**Figure 1.1**) (Grant et al., 2019). In the CNS, pial arteries and penetrating arterioles (named because they penetrate from pial arteries into the brain parenchyma) are covered by a continuous layer of ring-shaped SMCs (Hill et al., 2015; Grant et al., 2019). This penetrating arteriole is commonly defined as the "0^{th} order" vessel, as all downstream branches are subsequently numbered[1] in order of appearance (Hall et al., 2014; Hill et al., 2015; Grant et al., 2019). Vessels of the subsequent ~3-4 branch orders are variously defined as capillaries (Attwell et al., 2016), pre-capillary arterioles (Hill et al., 2015), or the arteriole-capillary transition (ACT) zone (Hartmann et al., 2022)*. Regardless of the nomenclature, these

* Although the ACT terminology is increasingly used, the term "capillary" will be used to refer to all vessels downstream of the penetrating arteriole (before the eventual transition to post-capillary venules) due to brevity and clarity when referencing early works. However, branch orders will be included, and the reader should be aware of the important distinctions between vascular segments.

proximal vessels can be distinguished from subsequent vessels, approximately greater than or equal to four branch order in the cortex and which are defined as classical capillaries, by numerous properties (such as diameter and contractility). Capillaries are contacted by pericytes, which, since their earliest descriptions, are defined by their "bump on a log" morphology – a highly visible soma. Although it is historically accurate to define pericytes by this feature alone (Attwell et al., 2016), this practice has precluded much of what we now know of the heterogeneity within pericyte subtypes. Most striking is the molecular, morphological, and functional divergence between the pericytes which reside on the 1st to 3rd (sometimes 4th) order capillaries, which are termed ensheathing pericytes (also proximal pericytes, or terminal SMCs), owing to their near complete coverage of the capillary endothelium, and the pericytes which contact vessels of greater than or equal to the 4th branch order, which are termed mid-capillary pericytes (in the brain) or distal pericytes (in the retina) and are of a mesh or thin-strand morphology (of which their nomenclature is sometimes divided based on these morphologies) (Grant et al., 2019).

Why do we care about this pericyte heterogeneity? To answer this question, it is critical to appreciate that the study of brain pericytes has long focused on understanding their ability (or lack thereof) to contract in physiological and disease states (Sims, 1986). But why is this single potential function of such importance? Many neurovascular papers open with some version of the canonical line that "the human brain uses 20% of the oxygen and nutrient supply, despite only representing 2% of body mass" (Clarke, 1999). Perhaps cliché, this phrase embodies the fact that the brain is an extremely metabolically active organ, and it follows that the efficient distribution of this large energy budget is imperative. The function of matching increases in neuronal activity (and thus, metabolic demand) with increased cerebral blood flow (CBF) to activated brain regions is termed neurovascular coupling (NVC) (Iadecola, 2017). Classically, CBF is controlled by

contractile SMCs on pial arteries and penetrating arterioles (Drew et al., 2011; Sekiguchi et al., 2014; Rungta et al., 2018). However, the constriction or dilation of these upstream vessels will redirect CBF over a large brain area and cannot alone account for the perceived specificity of NVC.

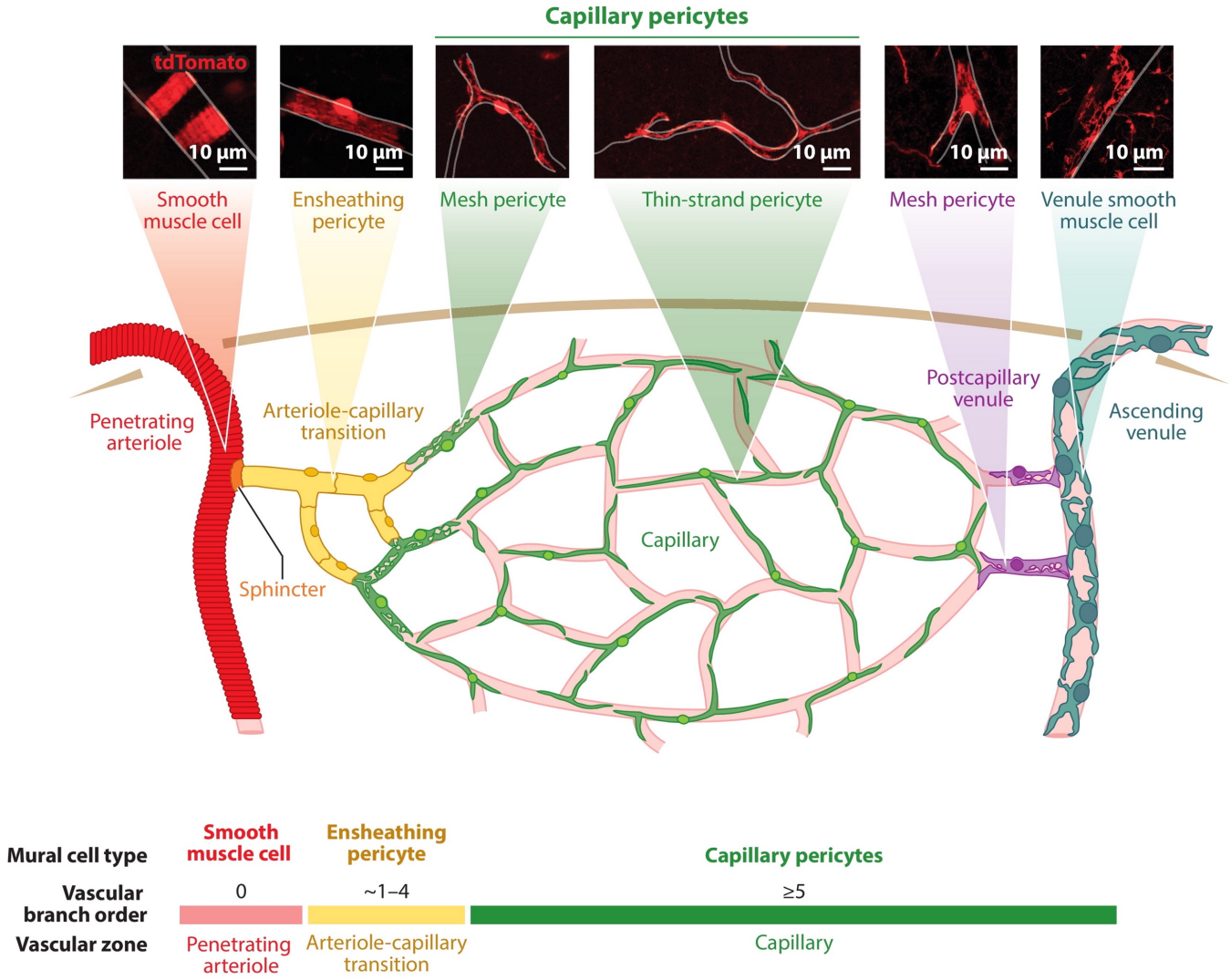

Figure 1.1: Morphological heterogeneity of mural cells across vascular zones. Adapted from Hartmann et al., 2022 with permission from Annual Reviews.

Therefore, the concept that pericytes, the mural cells of the capillaries, control CBF on a precise level has long been an intriguing hypothesis. Both historical and contemporary attempts at testing this hypothesis have produced opposing conclusions (Sims, 1986; Hartmann et al., 2022).

Indeed, seminal studies in the early 21st-century highlighted the contractile properties of "pericytes". In *ex vivo* preparations, pericytes contract in response to electrical stimulation, noradrenaline, and other vasoactive compounds including ATP, endothelin-1, and the thromboxane A2 receptor agonist U46619 (Peppiatt et al., 2006; Fernández-Klett et al., 2010; Hall et al., 2014; Nortley et al., 2019). Pericyte-mediated capillary constriction also occurs in pathology, including *ex vivo* oxygen-glucose deprivation (Hall et al., 2014) and *in vivo* middle cerebral artery occlusion (Yemisci et al., 2009), as well as in response to amyloid β (Nortley et al., 2019). On the contrary, the excitatory neurotransmitter glutamate (through release of prostaglandin E_2) dilates capillaries contacted by "pericytes", setting up a model that implicates pericytes in NVC (Hall et al., 2014; Mishra et al., 2016). Indeed, stimulation of the mouse whisker pad is matched by vessel dilations of somatosensory cortex penetrating arterioles and capillaries up to the 4th branch order (with decreasing response rates at higher branch orders) (Hall et al., 2014). Nevertheless, a 2015 study concluded that "pericytes" are not involved in NVC and do not constrict during ischemia, despite replicating previous results with *in vivo* experimentation (Hill et al., 2015). The authors chose to define mural cells as SMCs or pericytes based on their coverage of the endothelium and expression of the α-SMA protein, rather than the presence of a "bump-on-the-log" soma. Therefore, the mural cells on early branches from the penetrating arteriole were defined as SMCs, rather than pericytes. Although its novelty is largely due to this nomenclature discrepancy, the work of Hill et al. 2015 was critical for the neurovascular field to accept the early seminal studies as referring to the (now described) ensheathing pericyte subtype and ushered in an era in which

the pericyte subtype being studied is now specifically defined. Furthermore, the heterogeneity of pericyte function has since received renewed focus.

Subsequent *in vivo* studies have confirmed that other mural cells aside from arteriole SMCs are important contributors in the neurovascular coupling response. This includes a specialized mural cell known as a precapillary sphincter, which resides at the transition from the penetrating arteriole to the first-order capillary and may be responsible for the most substantial changes in cerebral blood flow (Grubb et al., 2020), as well as ensheathing pericytes. Vessels contacted by precapillary sphincters and ensheathing pericytes exhibit faster diameter changes in response to synaptic activation, vasoconstrictors, and vasodilators than upstream or downstream mural cells in the somatosensory cortex (Cai et al., 2018; Zambach et al., 2021). Likewise, a study examining the dynamics of mural cells along the vascular arbour of the mouse olfactory bulb in response to odor uncovered that 1st-order ensheathing pericytes and parenchymal arteriole SMCs (together termed the primary unit) dilate first following downstream synaptic activation (Rungta et al., 2018).

In addition to function, it has only recently been appreciated that mural cells also display exceptional diversity in transcriptome signatures. Early mRNA-sequencing studies of the brain which included the vasculature were performed at a bulk level and failed to even differentiate between endothelial cells and pericytes due to their tight physical association (Zhang et al., 2014). In 2018, a pivotal single-cell RNA-sequencing effort profiling > 3300 cells specifically dissociated from isolated mouse brain vasculature attempted to characterize changes in gene expression along the arteriovenous axis (Vanlandewijck et al., 2018). Endothelial cells displayed gradual alterations in gene expression along this axis, consistent with the idea of the vasculature as a singular continuum (Vanlandewijck et al., 2018). Strikingly, however, the expression profiles of mural cells

could not be assigned to a single arteriovenous continuum, but rather two discrete subclasses (Vanlandewijck et al., 2018). Mid-capillary pericytes were classified as existing in a continuum with venule SMCs, while SMCs of arteries exist in a distinct continuum with SMCs of arterioles (Vanlandewijck et al., 2018). Critically, mural cells of lower-order capillaries could not be distinguished from arteriole SMCs, suggesting that ensheathing pericytes may be more related to SMCs on a molecular level (Vanlandewijck et al., 2018). It is also important to note that, despite containing a significant plurality of the cells studied (1088 cells), the large pericyte cluster (putatively mid-capillary pericytes) could not be subclustered with the analysis protocol (Vanlandewijck et al., 2018). Altogether, these results suggest that there are abrupt regions of molecular (and perhaps, functional) transition within brain mural cells, most prominently at the transition from lower-order to higher-order capillaries. Furthermore, they provide justification for studying mid-capillary pericytes (i.e. "true" pericytes) as a singular population.

In addition to these signature differences, the most defining feature of mural cell transcriptome heterogeneity concerns α-SMA expression. α-SMA is a protein essential for the rapid actomyosin-based contraction of SMCs, and thereby directly links mural cell transcriptome differences to the contractility debate. This SMC contraction is Ca^{2+}-dependent, as Ca^{2+} influx through L-type VGCCs leads to increases in intracellular Ca^{2+}, which binds with calmodulin to form the Ca^{2+}-calmodulin complex. The Ca^{2+}-calmodulin complex activates myosin light-chain kinase, which phosphorylates myosin to induce α-SMA-myosin binding and cellular contraction. As mentioned, robust α-SMA expression is commonly believed to be restricted to SMCs and ensheathing pericytes on the 1^{st}-4^{th} capillary branch orders, as verified by immunohistochemistry (Nehls and Drenckhahn, 1991; Grant et al., 2019) and reporter fluorescent protein expression driven Acta2 (the α-SMA coding gene) (Hill et al., 2015; Gonzales et al., 2020). Pericytes on

higher order capillaries may express some α-SMA, as one study has demonstrated α-SMA expression by immunohistochemistry in retinal distal pericytes (> 5 capillary branch order) with fixation techniques designed to prevent rapid depolymerization of actin filaments (Alarcon-Martinez et al., 2018). While these conflicting results have yet to be resolved, α-SMA expression is definitively lower in mural cells of higher order capillaries. Furthermore, it remains to be experimentally determined whether the putative contractile machinery of mid-capillary pericytes requires this relatively low amount of α-SMA or is instead composed of cytoskeletal actin (Hartmann et al., 2021).

Largely following heterogeneity in contractile machinery, contractile phenotype clearly differs within mural cell subtypes. Ensheathing pericytes and SMCs rapidly constrict vessels in response to optogenetic stimulation, while cortical pericytes of thin-strand morphology constrict capillaries, albeit on a timescale of minutes (Nelson et al., 2020; Hartmann et al., 2021). Both fast and slow constrictions are inhibited by the Rho-kinase inhibitor fasudil, which suggests that cytoskeletal rearrangement is required by both forms (Hartmann et al., 2021). These results gathered with optogenetic stimulation, which likely produces unphysiological cell manipulations, are supported by results from mouse retinal and cortical preparations, in which distal pericytes constricted capillaries following stimulation with the vasoactive compound U46619 (Hernández-Klett et al., 2010; Gonzales et al., 2020; Glück et al., 2021), again, on a slower timescale than upstream pericytes (Gonzales et al., 2020). Furthermore, it is unlikely that the longitudinal processes of thin-stranded pericytes position these cells to exert the radial force required for SMC-like contraction (Hill et al., 2015; Grutzendler and Nedergaard, 2019). While the contractile phenotype of mid-capillary pericytes is definitively different from that of SMCs and ensheathing pericytes, it too remains undefined.

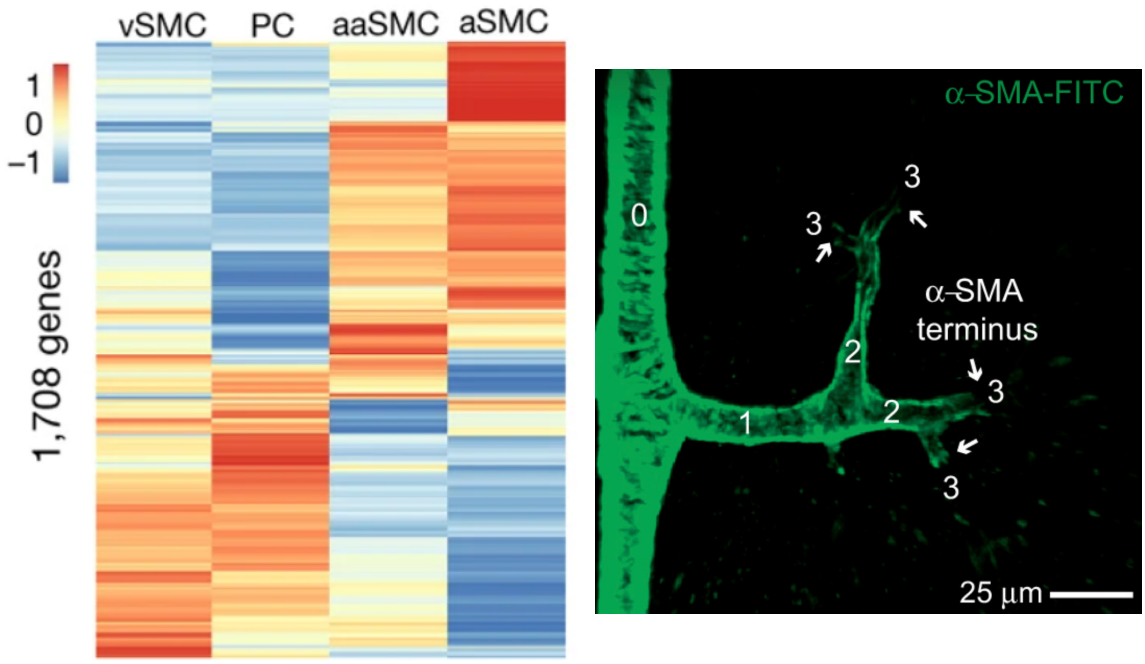

Figure 1.2: Molecular heterogeneity of mural cells. Left, differential expression of 1708 genes in mural cell subtypes. vSMC = venule smooth muscle cell, PC = pericyte, aaSMC = arteriole smooth muscle cell (although generally believed to include ensheathing pericytes), aSMC = arterial smooth muscle cell. Right, α-SMA expression in mural cells showing detectable levels up to the third branch order. Adapted from Vanlandewijck et al., 2018 and Grant et al., 2019 with permission from Springer Nature and SAGE Publications.

1.2 Non-contractile Pericyte Functions at the Neurovascular Unit

Pericytes are particularly numerous in the brain (for example, perhaps up to 10-100 times more numerous than in skeletal muscle) (Armulik et al., 2011), suggestive of a heightened functional importance in the CNS. Indeed, aside from their contractile ability and roles in neurovascular coupling that are still being fully characterized, pericytes are implicated in numerous CNS homeostatic functions and disease states. As the goal of uncovering pericyte signaling pathways is to understand pericyte function, a brief review of the best characterized brain pericyte functions is provided.

1.2.1 Blood-Brain Barrier Regulation

The term blood-brain barrier (BBB) describes the selective semipermeable membrane that restricts access of certain molecules and cells in the blood to the brain. The BBB is formed primarily by endothelial cells bound together by tight junctions, which severely limits paracellular transport of solutes, but is substantially regulated by pericytes, which intimately contact endothelial cells within the basement membrane. Three seminal studies specifically examined pericyte contributions to the BBB in development, adulthood, and aging by generating transgenic mice null or hypomorphic for the *Pdgfb* or *Pdgfrb* allele (Armulik et al., 2010; Bell et al., 2010; Daneman et al., 2010). PDGFβ is a survival factor released by endothelial cells that binds to pericytic PDGFRβ; therefore, these models lead to varying levels of pericyte depletion. Pericytes are required for functional formation of the BBB during embryogenesis, including the sealing of tight junctions and suppression of vascular permeabilizing proteins (Daneman et al., 2010). Increased BBB permeability is further observed in mice using a pericyte-deficient model that allows for adulthood viability (Armulik et al., 2010). Extended analysis of aged mice displayed

that the accumulation of toxic blood-derived proteins increases with age in pericyte-deficient mice, suggesting a link to neurodegenerative disease (Bell et al., 2010). Indeed, BBB dysfunction and reduction of pericyte coverage is found in Alzheimer's disease (Halliday et al., 2016; Miners et al., 2018). Recent investigations of hypomorphic Pdgfb mice revealed that pericytes are required to limit extravasation of leukocytes into the brain during experimental autoimmune encephalitis (EAE) (Török et al., 2021), and accumulation of fibrinogen and fibrin, which are toxic to oligodendrocytes (Montagne et al., 2018). Although Pdgfrb is indeed an important pericyte marker, it is also highly expressed in SMCs and fibroblasts, among other CNS cell types. Therefore, a more recent study achieved pericyte-specificity with an innovative strategy regulating the expression of inducible Cre with a combined requirement for activity *Pdgfrb* and *Cspg4* promoters (Nikolakopoulou et al., 2019). Crossing this mouse line with a line carrying the Cre-dependent diptheria toxin receptor allowed for selective ablation of pericytes in adult mice, which indeed produced BBB breakdown, reductions in CBF, and neuronal loss (Nikolakopoulou et al., 2019). While these studies conclusively show that pericytes are required for a blood-brain barrier homeostasis, results obtained with pericyte-depletion protocols must be supplemented by future investigations into specific cellular mechanisms mediating this regulation. Recent work examining humans with the E4 variant of apolipoprotein E (the greatest risk allele for the development of Alzheimer's disease) suggests that this genotype is associated with BBB breakdown as well as increased activation of matrix metalloproteinase-9 (which degrades the BBB), and correlated increased pericyte injury with increased cognitive decline in *APOE4* carriers (Montagne et al., 2020).

1.2.2 Neuroimmune Regulation

Brain pericytes also possess numerous putative roles during neuroinflammation. Cultured brain pericytes are immunoactive, responding to stimulation with the endotoxin lipopolysaccharides (LPS) by releasing a plethora of proinflammatory cytokines and chemokines (Kovac et al., 2011; Guijarro-Munoz et al., 2014). While pericytes are required to limit endothelial expression of ICAM-1 and VCAM-1, proteins which facilitate leukocyte adhesion (Török et al., 2021), they contradictorily express these molecules themselves (Proebstl et al., 2012). Brain pericytes may also express phagocytotic and antigen-presenting capabilities (Balabanov et al., 1996; Balabanov et al., 1999; Rustenhoven et al., 2016). Isolated cultures of pericytes have been the most utilized tool to study pericyte contribution to neuroinflammation, so these early results must be treated with caution in light of the transcriptome alterations observed in these cell cultures (Verbeek et al., 1994; Boado and Pardridge, 1994). In vivo, however, PDGFRβ^{+} cells that match the transcriptome of mid-capillary pericytes secrete the chemokine CCL2, which subsequently alters neuronal excitability within 2 hours of LPS-mediated systemic inflammation (Duan et al., 2018), suggesting that pericytes may indeed be initiators of some neuroinflammatory cascades. Given the transcriptomic and morphological changes to brain pericytes in culture (Verbeek et al., 1994; Boado and Pardridge, 1994), additional in vivo experimentation is required to define the precise contributions of pericyte subtypes to acute and chronic neuroinflammation.

1.2.3 Scar Formation and Stem Cell Properties

There are numerous additional CNS functions that have been attributed to pericyte-like cells. However, it appears that many studies supporting these claims are based on the perivascular location of the studied cells and/or marker proteins also found in other cells of the neurovascular

unit, often perivascular fibroblasts. It is also likely that the nondescript etymology of peri - cyte (which can be translated as surrounding – cell) is responsible for much of the confusion. As the precise contribution of *bonafide* pericytes to tantalizing CNS functions such as scar tissue formation and stem cell activity is unresolved, these functions are discussed together.

Following CNS lesions, scar tissue is created from non-neuronal cells to seal off the injured area. This scar tissue is divided into a glial component, mostly made up of reactive astrocytes, and a fibrotic component that secrets extracellular matrix proteins (Dias and Göritz, 2018). A subset of PDGFRβ^{+} perivascular cells that express the protein GLAST, originally named "type A pericytes" is the major contributor to the fibrotic portion of the scar in spinal cord injury (Göritz et al., 2011; Dias et al., 2021) and EAE (Dias et al., 2021), a mouse model of multiple sclerosis. However, the fact that these cells also express Col1a1 (a fibroblast marker not expressed in pericytes) and are commonly found associated with large-diameter blood vessels (as fibroblasts canonically are), has ignited another nomenclature controversy (Soderblom et al., 2013; Yahn et al., 2020; Dias et al., 2021).

Mesenchymal stem cells (MSCs) are a type of adult multipotent stem cell believed to be found in numerous organs, including the brain. Perivascular cells positive for PDGFRβ, NG2, MCAM, and ALPL can be isolated from non-neuronal tissue and differentiated into multiple cell lineages, which suggested that pericytes may act as stem cells across organs (Crisan et al., 2008). Indeed, NG2^{+}nestin^{+} cells cultured from isolated rat brain vessels could be induced to form spheroids containing cells possessing markers for astrocytes, oligodendrocytes, and neurons (Dore-Duffy et al., 2006). Ischemia induces nestin expression (a marker for neural stem cells) in PDGFRB^{+}NG2^{+} cells, which can be isolated and cultured to differentiate into a range of neural and vascular cell types, as well as microglia (Nakagomi et al., 2015; Sakuma et al., 2016). To

address whether these stem cell properties are a result of the cultured environment or are maintained in living animals, a study employed a Tbx18-CreERT2 mouse line to exclusively track the progeny of pericytes (rather than other PDGFRβ^{+} cells) following aging and injury in vivo (Guimarães-Camboa et al., 2018). Tbx18::GFP^{+} cells retained their pericyte identity across these conditions in vivo in numerous organs, including the brain, and did not differentiate into other cell lineages (Guimarães-Camboa et al., 2018). However, like previous culture studies, Tbx18^{+} cells were found to behave as MSCs in vitro (Guimarães-Camboa et al., 2018). Therefore, the physiological stemness of brain pericytes remains undefined.

1.3 Ca^{2+} Signaling

1.3.1 A Brief Introduction to Ca^{2+} Signaling

Ca^{2+} serves as a ubiquitous signaling molecule throughout biology and is a fundamental regulator of numerous cellular processes, including contractility, motility, proliferation, transcription, and apoptosis. Intracellular Ca^{2+} levels fluctuate with time, a process termed Ca^{2+} signaling, in a manner that is tightly controlled to match extracellular and intrinsic stimuli to precise cellular functions. The Ca^{2+} signaling network involves the concerted action of plasmalemmal, endoplasmic reticulum, and mitochondrial proteins, including ion channels, exchangers, and pumps **(Figure 1.3)**. These proteins work to temporally and spatially regulate Ca^{2+} influx, Ca^{2+} uptake/release to/from organelle stores, and Ca^{2+} extrusion. The Ca^{2+} signaling network is further regulated by effector proteins, including those downstream of G protein-coupled receptors or receptor tyrosine kinases. Ca^{2+} signaling pathways are plentiful and do not exist in isolation (for a review, see Clapham, 2007). However, the best characterized and perhaps most

utilized mechanisms: voltage-gated Ca^{2+} entry, Ca^{2+} entry through non-selective cation channels (transient receptor potential channels), store-operated Ca^{2+} entry, and Ca^{2+} release from endoplasmic reticulum stores, are discussed in detail below.

1.3.2 Voltage-Gated Ca^{2+} Channels

Voltage-gated calcium channels (VGCCs) are a group of ion channels which are usually composed of four subunits (α1, β, α2d, and γ), with α1 representing the primary subunit. The α1 subunit is the pore-forming member and contains four homologous domains of six transmembrane a-helices, with the fourth transmembrane helix (termed S4) acting as the primary voltage sensor and the fifth and sixth helices (S5-S6) forming the inner pore. The gene which encodes a channel's α1 subunit dictates the channel type and the channel's biophysical and pharmacological properties. These types include the L-type VGCC channels (Cav1.1, 1.2, 1.3, and 1.4), the P/Q-type (Cav2.1), N-type (Cav2.2), R-type (Cav2.3) and T-type (Cav3.1, 3.2, 3.3).

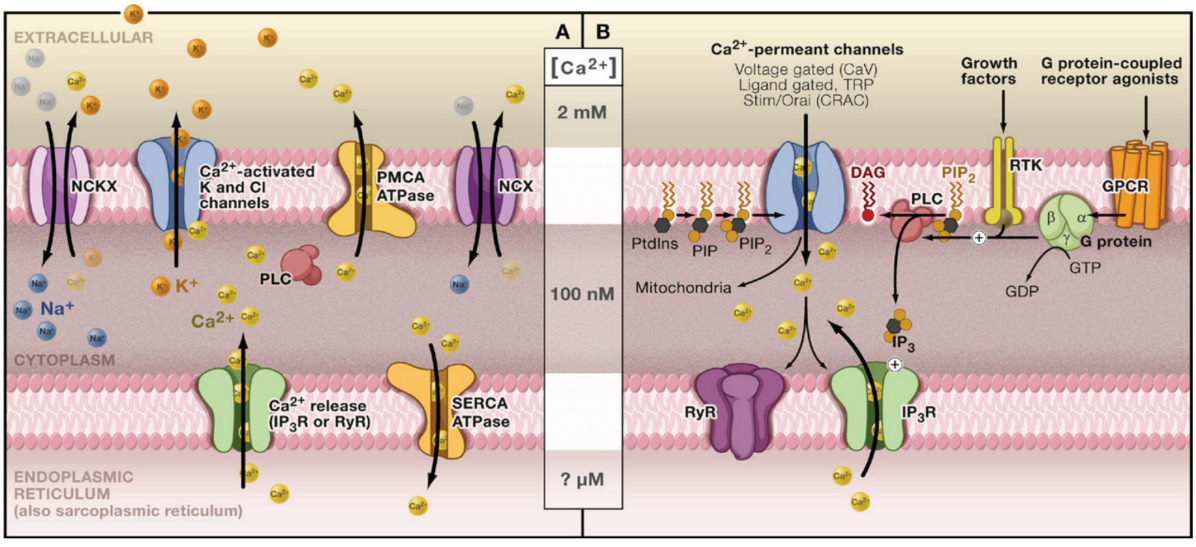

Figure 1.3: An overview of Ca^{2+}-permeable channels. Reprinted from Clapham, 2007 with permission from Elsevier.

The L-type channels are characterized by their activation at a high voltage (HVA), large single-channel conductance, slow voltage-dependent activation, and strong inhibition by the class of ion channel modulators known as dihydropyridines (e.g., nifedipine, nimodipine, nicardipine) at high nanomolar concentrations (Catterall, 2011). Depending on the specific α1 subunit and other factors, including auxiliary channel subunits and channel phosphorylation, L-type VGCCs open and conduct a highly Ca^{2+}-selective current when a cell is depolarized to membrane potentials beyond -30 mV, although this can be as low as -55 mV for the Cav1.3 subtype (Xu and Lipscombe, 2001). L-type VGCCs are the best studied of this channel family and possess a plethora of important roles in classically excitable cells. L-type VGCCs are prevalent in neuronal cell bodies and dendrites, which positions them to control Ca^{2+}-dependent transcription pathways, such as CREB-dependent gene expression downstream of long-term potentiation (Wheeler et al., 2012), suggesting an importance in learning and memory (Moosmang et al., 2005; Langwieser et a., 2010). Nevertheless, the best-described role of L-type VGCCs is their initiation of excitation-contraction coupling in skeletal, cardiac, and smooth muscle cells, albeit through differing mechanisms. As HVA channels, cardiac muscle Cav1.2 channels open in response to action potentials, conducting a significant amount of Ca^{2+} into the cell that acts as an agonist for Ca^{2+} release from intracellular stores through ryanodine receptors (discussed in detail below). This Ca^{2+} release amplifies the Ca^{2+} influx, further driving Ca^{2+} release (a process termed Ca^{2+}-induced-Ca^{2+}-release), leading to activation of actomyosin-based contraction (Fabiato, 1983; Näbuer et al., 1989). A similar process occurs during skeletal muscle contraction, however, a transformational change in Cav1.1 channels activates ryanodine receptors, independent of Ca^{2+} influx (Armstrong et al., 1972; Tanabe et al., 1990). L-type VGCCs are the predominant contributor to $[Ca^{2+}]i$ in smooth muscle cells, and thereby maintain the elevated Ca^{2+} level required for their contraction

(Knot and Nelson, 1998). In these cells, RyRs paradoxically oppose this Ca^{2+} influx through activation of a hyperpolarizing pathway (discussed in detail below) (Nelson et al., 1995).

P/Q-type, N-type, and R-type VGCCs are also high voltage channels with an activation threshold around -40 mV (Adams et al., 2009). They are found predominantly in neurons, where their perisynaptic localization positions them to regulate neurotransmitter release in response to action potentials (Westenbroek et al., 1992; Wheeler et al., 1994). As such, genetic mutations of these channels (in particular, Cav2.1) give rise to pathologies including ataxias and familial hemiplegic migraine type 1 (Pietrobon, 2010).

T-type VGCCs are low voltage activated (LVA) channels, which conduct Ca^{2+} entry at membrane potentials around -60 mV. Unlike the HVA channels, LVA channels have small single channel conductance, rapid gating kinetics, and are composed solely of the α1 subunit (Perez-Reyes, 2003). T-type channels have fast voltage-dependent inactivation, but rapidly recover following a brief hyperpolarizing pulse. Together, these properties make T-type VGCCs important contributors to cardiac pacemaker current (Mangoni et al., 2006), rhythmic firing of action potentials (Cheong and Shin, 2013), and thalamic burst firing (Kim et al., 2001). Upregulation of T-type currents in corticothalamic circuits underlies absence seizures (Tringham et al., 2012; Cheong and Shin, 2013). T-type VGCCs were originally noted for their insensitivity to dihydropyridines, a class of L-type VGCC inhibitors (Nilius et al., 1985). Indeed, the potential therapeutic action of inhibiting T-type VGCCs in absence seizures has led to the recent development of antagonists with greater specificity (Tringham et al., 2012). T-type channels also contribute to vascular function. Notably, in cerebral arterial SMCs, Cav3.2 channels are localized to microdomains where they activate the RyR-mediated hyperpolarization pathway which counteracts constriction (Harraz et al., 2014).

1.3.3 Transient Receptor Potential Channels

The Transient Receptor Potential (TRP) channels form a large channel family of plasma membrane non-selective cation channels. Although the ratio of their permeability to monovalent and divalent cations differs, TRP channels often display significant conductance of Ca^{2+} under a range of physiological contexts (Hariharan et al., 2020). Mammalian cells encode for six subfamilies of TRP channels, named as ankyrin (TRPA), canonical (TRPC), melastain (TRPM), polycystic (TRPP), vanilloid (TRPV). All TRP channels are tetramers formed from subunits with a six transmembrane structure; the ability of these subunits to form heteromers with other subunits from their family greatly increases the diversity of these channels. In total, TRP channels respond to a variety of stimuli, including temperature, cell swelling, mechanical stress, pH, and stimulation of plasma membrane receptors (Clapham, 2003). Many TRP channels are activated by multiple mechanisms, and work is still ongoing to fully characterize these channels. Given this diversity, it is perhaps best to specifically review the TRP channels with known roles in the vasculature. TRPC3 contributes to receptor-mediated vasoconstriction of cerebral arterial SMCs in response to ET-1, angiotensin II, and UTP (Reading et al., 2005; Peppiatt-Wildman et al., 2007; Liu et al., 2009). TRPC6 participates in both receptor-mediated constriction of vascular SMCs, but also in pressure-induced constrictions, whereby it contributes to the myogenic response: an autoregulatory mechanism to keep blood flow constant with changes in blood pressure (Welsh et al., 2002; Inoue et al., 2009; Gonzales et al., 2014). TRPM4 is impermeable to Ca^{2+} but required for the myogenic response (Earley et al., 2004), where it contributes a substantial depolarizing current which activates VGCCs (Gonzales et al., 2010; Gonzales et al., 2014). TRPV4 is a highly Ca^{2+}-permeable TRP channel expressed in endothelial cells, where it activates hyperpolarizing currents through intermediate- and small-conductance Ca^{2+}-activated K^+ channels that transmitted

to SMCs through gap junctions (Sonkusare et al., 2012). In summary, TRP channels are substantial contributors to a host of contractile responses in the vasculature.

1.3.4 Intracellular Calcium Channels

Given the importance of Ca^{2+} as a signaling molecule, cells contribute substantial resources to keeping the intracellular Ca^{2+} concentration around 100 nM, substantially lower than the 1 – 2 mM Ca^{2+} found in the extracellular space. This is primarily accomplished by the actions of two ATP-consuming pumps: the plasma membrane Ca^{2+} ATPase (PMCA), which extrudes Ca^{2+} across the plasma membrane, and the sarco-endoplasmic reticulum Ca^{2+} ATPase (SERCA) which stores Ca^{2+} in large endoplasmic reticulum (ER) (or, in the muscle, sarcoplasmic reticulum (SR)) pools, where it is sustained between 100-800 μM. Ca^{2+} can be released from these pools by IP_3Rs or RyRs, which both function as massive intracellular Ca^{2+} channels with molecular masses of 1-2 MDa (Woll and Van Petegem, 2022). Both release channels are tightly regulated by Ca^{2+}. Cytosolic Ca^{2+} is an agonist at low to intermediate concentrations, but acts as an antagonist at high concentrations, authorizing negative feedback (Fill and Copello, 2002; Taylor and Tovey, 2010). Ca^{2+} release from IP_3Rs and RyRs is therefore able to temporally activate nearby release channels (a process termed Ca^{2+}-induced- Ca^{2+} release), which is responsible for the signature "Ca^{2+} wave" signal produced by these channels. In addition, luminal Ca^{2+} can also activate IP_3Rs and RyRs, permitting Ca^{2+} release when stores become overfilled (Palade et al., 1983; Missiaen et al., 1991). Both channels exist in three isoforms (IP_3R1-3, RyR1-3). All are broadly expressed, although RyR2 is canonically found in cardiac and smooth muscle, while RyR1 is essential for skeletal muscle contraction.

Despite these similarities, the release channels play distinct physiological roles. IP_3Rs are potently activated by the signalling molecule IP_3, which is elevated in cells in response to stimulation of Gq-coupled receptors or receptor tyrosine kinases on the plasma membrane (discussed in detail in section 1.5.2). The magnitude of IP_3 elevation will depend on the extracellular agonist concentration and the number of receptors expressed, and the downstream Ca^{2+} signal will also depend on the number of IP_3Rs and ER Ca^{2+} load. Therefore, IP_3Rs can produce Ca^{2+} signals with diverse spatiotemporal profiles in response to given stimuli, including spatially restricted "puffs", which arise from the opening of a handful of IP_3Rs, or the aforementioned "Ca^{2+} wave" (Hill-Eubanks et al., 2011). IP_3R-mediated Ca^{2+} waves are required for SMC contraction in response to vasoconstrictors, such as UTP, ATP, thromboxane, and angiotensin II (Jaggar and Nelson, 2000; Bayguinov et al., 2000; Hashimoto et al., 2005; Lin et al., 2016). In some instances, these waves can activate calcium-activated chloride channels (Cl_{Ca}), which can lead to depolarization and additional Ca^{2+} elevations through VGCCs (Leblanc et al., 2005). In general, Ca^{2+} release from IP_3Rs is a ubiquitous signaling pathway for cells to respond to agonists.

Ca^{2+} is the primary physiological activator of RyRs. While they are present in numerous cells, including neurons, RyRs are defining features of muscle cells, where, as mentioned, they mediate mechanisms of excitation-contraction coupling. In cerebral SMCs, activation of L- and T-type VGCCs induces a brief (~50 msec), spatially confined, and Ca^{2+}-dependent release from a handful of RyRs – termed a "Ca^{2+} spark" (Nelson et al., 1995; Hill-Eubanks et al., 2011). The spark is the most elementary unit of RyR Ca^{2+} release and activates local large-conductance Ca^{2+} activated potassium channels (BK_{Ca}) at the plasma membrane, which exert a substantial hyperpolarizing influence on the cell (Nelson et al., 1995; Perez et al., 1999). Successive Ca^{2+}

sparks can summate to substantially increase intracellular Ca^{2+}, or they may initiate a propagating Ca^{2+} wave, sometimes with involvement of IP_3Rs (Hill-Eubanks et al., 2011). Additional modulators of RyRs include ATP, which links these channels to cellular metabolism (Meissner, 1984; Xu et al., 1996) and caffeine, which is capable of initiating Ca^{2+} waves in some SMCs (Heppnar et al., 2002). RyRs are also present in non-excitable cells, where they appear to be activated by second messengers such as cyclic adenosine 5-diphosphoribose (cADPR) and nicotinic acid adenine dinucleotide 2'-phosphate (NAADP) and involved in T lymphocyte activation (Thakur et al., 2012; Diercks et al., 2018). In general, however, study of the functional significance of RyRs in non-excitable cells lags that of IP_3Rs (Fomina, 2021).

1.3.5 Store-Operated Calcium Entry (SOCE)

Shortly following the discovery of IP_3-mediated Ca^{2+} release, it became evident that an extracellular Ca^{2+} influx pathway is coincidentally activated upon store depletion in non-excitable cells. Importantly, this pathway is independent of the voltage-gated channels that are inherent to excitable cells (Putney, 1986). Although a strikingly accurate model coupling store depletion to Ca^{2+} influx was proposed in 1986 (Putney, 1986), the electrophysiologic properties, cellular mechanisms, and channel molecular identities of this pathway remained elusive for decades. Hypotheses of direct IP_3 activation of extracellular influx, an ER-released diffusible second messenger, direct IP_3R coupling to a plasmalemmal channel, and transient potential receptor canonical channels as store-operated channels were created and subsequently disproven (Lewis, 2011). Importantly, the discovery of the SERCA pump inhibitors thapsigargin and cyclopiazonic acid proved that SOCE is dictated by the filled state of internal store Ca^{2+} rather than cytosolic IP_3 levels (Takemura et al., 1989), while patch clamp recordings in mast cells revealed an influx

current activated by IP_3 and store depletion (Hoth and Penner, 1992). This current, termed I_{CRAC} (Ca^{2+}-release-activated-Ca^{2+}-channel) is extremely Ca^{2+} selective (pCa^{2+}:pNa^{+} > 1000), with a unitary conductance of only 9-24 fS, and is the prototypical signature of SOCE (Hoth and Penner, 1993; Zweifach and Lewis, 1993).

In 2005, independent genetic knockdown screens in drosophila and mammalian cells identified two intracellular proteins, STIM1 and STIM2, as the ER Ca^{2+} sensors necessary for SOCE (Liou et al., 2005; Roos et al., 2005). Importantly, STIM proteins reside in the ER, contain a Ca^{2+} binding domain on their luminal side, and translocate to plasma membrane puncta upon store depletion (Liou et al., 2005). STIM1 has a lower affinity for Ca^{2+} than STIM2 and is the primary STIM protein underlying SOCE in maximal store-depletion protocols, while STIM2, activated by submaximal depletion, is essential for maintaining basal cytosolic and ER Ca^{2+} levels (Brandman et al., 2007). Subsequent screens identified the Orai family (Orai1, 2, 3) of proteins as the channels which mediate SOCE upon coupling with STIM (Feske et al., 2006; Vig et al., 2006; Zhang et al., 2006). Despite significant homology, the Orai channels each possess distinct biophysical and pharmacological properties that can be further modulated by their formation into functional homotetrameric or heterotetrameric channels. Perhaps most notable is the inhibition of Orai1 but potentiation of Orai3 currents by high micromolar concentrations of the ion channel modulator 2-aminoethoxydiphenyl borate (2-APB) (Prakriya and Lewis, 2001). Orai1, which is necessary for SOCE and I_{CRAC} in lymphocytes (Feske et al., 2006), is by far the best studied Orai member, while research is only beginning to elucidate the unique biological significance of Orai2 and Orai3 (Hoth and Niemeyer, 2013; Emrich et al., 2021). It is important to note that prior to the discovery of the Orai channels, TRPC channels were long hypothesized to be store-operated. However, these channels are activated by DAG downstream of PLC, carry a non-selective cation

current (termed I_{SOC}) that is distinct from I_{CRAC}, do not conclusively associate with STIM proteins, and their activation is not definitively dependent on $[Ca^{2+}]_{ER}$ (DeHaven et al., 2009).

Canonically, the sole function of SOCE is to refill ER stores following depletion by Ca^{2+} release. However, the coupling between SOCE entry and SERCA-mediated uptake is not tight as originally hypothesized. Indeed, as revealed by cytosolic Ca^{2+} indicators, SOCE also dictates cytosolic Ca^{2+} levels, with profound implications for cellular functions. In lymphocytes, Orai-mediated SOCE, which follows activation of the PLC-coupled T or B cell receptor, is necessary for calcineurin activation, subsequent nuclear translocation of the NFAT family of transcription factors, and upregulation of cytokine transcription (Gwack et al., 2007). SOCE-dependent NFAT translocation is also observable in non-immune cell types, with important implications, for example, in neural progenitor proliferation (Somasundaram et al., 2014). Recent work suggests that unique interactions between subsets of the Orai and STIM isoforms allows differential activation of SOCE based on agonist strength, which subsequently encodes differential activation of NFAT isoforms (Yoast et al., 2020; Emrich et al., 2021).

SOCE further has emerging roles in excitable cells in which Ca^{2+} influx is classically dominated by L-type VGCCs. For example, SOCE is an important contributor to skeletal muscle contractility, whereby rapid SOCE activation contributes to the maintenance of ryanodine-sensitive stores (Pearce et al., 2022). Likewise, SOCE may have unique functions in regulating smooth muscle proliferation and migration (Potier et al., 2009). In the central nervous system, SOCE mediates diverse functions in neuronal and non-neuronal cells. For example, excessive Orai2 SOCE is implicated in cortical neuron Ca^{2+} overload following ischemia (Stegner et al., 2019), but some level of SOCE is required for the maintenance of dendritic spines in hippocampal neurons (Maneshi et al., 2020). Microglia, the resident immune cell of the brain, display SOCE

downstream of purinergic receptor activation by ATP, which functions as a danger-associated molecule in neurological disease (Michaelis et al., 2015). TREM2-KO mice exhibit excessive SOCE that inhibits microglia motility (Jairaman et al., 2022), and Orai1 SOCE upregulates synthesis of proinflammatory cytokines in spinal microglia to promote neuropathic pain (Tsujikawa et al., 2023). Astrocytes, another major glial cell, display significant SOCE following purinergic and protease-receptor activation that evokes release of gliotransmitters (Toth et al., 2019). Furthermore, reduction of functional STIM1 was recently associated with astrocyte Ca2+ hypoactivity in a mouse model of Alzheimer's disease (Lia et al., 2023). Interestingly, recent in situ studies have suggested that constitutively active SOCE is required to maintain astrocytic IP_3-sensitive Ca^{2+} stores and spontaneous Ca^{2+} signaling (Sakuragi et al., 2017; Okubo et al., 2020). Despite being initially regarded as a primitive and single-function Ca^{2+} entry pathway, it is becoming increasingly evident that SOCE assumes significant and cell type specific functions that demand detailed study.

1.4 Ca^{2+} Signaling and Functions in Brain Pericytes

Despite the implied importance of calcium to a potential pericyte contractility (among other physiological roles), the mechanisms and functional effects of pericyte Ca^{2+} signaling are largely underexamined. An early study into the Ca^{2+} influx pathways in cultured rat brain pericyte found that cell depolarization with 60 mM K^+ induced Ca2+ influx in pericytes that was blocked by the L-type VGCC inhibitor nicardipine (Kamouchi et al., 2004). Stimulation of these pericytes with vasoactive substances including angiotensin II and ET-1 induced a brief Ca^{2+} transient followed by a sustained Ca^{2+} plateau that was incompletely blocked by nicardipine, indicative of activation of an additional Ca^{2+} influx pathway following IP_3R activation (Kamouchi et al., 2004). It is

important to note that common conditions to culture brain pericytes induces expression of α-SMA (Verbeek et al., 1994; Boado and Pardridge, 1994), which suggests that these cells are more akin to the α-SMA-expressing ensheathing pericyte subtype. Interestingly, current recordings from isolated microvessels from mouse retina have revealed that L-type VGCC activity is indeed robust in ensheathing-type pericytes but is sharply reduced within pericytes of the mid-capillary bed (Matsushita et al., 2010). Consistent with a reduced functional expression of L-type VGCCs in pericytes contacting higher-order capillaries, Ca^{2+} influx in mid-capillary pericytes following stimulation with high K^+ was substantially blunted in comparison to ensheathing-type pericytes (Matsushita et al., 2010). Removal of extracellular Ca^{2+} prevents putative ensheathing-type retinal pericyte capillary constriction following electrical stimulation, confirming a causal link between Ca^{2+} influx into pericytes and contractility (Peppiatt et al., 2006).

While early studies of pericyte Ca^{2+} signaling harnessed ratiometric Ca^{2+} imaging tools such as Fura-2AM to study singular Ca^{2+} signals in response to depolarization, this experimental design does not capture the true physiological diversity of Ca^{2+} signals. Indeed, pioneering *in vivo* imaging of cortical pericyte Ca^{2+} signaling using genetically encoded calcium indicators (GECI) revealed that all mural cells, including all pericyte subtypes, exhibit spontaneous fluctuations in Ca^{2+} within microdomains of the cell, which are termed Ca^{2+} transients (Hill et al., 2015; Rungta et al., 2018). In SMCs and ensheathing pericytes, an increase in intracellular Ca^{2+} is correlated to a decrease in underlying vessel diameter, while no similar correlation (or at least a correlation resolvable with 2-photon imaging), is observed at capillaries contacted by mid-capillary pericytes (Hill et al., 2015; Glück et al., 2021). Nevertheless, intracellular Ca^{2+} levels and Ca^{2+} transient frequency in mid-capillary pericytes is reduced following local increases in neuronal activity by physiological stimuli in the olfactory bulb (Rungta et al., 2018) and retina (Alarcon-Martinez et

al., 2020), as well as by chemogenetic activation of neurons in the somatosensory cortex (Glück et al., 2021). This reduction in Ca^{2+} signaling is coupled to a subsequent dilation of the underlying capillaries, although as shown in the olfactory bulb, this mid-capillary pericyte Ca^{2+} reduction and mid-capillary vessel dilation is delayed relative to the corresponding changes in upstream vessels (Rungta et al., 2018). Altogether, these *in vivo* studies suggest that ensheathing pericyte Ca^{2+} signaling is important for their rapid contractile function, as in SMCs. While a decrease in intracellular Ca^{2+} and subsequent capillary dilation following local neuronal activation suggests that there may also be a physiological contractile function of mid-capillary pericyte Ca^{2+} signals, it is currently unclear if these are merely passive effects following upstream mural cell Ca^{2+} decreases and increases in local blood flow (Rungta et al., 2018).

The application of GECIs (such as GCaMP6f) to *ex vivo* experimentation has allowed for renewed interest in examining the mechanisms of brain pericyte Ca^{2+} signaling. Imaging of GCaMP6f in pericytes expressing Acta2 (presumably ensheathing type) in a mouse retinal mount preparation revealed that the Ca^{2+} activity of ensheathing pericytes in an *ex vivo* preparation lacking intraluminal pressure is largely reduced in comparison to in vivo settings, which suggests that ensheathing pericyte Ca^{2+} activity is dependent on myogenic tone at rest (Gonzales et al., 2020). Nevertheless, Ca^{2+} transient frequency in these cells was robustly elevated upon application of 60 mM K^+ solution or the thromboxane A2 receptor agonist U46619, indicating that ensheathing pericytes possess both functional L-type VGCCs and IP_3 receptors that contribute to the generation of Ca^{2+} transients (Gonzales et al., 2020). These Ca^{2+} signaling pathways appear to act cooperatively in ensheathing pericytes. For example, IP_3 receptor activation following application of ET-1 activates the Ca^{2+}-activated chloride channel TMEM16A in ensheathing pericytes from cortical brain slices. As pericytes have high intracellular Cl^- concentration, opening of TMEM16A

channels leads to chloride efflux, depolarization, and Ca^{2+} influx through opened L-type VGCCs (Korte et al., 2022). Other ion channels may additionally contribute to ensheathing pericyte Ca^{2+} signaling. Interestingly however, an attempt at pharmacologically modulating RyRs in retinal ensheathing pericytes (a channel critical to SMC function) displayed a lack of functional expression (Gonzales et al., 2020).

Direct study of Ca^{2+} signaling in mid-capillary pericytes is only beginning to emerge. In contrast to ensheathing pericytes, mid-capillary pericyte Ca^{2+} transients are largely maintained in *ex vivo* preparations lacking intraluminal pressure, suggesting that these signals occur independently of myogenic tone (Glück et al., 2021). Consistent with a reduced functional expression of VGCCs in retinal mid-capillary pericytes at rest, preliminary pharmacological modulation of cortical mid-capillary pericyte Ca^{2+} signals found that they were only minimally sensitive to a high concentration (100 μM) of the L-type VGCC inhibitor nimodipine, while instead being largely inhibited by the non-specific cation channel blocker SKF-96365 (Glück et al., 2021). Mid-capillary pericytes respond to a diverse array of G_q-GPCR coupled agonists, including U46619, ET-1, and ATP with a sustained and global Ca^{2+} elevation (Glück et a., 2021), indicating that Ca^{2+} release through IP_3R, and potentially downstream or interconnected Ca^{2+} signaling pathways, may have a prominent role in mid-capillary pericytes. However, experimentation suggests that L-type VGCCs may play a significant role in modulating pericyte Ca^{2+} in disease. Distinct pericytes on neighboring capillaries of the mouse retina are sometimes connected by a thin organelle-containing structure called an inter-pericyte tunneling nanotube (IP-TNT) (Alarcon-Martinez et al., 2020). This structure allows for intercellular Ca^{2+} waves to spread between cells, which is essential for IP-TNT mediated neurovascular coupling. In retinal ischemia and glaucoma, the frequency of capillary pericyte Ca^{2+} transients and intercellular waves is reduced, but basal

Ca^{2+} is elevated through the opening of L-type VGCCs, impairing neurovascular coupling (Alarcon-Martinez et al., 2020; Alarcon-Martinez et al., 2022). Pharmacological inhibition or genetic knockout of L-type VGCCs restores Ca^{2+} homeostasis and IP-TNT mediated neurovascular coupling, suggesting that excessive L-type VGCC entry is deleterious.

1.5 G Protein-Coupled Receptor Signaling in Brain Pericytes

1.5.1 A Brief Overview of G Protein-Coupled Receptor Signaling

In addition to Ca^{2+}, cells possess several other second messenger molecules that serve to transduce extracellular stimuli into intracellular effects. Many of these messengers, including cyclic AMP (cAMP), IP_3, and diacylglycerol (DAG) are found (and often, coincidentally modulated) within the G protein-coupled receptor (GPCR) signaling system, for which a broad overview will be provided. It is also important to note that Ca^{2+} channels are themselves significant targets of GPCR signaling, as well as that Ca^{2+} can modulate some G protein isoforms. It is essential to consider such reciprocal relationships when discussing these second messenger systems.

GPCRs consist of seven transmembrane α-helices which form, among other domains, an extracellular ligand binding domain and an intracellular G protein binding domain (Rosenbaum et al., 2009). Binding of a ligand (which depending on the specific GPCR could be a neurotransmitter, hormone, inflammatory mediator, or vasoactive protein, among others) induces a conformational change in the intracellular heteromeric G protein, by which the alpha subunit (Gα) of the G protein exchanges GDP for GTP and dissociates from the β and γ subunits. G proteins are broadly categorized by their α subunit into three major classes, which dictates the downstream effects of

this signaling. Of these, G_q activates that phosphatidylinositol signaling pathway, while G_s and G_i activate and inhibit the cAMP signaling pathway, respectively.

1.5.2 The Phosphatidylinositol Pathway in Brain Pericytes

The G_q pathway is the best characterized G protein signaling pathway in brain pericytes. In this pathway, the activated α_q subunit activates PLC, which cleaves phosphatidylinositol 4,5-bisphosphate (PIP_2) into IP_3 and DAG. Pericytes possess a plethora G_q-GPCRs that should allow them to mobilize Ca^{2+} through IP_3R release in response to a wide array of stimuli (Hariharin et al., 2020; Vanlandewijck et al., 2018). Indeed, cultured pericytes possess a contractile response to numerous ligands, including angiotensin II (Matsugi et al., 1997), ATP (Hørlyck et a., 2021), serotonin (Kamouchi et al., 2004), thromboxane A2 (Dodge et a., 1991), and endothelin-1 (Dehouck et al., 1997), which suggests functional expression of the G_q-GPCRs associated with these agonists (AGTR1, P2RY1, HTR2A/HTR2B, TBXA2R, and EDNRA, respectively). The thromboxane A2 and endothelin-A receptors are the most highly expressed G_q-GPCRs in pericytes at the mRNA level (Hariharin et al., 2020; Vanlandewijck et al., 2018) and are also the best characterized in *ex vivo* and *in vivo* settings. Both thromboxane A2 (and its analogue U46619) and ET-1 are potent vasoconstrictors, well noted for their effects on SMCs (Dorn and Becker, 1993; Yanagisawa et al., 1988). U46619 induces constrictions of capillaries contacted by diverse pericyte subtypes in the brain slice and living brain, including those that appear to be of mesh or thin-strand morphology (Fernández-Klett et al., 2010; Glück et al., 2021), or are confirmed distal retinal pericytes (Gonzales et al., 2020). At least in the brain slice, this constriction is correlated with a robust increase in pericyte $[Ca^{2+}]_i$ (Gonzales et al., 2020; Glück et al., 2021), and both the contractile and Ca^{2+} responses are abolished following sustained washout of U46619 (Glück et al.,

2021). Thromboxane A2 and ET-1 are also central to pericyte pathology and are released from nearby cells of the neurovascular unit, including endothelial cells, astrocytes, and neurons, in ischemia (Korte et al., 2022). ET-1 is also released by pericytes downstream of amyloid β accumulation in rat and human cortical brain slices, whereby it signals to capillary pericytes in an autocrine manner, increasing intracellular Ca^{2+} and constricting underlying capillaries (Nortley et al., 2019). However, aside from the high concentrations of thromboxane A2 and ET-1 that act on pericytes in pathology and experimental settings, both molecules are likely constitutively present at the neurovascular interface (Hariharan et al., 2020). Understanding how fluctuating concentrations of these vasoactive substances modulates pericyte Ca^{2+}, and perhaps local cerebral blood flow, remains an intriguing concept to explore.

Although the Ca^{2+} mobilizing effects of G_q-GPCR agonists in pericytes are widely attributed to their effects downstream of IP_3 production, DAG can also induce $[Ca^{2+}]_i$ changes through modulation of non-selective cation channels or VGCCs. TRPC3 and TRPC6 are directly activated by DAG, as are TRPC3/6-containing heteromeric TRPC channels (Hofmann et al., 1999). The principial action of DAG in the phosphatidylinositol pathway is to stimulate protein kinase C (PKC), which can exert its own effects on plasmalemmal channels. For example, PKC phosphorylation of TRPC1, TRPV1, TRPV6 induces channel activation (Ahmmed et al., 2004; Numazaki et al., 2002; Yao et al., 2005), while PKC phosphorylation of TRPM4 increases its sensitivity to Ca^{2+} activation (Nilius et al., 2005). Phosphorylation is a major regulator of L-type VGCCs, and indeed, phosphorylation of Cav1.2 by PKC increases current amplitude (Yang et al., 2005). As pericytes express many of these ion channels on a transcript level (Hariharan et al., 2020; Vanlandewijck et al., 2018), additional work is required to clarify their precise modulation by the G_q signaling pathway.

1.5.3 The cAMP Pathway in Brain Pericytes

Brain pericytes also express a vast array of G_s- and G_i-coupled GPCRs (Hariharan et al., 2020; Vanlandewijck et al., 2018), which suggests that the cAMP signaling pathway is also a significant regulator of pericyte function. In the G_s pathway, the activated $G\alpha_s$ subunit stimulates adenylyl cyclase, which elevates production of cAMP. Protein kinase A is the major downstream target of cAMP and exerts much of the effects of the G_s pathway by phosphorylating target proteins. The α subunit of the G_i pathway inhibits adenylyl cyclase, thereby opposing the G_s pathway. The best studied G_s-GPCR in brain pericytes is the A_{2A} receptor, which is activated by the nucleotide adenosine, a known vasodilator that is also released in pathologies such as hypoxia and ischemia (Latini et al., 1999; Roth et al., 1997). In isolated retinal microvessels and isolated brain pericytes, adenosine activates K_{ATP} (Kir6.1) potassium channels through the G_s-GPCR/cAMP/PKA pathway (Li and Puro, 2001; Sancho et al., 2022). K_{ATP} channels are highly expressed in mid-capillary pericytes and are substantial contributors to pericyte resting membrane potential (Li and Puro, 2001; Sancho et al., 2022). Theoretically, activation A_{2A}Rs or other G_s-GPCRs (as well as G_i-GPCRs) could impart significant, and sometimes conflicting, effects on pericyte Ca^{2+}. For example, K_{ATP} channel activation signaling hyperpolarizes pericytes, which would be expected to decrease Ca^{2+} influx through voltage-gated Ca^{2+} channels but increase influx through non-voltage-gated channels (such as non-selective cation or store-operated Ca^{2+} channels) by increasing the driving force for Ca^{2+}. In addition, both cAMP/PKA can exert numerous effects on a variety of ion channels. Like PKC, phosphorylation of L-type VGCCs by PKA increases current amplitude (Keef et al., 2001), which could, to some degree, oppose the effects of KATP-mediated hyperpolarization. PKA induces an increase in channel open probability of both IP_3Rs

and RyRs (Woll and Van Petegem, 2022), further implicating the G_s pathway as a potential regulator of pericyte Ca^{2+} signaling.

Investigations into G_i-GPCRs in brain pericytes are only beginning to emerge. Interestingly, G_i activation downstream of noradrenaline stimulation constricts ensheathing pericytes, although this effect was not correlated to a change in pericyte $[Ca^{2+}]_i$ (Korte et al., 2023). Additional experimentation is required to examine the effects of pericyte constriction and Ca^{2+} in response to other G_s and G_i agonists, as well as the influence of the cAMP/PKA pathway on pericyte Ca^{2+} signaling.

1.6 Research Objectives, Hypothesis, and Experimental Design

The overall objective of this work was to uncover the calcium signaling mechanisms responsible for spontaneous Ca^{2+} transients and G_q-GPCR mediated Ca^{2+} elevations in brain mid-capillary pericytes. We hypothesized that Ca2+ transients in mid-capillary pericytes would be mediated by L- or T-type VGCCs given the brief and localized spatiotemporal profile of these transients, the high mRNA expression of Cav1.2 and Cav3.2 in mid-capillary pericytes (Vanlandewijck et al., 2018), previous recordings of pericyte resting membrane potentials which would permit opening of VGCCs (Li et al., 2011; Hall et al., 2014; Hariharan et al., 2022; Korte et al., 2022; Sancho et al., 2022), and the importance of VGCCs to Ca^{2+} signaling in more proximal brain mural cells. We tested this hypothesis by probing the involvement of specific ion channels and associated proteins with pharmacological and ion substitution experiments in *ex vivo* cortical brain slices from transgenic mice expressing the calcium indicator GCaMP6f in mural cells (PDGFRβ-Cre;GCaMP6f).

Chapter 2

Orai, RyR, and IP_3R channels cooperatively regulate calcium signaling in brain mid-capillary pericytes

Braxton Phillips[1,2,3], Jenna Clark[1,2,3], Éric Martineau[2,3], Ravi L. Rungta[2,3*]

1 Department of Neurosciences, Université de Montréal, Montréal, QC, Canada
2 Department of Stomatology, Faculty of Dental Medicine, Université de Montréal, Montréal, QC, Canada
3 Centre interdisciplinaire de recherche sur le cerveau et l'apprentissage, Université de Montréal, Montréal, QC, Canada

* Corresponding author: ravi.rungta@umontreal.ca

Manuscript published in *Communications Biology*

2.1 Abstract

Pericytes are multifunctional cells of the vasculature that are vital to brain homeostasis, yet many of their fundamental physiological properties, such as Ca^{2+} signaling pathways, remain unexplored. We performed pharmacological and ion substitution experiments to investigate the mechanisms underlying pericyte Ca^{2+} signaling in acute cortical brain slices of PDGFRβ-Cre::GCaMP6f mice. We report that mid-capillary pericyte Ca^{2+} signalling differs from ensheathing type pericytes in that it is largely independent of L- and T-type voltage-gated calcium channels. Instead, Ca^{2+} signals in mid-capillary pericytes were inhibited by multiple Orai channel blockers, which also inhibited Ca^{2+} entry triggered by endoplasmic reticulum (ER) store depletion. An investigation into store release pathways indicated that Ca^{2+} transients in mid-capillary pericytes occur through a combination of IP_3R and RyR activation, and that Orai store-operated calcium entry (SOCE) is required to sustain and amplify intracellular Ca^{2+} increases evoked by the GqGPCR agonist endothelin-1. These results suggest that Ca^{2+} influx via Orai channels reciprocally regulates IP_3R and RyR release pathways in the ER, which together generate spontaneous Ca^{2+} transients and amplify Gq-coupled Ca^{2+} elevations in mid-capillary pericytes. Thus, SOCE is a major regulator of pericyte Ca^{2+} and a target for manipulating their function in health and disease.

2.2 Introduction

The mural cells of the brain are multifunctional cells organized in a continuum along the arterio-venous axis of the cerebral vasculature. This continuum is grouped into distinct cell types, which includes smooth muscle cells on penetrating arterioles (aSMCs), pre-capillary sphincters and ensheathing pericytes (also named terminal SMCs) of the arteriole-to-capillary transition zone, pericytes of the mid-capillary bed (of mesh and thin-strand morphology – here collectively referred to as mid-capillary pericytes), and venule smooth muscle cells (Hartmann et al., 2022; Grubb et al., 2021). Although they share a common origin (Armulik et al., 2011) and similar nomenclature, these cell types have numerous morphological (Grant et al., 2019; Ratelade et al., 2020), transcriptomic (Vanlandewijck et al., 2018; Yang et al., 2022), and functional differences (Rungta et al., 2018; Hartmann et al., 2021). For example, aSMCs and ensheathing pericytes fully encircle and exhibit near complete coverage of the endothelial tube, highly express alpha smooth muscle actin (α-SMA), and undoubtedly regulate cerebral blood flow (CBF) (Hall et al., 2014; Rungta et al., 2018). Mid-capillary pericytes have thin or mesh-like processes that run longitudinal to the vessel, express little to no α-SMA, and their role in controlling CBF in physiological contexts remains poorly defined. Nevertheless, blood flow control aside, mid-capillary pericytes have numerous functions in health and disease, such as blood-brain-barrier regulation (Armulik et al., 2010; Bell et al., 2010; Daneman et al., 2010) neuroimmune regulation (Rustenhoven et al., 2017), angiogenesis (Gerhardt and Betsholtz, 2003), glial scar formation (Dias et al., 2021), and suggested stem cell-like properties (Nakagomi et al., 2015). Yet, despite these important functions, the basic physiological properties of brain mid-capillary pericytes, including the mechanisms that regulate their Ca^{2+} signaling, remain understudied.

All mural cells exhibit spontaneous fluctuations in intracellular Ca^{2+}, which are termed Ca^{2+} transients (Hill et al., 2015; Rungta et al., 2018; Glück et al., 2021). Whereas the mechanisms underlying calcium signaling and contraction in aSMCs have been studied in detail (e.g., Nelson et al., 1995; Knot and Nelson, 1998; Collier et al., 2000; Moosmang et al., 2003; Dabertrand et al., 2012; Lin et al., 2016), investigations into brain pericyte Ca^{2+} signaling mechanism are only beginning to emerge. In ensheathing-type pericytes, Ca^{2+} transients can be caused by transmembrane influx through voltage-gated Ca^{2+} channels (VGCCs) and inositol 1,4,5-trisphosphate receptor (IP_3R) signaling that recruits the Ca^{2+} required for α-SMA-mediated contraction (Gonzales et al., 2020; Korte et al., 2022). Mid-capillary pericytes also exhibit Ca^{2+} transients with similar properties *in vivo* and *in vitro*, which are confined to spatial microdomains and modulated by neuronal activity (Rungta et al., 2018; Alarcon-Martinez et al., 2020; Glück et al., 2021). Interestingly, a recent study reported that in resting conditions mid-capillary pericyte Ca^{2+} transients were only minimally sensitive to the potent L-type VGCC blocker nimodipine but were largely inhibited by the non-selective ion channel blocker SKF-96365 (Glück et al., 2021), consistent with a prior study reporting reduced functional expression of VGCCs on distal retinal capillaries (Matsushita et al., 2010). In addition to non-selective cation TRPC channels, SKF-96365 blocks several other Ca^{2+} channels that are highly expressed in mid-capillary pericytes such as T-type VGCCs (Singh et al., 2010), and the Orai family of store-operated Ca^{2+} channels (Várnai et al., 2009). Mid-capillary pericytes also express a plethora of Gq-coupled receptors (Vanlandewijck et al., 2018; Hariharan et al., 2020), which when activated would be expected to trigger Ca^{2+} release from internal stores via IP_3R signaling. Therefore, a more detailed investigation is required to understand the cellular mechanisms underlying Ca^{2+} signaling in mid-

capillary pericytes, their voltage dependence, and the interplay between Ca^{2+} release from internal stores and transmembrane influx.

Here, we utilized pharmacology experiments on acute cortical brain slices from transgenic mice expressing a fluorescent calcium indicator, GCaMP6f, in brain mural cells expressing PDGFRβ (PDGFRβ-Cre;GCaMP6f mice) to delineate the mechanisms underlying Ca^{2+} signaling in brain pericytes. Surprisingly, in contrast to ensheathing type pericytes which we show exhibit Ca^{2+} transients that are partially dependent on VGCCs, mid-capillary pericyte Ca^{2+} signals are largely unaffected by inhibition of VGCCs. We show that mid-capillary pericyte Ca^{2+} transients are, instead, primarily mediated by an interplay between store operated Ca^{2+} entry (SOCE) channels and release of Ca^{2+} from internal stores by IP_3Rs and ryanodine receptors (RyRs). Underscoring the potential importance of pericyte SOCE channels, we further demonstrate that they amplify Gq-coupled $[Ca^{2+}]_i$ elevations evoked by the potent vasoconstrictor endothelin-1 (ET-1).

2.3 Methods

2.3.1 Ethics statement and animals

All procedures conformed to the guidelines of the Canadian Council on Animal Care and were approved by the "Comité de déontologie sur l'expérimentation animale" (CDEA) of the Université de Montréal (QC, Canada). PDGFRβ-Cre mice (Cuttler et al., 2011) were crossed with Ai95(RCL-GCaMP6f)-D reporter mice (Jackson Laboratory) to obtain PDGFRβ-Cre; GCaMP6f-floxed double transgenic mice. Male and female mice aged P28-P163 were used in experiments.

2.3.2 Acute brain slice preparation

Prior to slicing, mice were put into deep anesthesia with isoflurane and 50 µL of Rhodamine B isothiocyanate-Dextran (70 kDa, 2.5% wt:vol, Sigma-Aldrich) was injected retro-orbitally to label the vessel lumen. Mice were euthanized by decapitation. Following extraction from the skull, brains were placed into ice-cold NMDG-based slicing solution containing (in mM): 120 N-Methyl-D-glucamine, 3 KCl, 25 $NaHCO_3$, 7 $MgCl_2$-$6H_2O$, 1 NaH_2PO_4-H_2O, 20 Glucose, 2.4 Na-pyruvate, 1.3 Na-ascorbate, 1 $CaCl_2$-H_2O. Then, 300 µm thick coronal cortical slices were cut with a Leica VT 1200S Vibratome. Slices were transferred to a custom chamber with artificial cerebral spinal fluid (ACSF) containing (in mM): 126 NaCl, 2.5 KCl, 26 $NaHCO_3$, 1.5 $MgCl_2$-$6H_2O$, 1.3 NaH_2PO_4-H_2O, 10 Glucose, 1.2 $CaCl_2$ at 36 °C for 10 minutes. Slices were then recovered in the chamber at room temperature until use. The fluorescent dye TO-PRO-3 has previously been shown to robustly label mid-capillary pericytes in fixed tissue (Mai-Morente et al., 2021), and we have adapted this for imaging in acutely prepared live brain slices. Prior to use, slices were incubated in 1 µM TO-PRO-3 diluted in ACSF for 20 minutes at room temperature to label and identify the pericyte soma. All solutions used were continuously gassed with 95% O_2 and 5% CO_2.

2.3.3 Pharmacology and ion substitution

All salts were obtained from Sigma-Aldrich. Please refer to **Table 2.3** for identifiers, and vehicles of reagents used. Time 0 represents the start of the first acquisition when the new solution is estimated to have reached the bath (estimated based on the flow rate). For Ca^{2+}-free ACSF, $CaCl_2$ was omitted from the ACSF and 2 mM EGTA was added. For 60 mM K^+ ACSF, equimolar NaCl was replaced with KCl. Slices were perfused with TTX for 10 -20 minutes prior to imaging.

For 60mM K^+ experiments, slices were perfused with 60mM K^+ for 10 -20 minutes prior to application of VGCC blockers.

2.3.4 Confocal imaging

Imaging was performed with a Zeiss LSM 510 laser scanning confocal microscope with a 40X water immersion objective lens (0.8NA). Pericytes in cortical brain slices were located by TO-PRO-3 and GCaMP6f co-localization and association with a Rhodamine B labelled vessel. GCaMP6f was excited with a 488 nm LED laser and was detected after passing through a 505-530 nm bandpass filter. TO-PRO-3 and Rhodamine B were excited with a 633 nm and 543 nm HeNe laser respectively, which were generally turned off during Ca^{2+} imaging. Ensheathing pericytes in a subset of explicitly labeled experiments were identified based on GCaMP fluorescence almost fully enwrapping the vessel and were definitively confirmed to be within 3 branch orders of the penetrating arteriole. Mid-capillary pericytes were selected for all other experiments on the basis of: 1) Morphology: thin-stand or mesh morphology in which processes clearly did not fully enwrap the vessel (notably different than those found on first 3 branches), 2) being positive for TO-PRO-3 labelling, and 3) the lack of an arteriole detected within 4 branches of the capillary using the Rhodamine B signal. In several cases for mid-capillary pericytes they could not be traced back 4 branches and an arteriole was not visible in the field of view, in these cases only criteria 1 and 2 were used. To measure calcium transient frequency over time, 50-second image acquisitions were made every 3-4 minutes in frame scanning mode at a 2 Hz sample rate. To record SOCE experiments and $[Ca^{2+}]_i$ rises evoked by agonists, a single acquisition was made in frame scanning mode at a 2 Hz sample rate. Slices were perfused with ACSF at 2 mL/minute and were kept at 34 ± 2 °C during experiments.

2.3.5 Data collection and analysis

Between frame XY-plane translational movement and within frame distortion were removed using a custom non-rigid alignment MATLAB algorithm, based on the *imregdemons* (AccumulatedFieldSmoothing = 2.5; PyramidLevels = 4; 32, 16, 8 and 4 iterations respectively for each pyramid level) and *imwarp* MATLAB functions (https://scanbox.org/2016/06/30/non-rigid-image-alignment-in-twenty-lines-of-matlab/). Hand-drawn regions of interest (ROI) separated pericyte somas from processes. The Astrocyte Quantification and Analysis (AQuA) MATLAB tool (Wang et al., 2019) was used for unbiased event-based Ca^{2+} transient analysis. A Gaussian filter was applied to the images ($\sigma = 2$), minimum event size was set to (pixels): 5/pixel size (μm), and detected events occurring in the same frame separated by (in pixels) 1/pixel size (μm) were merged. Event threshold parameters were set to reliably detect the majority of pericyte Ca^{2+} signaling events with minimal detection of false events outside the cell boundaries. Identical analysis parameters were used for all time series of a given cell and experiment. In experiments in which movies were collected at differing timepoints and average data was shown, a linear interpolation between data points was performed. Ca^{2+} transients following agonist application (ET1 or U46619) in Ca^{2+} free solution (**Figure 2.1f, g**) or GSK-7975A (**Figure 2.6c, d**) was only momentarily increased after agonist application before stores became depleted and was therefore analyzed over a brief period during which the agonists visibly evoked an increase in transient signals: ET-1 in Ca^{2+}-free (65.2 ± 16.31 seconds); U46619 (78.86 ± 12.53 seconds); ET-1 in GSK-7975A (149.1 +/- 7.841 seconds). To compare ET-1 responses at 5, 10, and 30 minutes in Ca^{2+}-free solution (**Figure 2.S2**), Ca^{2+} transient frequency following ET-1 application was analyzed over a 50 second timeframe from when the agonist first evoked signals. To examine changes in ensheathing pericyte Ca^{2+} transient frequency following application of 60 mM $[K^+]_{ex}$, an arteriole

was located and single 50-second acquisitions of all pericytes 1-3 branch orders downstream of the arteriole were taken before and 9-18 minutes after 60 mM $[K^+]_{ex}$ application. Ca^{2+} transient data during all other treatments in **Figures 2.2-2.4** was measured from 10-20 minutes after drug application unless otherwise stated. Transient frequency was normalized to 10 μm of pericyte processes (referred to as 'length'). To measure SOCE and $[Ca^{2+}]_i$ rises evoked by ET-1 in **Figures 2.5-2.6**, background fluorescence was subtracted, a hand-drawn ROI was placed around the soma, and $\Delta F/F$ was averaged 30 seconds around the peak value recorded. Event density heat maps in figures represent the fraction of frames in which an active event was present in each pixel. To measure resting Ca^{2+} levels (**Figure 2.S4; Table 2.1, 2.2**) , a hand-drawn ROI was placed around the soma and an average fluorescence value was calculated from pixels in which AQuA did not detect an event for a given frame. Only cells in which the soma was in focus were included for this analysis. 5 cells were excluded due to improper alignment of translational movement between recordings, and 6 cells were excluded as outliers following identification with the ROUT test (Q = 10%).

2.3.6 Statistics

For all paired data with two groups a two-tailed paired Students' t-test was conducted. For paired data with three groups, a one-way repeated measures ANOVA was conducted, which if significant, was followed by Tukey's or Šidák's post-hoc test (see Figure Legends). For all other statistical comparisons normality was first assessed with a Shapiro-Wilk normality test. If this test failed, statistics were calculated by a Kruskal-Wallis non-parametric test, followed by Dunn's multiple comparisons test.

2.4 Results

Pericyte Ca^{2+} signals were visualized with confocal imaging in acute cortical slices from PDGFRβ-Cre;GCaMP6f mice. The capillary lumen was labeled with an intravenous (I.V.) injection of RhodamineB-Dextran (70kDa) and pericyte somas were labelled with the recently described pericyte specific dye TO-PRO-3 (Mai-Morente et al., 2021) (**Figure 2.1a**). The spontaneous and spatially incoherent nature of mid-capillary pericyte Ca^{2+} transients lead us to take advantage of the recently developed event-based analysis tool AQuA, which was developed precisely for unbiased analysis of such signals, but in astrocytes (Wang et al., 2019). When applied to pericytes, AQuA was found suitable for extracting several properties of these pericyte Ca^{2+} transients, such as overall event frequency, amplitude, area, and duration (**Figure 2.S1a-c; Tables 2.1, 2.2**). Indeed, Ca^{2+} transient frequency in mid-capillary pericyte somas as measured by AQuA was well-matched to measurements made with a region-of-interest based approach (**Figures 2.1b-d, 2.S1**).

We first tested whether these Ca^{2+} transients depended on extracellular Ca^{2+} ($[Ca^{2+}]_{ex}$) by washing out $[Ca^{2+}]_{ex}$ from the perfused artificial cerebral spinal fluid (ACSF). Perfusion of 0 mM Ca^{2+}, 2 mM EGTA solution reversibly depressed the frequency of Ca^{2+} transients in both the processes and soma of the pericyte (**Figures 2.1b-e; 2.S1b-d**). The inhibition of Ca^{2+} transients by Ca^{2+}-free solution was rapid, reaching a maximal effect within 5 – 9 minutes (**Figure 2.S1e**). To test whether intracellular Ca^{2+} stores were completely depleted following 10 minutes in Ca^{2+} -free ACSF, we applied Gq-coupled GPCR agonists for either the endothelin (ET)-A or thromboxane A2 receptor, ET-1 and U46619, which increases intracellular pericyte Ca^{2+} in an IP_3-dependent manner. ET-1 and U46619 were still able to evoke Ca^{2+} transients in Ca^{2+}-free solution (**Figure 2.1f, g**), suggesting that Ca^{2+} stores were not fully depleted at this time point. However, after

prolonged exposure to Ca^{2+} free solution (30 minutes) signals generated by ET-1 application were severely blunted when compared to those induced at 5 and 10 minutes following $[Ca^{2+}]_{ex}$ removal (**Figure 2.S2**), suggesting a gradual run down of store Ca^{2+} levels in the absence of transmembrane Ca^{2+} influx, and a dependence on $[Ca^{2+}]_{ex}$ to maintain ER store Ca^{2+}. Intriguingly, in Ca^{2+} free solution the ET-1 and U46619 induced increases in Ca^{2+} transient frequency were temporary (ET-1, 248.2 +/- 46.52 seconds; U46619, 268.6 +/- 32.65 seconds) (**Figure 2.S2a**) in contrast to the sustained global elevation previously observed in normal $[Ca^{2+}]_{ex}$ solution (Glück et al., 2021). Altogether, these results suggest mid-capillary pericyte Ca^{2+} transients require a plasmalemmal influx pathway, either to directly generate the transients or to sustain constitutive intracellular store filling and release.

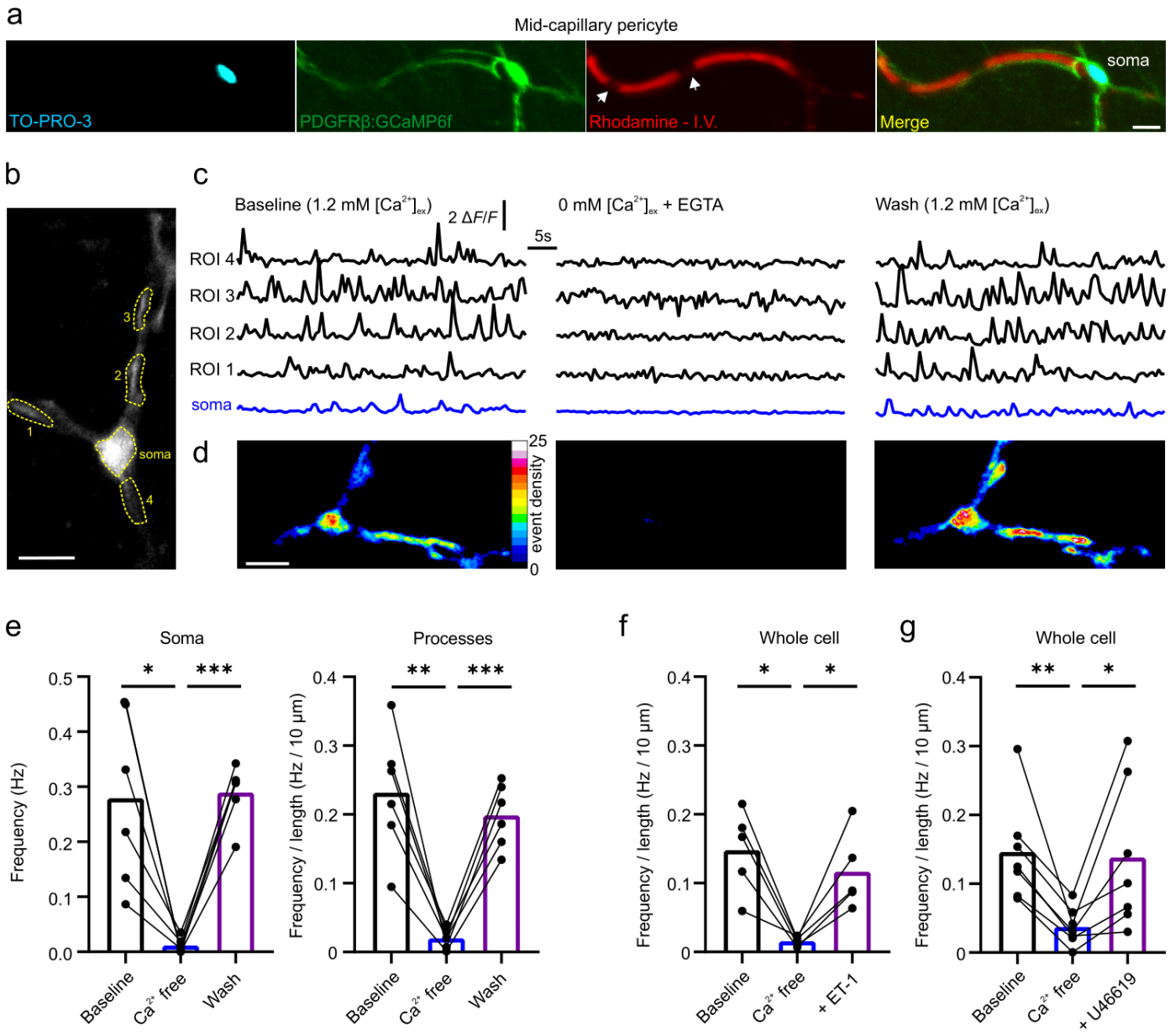
a
Mid-capillary pericyte
TO-PRO-3
PDGFRβ:GCaMP6f
Rhodamine - I.V.
soma
Merge
b
soma
c
Baseline (1.2 mM [Ca2+]ex)
2 ΔF/F
5s
0 mM [Ca2+]ex + EGTA
Wash (1.2 mM [Ca2+]ex)
ROI 4
ROI 3
ROI 2
ROI 1
soma
d
25
event density
0
e
Soma
Processes
Frequency (Hz)
Frequency / length (Hz / 10 µm)
Baseline
Ca2+ free
Wash
f
Whole cell
+ ET-1
g
Whole cell
+ U46619

Figure 2.1: Imaging of mid-capillary pericyte Ca^{2+} transients and their dependence on extracellular Ca^{2+}.
(a) Confocal z-projection of a pericyte expressing GCaMP6f (green) in an acute brain slice loaded with TO-PRO-3 (cyan) and contacting a capillary whose lumen is labeled with Rhodamine-dextran (Red) – arrow heads indicate red blood cells.
(b) Image of GCaMP6f fluorescent pericyte and ROIs selected for (**c**)
(c) ROI based analysis of fluorescent changes in ROIs from (**b**) at baseline (left), after 11 minutes in Ca^{2+} free ACSF (middle), and 5 minutes following wash back of Ca^{2+} containing ACSF (right).
(d) Heat maps of pericyte from (**b** and **c**) showing event density calculated from AQuA (percent time each pixel is active) in same conditions as above in (**c**).
(e) Summarized data showing effect of transiently removing and washing back $[Ca^{2+}]_{ex}$ on pericyte Ca^{2+} transient frequency in the soma and processes. Statistics were calculated by repeated measures one-way ANOVA followed by Tukey's multiple comparisons test, baseline and wash were not significantly different. Analysis window of Ca^{2+} free (4-13 minutes), wash (4-13 minutes) following exposure to solution. N (mice) = 3; n (cells) = 6.
(f, g) 10 nM ET-1 **(f)**, or 100 nM U46619 **(g)** increases Ca^{2+} transient frequency after 10 minutes exposure to Ca^{2+} free ACSF. Statistics were calculated by repeated measures one-way ANOVA followed by Šídák's multiple comparisons test. N = 2; n = 5 and N = 4; n = 7, respectively.
For statistical comparisons *$p < 0.05$, ** $p< 0.01$, *** $p< 0.001$. All image scale bars, 10 μm.

In ensheathing pericytes, depolarization triggers transmembrane influx of Ca^{2+} via VGCCs, thereby increasing Ca^{2+} transient frequency and $[Ca^{2+}]_i$ (Gonzales et al., 2020; Korte et al., 2022). Therefore, we tested the effect of blocking the predominantly expressed pericyte VGCC subtypes, $Ca_V1.2$ (L-type) and $Ca_V3.2$ (T-type), with nifedipine and Z944 (Tringham et al., 2012), respectively (**Figure 2.2a**). Application of nifedipine (20 μM) and Z944 (2 μM) had no effect on the frequency of Ca^{2+} transients, or baseline Ca^{2+} levels, in either the processes or soma (**Figures 2.2b, 2.S4, Tables 2.1, 2.2**). However, we could not exclude the possibility that VGCC transients would become more apparent if the membrane were depolarized, as previously reported for ensheathing type pericytes (Gonzales et al., 2020). Consistent with this previous report, Ca^{2+} transient frequency of ensheathing pericytes was robustly elevated by increasing extracellular K^+ concentration from 2.5 mM to 60 mM and was significantly reduced in the presence of VGCC blockers (**Figure 2.2c-g**, **Tables 2.1, 2.2**, 1st to 3rd branch order from penetrating arteriole). In contrast, depolarization with 60 mM $[K^+]_{ex}$ did not increase mid-capillary pericyte Ca^{2+} transient frequency (**Figure 2.2d)** and VGCC blockers still had no effect on mid-capillary pericyte Ca^{2+} transient frequency when applied in 60 mM $[K^+]_{ex}$ (**Figures 2.2c-g, Tables 2.1, 2.2**). To further test the effect of membrane voltage on mid-capillary pericyte Ca^{2+}, we pharmacologically altered K_{ATP} channel activity, whose modulation has been shown to have large effects on pericyte membrane potential (Li and Puro, 2001; Hariharan et al., 2022; Sancho et al., 2022). Consistent with our above results showing that mid-capillary Ca^{2+} transients were independent of VGCCs, application of pinacidil (10 μM), a K_{ATP} channel opener which hyperpolarizes pericytes, had no effect on transient frequency in processes or the soma (**Figure 2.2h**). Furthermore, glibenclamide (20 μM) a K_{ATP} channel blocker, decreased rather than increased transient frequency in mid-capillary pericyte processes (**Figure 2.2i**), suggesting that mid-capillary K_{ATP} channels were open

at rest, and that depolarization may actually decrease Ca^{2+} influx. As a note, all experiments were performed in tetrodotoxin (TTX, 500 nM) to block neuronal action potentials, which alone had no significant effect on the frequency of mid-capillary pericyte Ca^{2+} transients, consistent with a previous report (Glück et al., 2021), although resting $[Ca^{2+}]_i$ was slightly increased in TTX (**Figures 2.S3, 2.S4, Tables 2.1, 2.2**). Taken together, these results indicate that in contrast to ensheathing pericytes which exhibit elevated Ca^{2+} transients upon depolarization via VGCCs, mid-capillary pericyte Ca^{2+} transients are largely independent of VGCCs.

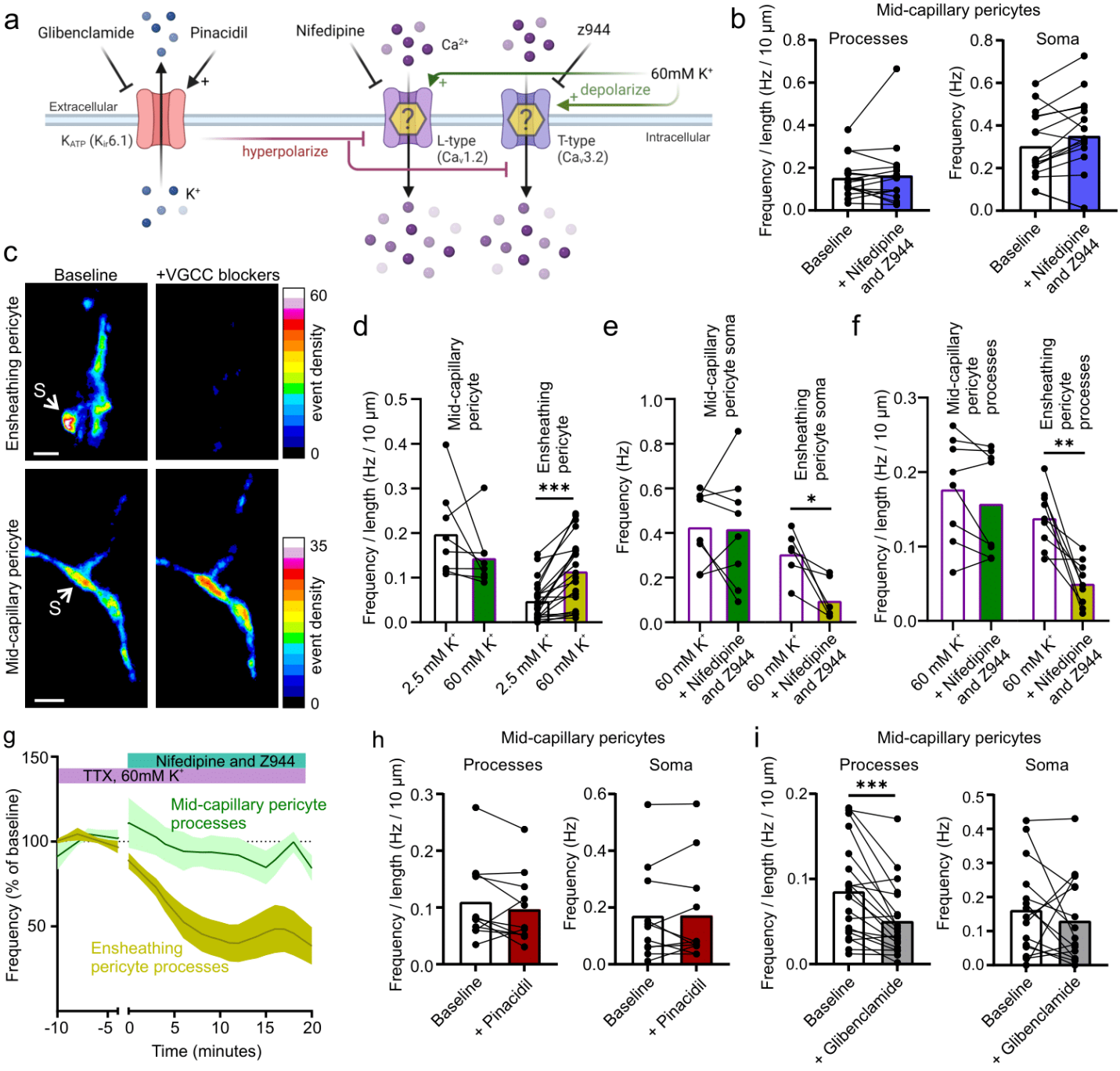
a
Glibenclamide
Pinacidil
Nifedipine
Ca2+
z944
60mM K+
depolarize
Extracellular
Intracellular
KATP (Kir6.1)
hyperpolarize
L-type (Cav1.2)
T-type (Cav3.2)
K+
b
Mid-capillary pericytes
Processes
Soma
Frequency / length (Hz / 10 µm)
Frequency (Hz)
Baseline
+ Nifedipine and Z944
c
Baseline
+VGCC blockers
Ensheathing pericyte
Mid-capillary pericyte
event density
d
Mid-capillary pericyte
Ensheathing pericyte
Frequency / length (Hz / 10 µm)
2.5 mM K+
60 mM K+
e
Mid-capillary pericyte soma
Ensheathing pericyte soma
Frequency (Hz)
60 mM K+ + Nifedipine and Z944
f
Mid-capillary pericyte processes
Ensheathing pericyte processes
g
Nifedipine and Z944
TTX, 60mM K+
Mid-capillary pericyte processes
Ensheathing pericyte processes
Frequency (% of baseline)
Time (minutes)
h
Mid-capillary pericytes
Processes
Soma
+ Pinacidil
i
Mid-capillary pericytes
Processes
Soma
+ Glibenclamide

Figure 2.2: Mid-capillary pericyte Ca^{2+} transients are not potentiated by depolarization or mediated by VGCCs.
(a) Schematic of experimental plan in Fig. 2. Created with biorender.com
(b) Blocking L-type and T-type VGCCs with 20 μM nifedipine and 2 μM Z944 does not reduce the frequency of Ca^{2+} transients in mid-capillary pericyte processes (N = 2, n = 16) or soma (N = 2, n = 16). Analysis was conducted 10-20 minutes after drugs reached the bath.
(c) Example images showing event density (percentage of frames an event was detected within each pixel) after application of 20 μM nifedipine and 2 μM Z944 in 60 mM $[K^+]_{ex}$, for an ensheathing pericyte (3rd order, top), and a mid-capillary pericyte (bottom). S points to soma.
(d) Summarized data showing that changing $[K^+]_{ex}$ from 2.5 to 60 mM does not increase the frequency of Ca^{2+} transients in mid-capillary pericytes (left, N = 2, n = 8), but does significantly increase Ca^{2+} transient frequency of ensheathing pericytes (1st-3rd order, N = 2, n = 21). Analysis done 9-18 minutes following 60 mM $[K^+]_{ex}$ exposure.
(e) Summarized data, showing application of 20 μM nifedipine and 2 μM Z944 in 60 mM $[K^+]_{ex}$ reduces Ca^{2+} transient frequency in ensheathing (N = 5, n = 6) but not mid-capillary pericyte soma (N = 4, n = 8). Analysis was conducted 10-20 minutes after drugs reached the bath.
(f) Summarized data, showing application of 20 μM nifedipine and 2 μM Z944 in 60 mM $[K^+]_{ex}$ reduces Ca^{2+} transient frequency in ensheathing (N = 5, n = 9) but not mid-capillary pericyte processes (N = 4, n = 8). Analysis was conducted 10-20 minutes after drugs reached the bath
(g) Time course of data shown in (**f**).
(h) Summarized data of K_{ATP} channel opener 10 μM pinacidil on mid-capillary pericyte Ca^{2+} transient frequency in process (N = 2, n = 11), and soma (N = 2, n = 11). Analysis was conducted 10-20 minutes after drugs reached the bath.
(i) Summarized data of K_{ATP} channel blocker 20 μM glibenclamide on mid-capillary pericyte Ca^{2+} transient frequency in process (N = 3, n = 20), and soma (N = 3, n = 15). Analysis was conducted 10-20 minutes after drugs reached the bath.
All experiments performed in 500 nM TTX. Shaded area **(g)** represents SEM. Time 0 represents the start of the first 50 second acquisition in the presence of the new bathing solution (when the solution is estimated to have reached the slice chamber). For statistical comparisons *$p < 0.05$, ** $p< 0.01$, *** $p< 0.001$. All image scale bars, 10 μm.

Having established a marked difference in the mechanisms of Ca^{2+} signalling between pericyte subtypes, we next examined the unidentified calcium influx pathway(s) required for the generation of Ca^{2+} transients in mid-capillary pericytes (**Figure 2.3a**). We first tested the non-specific ion channel blocker SKF-96365, which was previously reported to block mid-capillary pericyte Ca^{2+} transients (Glück et al., 2021). Consistent with this previous report, Ca^{2+} transient frequency in the processes and somas of these pericytes was largely diminished in the presence of SKF-96365 (100 μM) (**Figure 2.3b, Tables 2.1, 2.2**). As SKF-96365 is a potent TRPC channel blocker, and TRPC3/6 are non-selective cation channels highly expressed in pericytes (Vanlandewijck et al., 2018), we further examined the sensitivity of mid-capillary pericyte Ca^{2+} transients to the TRPC3 blocker, Pyr3 and the potent TRPC3/6 blocker GSK-2833503A. Mid-capillary pericyte Ca^{2+} transients were unaffected by TRPC3 inhibition with Pyr3 (20 μM), and inhibition of TRPC3/6 with GSK 2833503A (10 μM) (**Figure 2.3b, Tables 2.1, 2.2**), suggesting influx via another SKF-96365 sensitive pathway. Interestingly, mid-capillary pericytes highly express Orai1 and Orai3 Ca^{2+} channels (Vanlandewijck et al., 2018), and these channels are also sensitive to SKF-96365 (Várnai et al., 2009). We therefore tested the sensitivity of mid-capillary pericyte Ca^{2+} transients to the non-selective Orai channel blocker 2-APB. 2-APB is a potent Orai1 channel blocker at high concentration but potentiates Orai1 channels at low concentrations (Prakriya and Lewis, 2001). Consistent with the bidirectional concentration-dependent sensitivity of Orai1 channels to 2-APB, 10 μM 2-APB increased mid-capillary pericyte Ca^{2+} transient frequency, whereas 100 μM 2-APB nearly abolished all transients (**Figure 2.3c, Tables 2.1, 2.2**). Although the effects of 2-APB are supportive of Orai mediated Ca^{2+} entry, 2-APB has several off-target effects, such as inhibiting IP_3Rs and some TRP channels. Therefore, we tested the sensitivity of mid-capillary pericyte Ca^{2+} transients to the Orai-specific blocker GSK-7975A (Derler et al.,

2013). Indeed, GSK-7975A (40 μM) robustly reduced the frequency of Ca^{2+} transients in mid-capillary pericytes in both the soma and processes (**Figure 2.3d-g, Tables 2.1, 2.2)**. Additionally, we tested the effects of the recently developed compound IA65, which enhances Orai1/3 but inhibits Orai2 (Azimi et al., 2020; Zhang et al., 2020). Consistent with the high mRNA expression of Orai1 and Orai3 in mid-capillary pericytes, IA65 (10 μM) rapidly induced an elevation in resting Ca^{2+} levels (**Figure 2.3h, 2.S4**), although in contrast to 2-APB (10 μM), we did not observe an increase in Ca^{2+} transient frequency (**Tables 2.1, 2.2**).

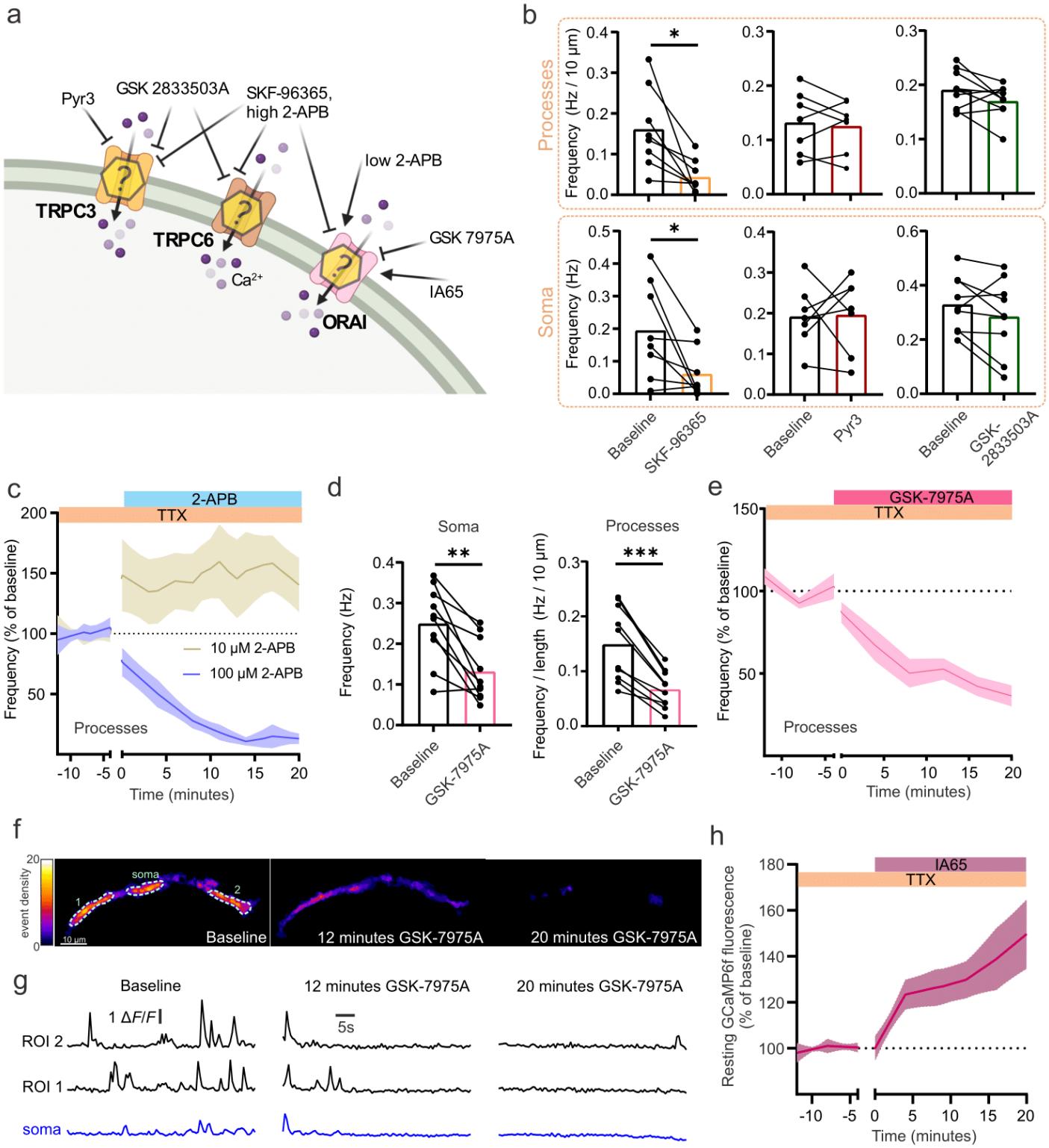
a
Pyr3
GSK 2833503A
SKF-96365,
high 2-APB
low 2-APB
TRPC3
TRPC6
GSK 7975A
Ca2+
IA65
ORAI
b
Processes
Soma
Frequency (Hz / 10 µm)
Frequency (Hz)
Baseline
SKF-96365
Pyr3
GSK-2833503A
c
2-APB
TTX
Frequency (% of baseline)
10 µM 2-APB
100 µM 2-APB
Processes
Time (minutes)
d
Soma
Processes
Frequency (Hz)
Frequency / length (Hz / 10 µm)
Baseline
GSK-7975A
e
GSK-7975A
TTX
Frequency (% of baseline)
Processes
Time (minutes)
f
event density
soma
1
2
10 µm
Baseline
12 minutes GSK-7975A
20 minutes GSK-7975A
g
Baseline
12 minutes GSK-7975A
20 minutes GSK-7975A
1 ΔF/F
5s
ROI 2
ROI 1
soma
h
IA65
TTX
Resting GCaMP6f fluorescence (% of baseline)
Time (minutes)

Figure 2.3: Mid-capillary pericyte Ca^{2+} transients signals are dependent on Orai Ca^{2+} channels

(a) Schematic of experimental plan and pharmacology. Created with biorender.com

(b) 100 μM SKF-96365 reduces the frequency of Ca^{2+} transients in mid-capillary pericyte processes (N = 3, n = 8) and soma (N = 3, n = 8). Neither of the TRPC3 or the TRPC3/6 antagonists, 20 μM Pyr3 or 10 μM GSK-2833503A, significantly reduce pericyte Ca^{2+} transient frequency, soma (N = 3, n = 7 and N = 2, n = 9, respectively) or processes (N = 3, n = 7 and N = 2, n = 9, respectively). Analysis was conducted 10-20 minutes after drugs reached the bath.

(c) Low concentration (10 μM) 2-APB increases whereas high concentration (100 μM) 2-APB reduces Ca^{2+} transient frequency in mid-capillary pericyte processes (N = 3, n = 9 for both analyses). Analysis was conducted 10-20 minutes after drugs reached the bath.

(d) The Orai channel inhibitor 40 μM GSK-7975A reduces Ca^{2+} transient frequency in both soma (left, N = 2, n = 10) and processes (right, N = 2, n = 10). Analysis was conducted 10-20 minutes after drugs reached the bath.

(e) Time course of data in (**d** right).

(f) Event density image of a pericyte showing a decrease in Ca^{2+} transients at different time points following application of GSK-7975A.

(g) Example traces of GCaMP6f signal over time in ROIs from soma and 2 regions of a pericytes processes matching heat maps in (**f**).

(h) Perfusion of the Orai1/3 enhancer IA65 (10 μM) increases resting Ca^{2+} (GCaMP6f fluorescence measured in the soma, N = 2, n = 8).

All experiments performed in 500 nM TTX. Shaded areas represent SEM. Time 0 represents the start of the first acquisition in the presence of the new bathing solution (when the solution is estimated to have reached the slice chamber). For statistical comparisons *$p < 0.05$, ** $p< 0.01$, *** $p< 0.001$.

While our data suggests that Ca^{2+} influx through Orai SOCE channels is required for the generation of spontaneous Ca^{2+} transients in mid-capillary pericytes, store-operated entry and store-release mechanisms are inextricably linked. Therefore, we set out to test the dependence of mid-capillary pericyte Ca^{2+} transients on store Ca^{2+} filling and release pathways (**Figure 2.4a**). If mid-capillary pericyte Ca^{2+} transients were dependent on store release, then blocking store filling would be expected to block the generation of the transients. Indeed, pharmacological inhibition of the sarco(endo)-plasmic reticulum calcium-ATPase (SERCA), with cyclopiazonic acid (CPA, 30 μM) abolished Ca^{2+} transients (**Figure 2.4b)** suggesting their dependence on store release. In parallel to the drop in transient frequency, CPA induced a global and sustained resting Ca^{2+} elevation (**Figure 2.4b**), consistent with the activation of Orai channels via ER Ca^{2+} depletion and STIM1/2 proteins. Given the dependence of the Ca^{2+} transients on store Ca^{2+}, we proceeded to investigate their dependence on the ER store release channels, IP_3Rs and RyRs. To test the relative contributions of these channels to mid-capillary pericyte Ca^{2+} transients, we either inhibited phospholipase C with U73122 (which prevents IP_3 production) or RyRs with the reversible antagonist tetracaine. Blocking IP_3 production with U73122 (25 μM) led a modest reduction in Ca^{2+} transient frequency in mid-capillary pericyte processes but not soma (**Figure 2.4c, d**), and the spatial area of the remaining transients was also reduced (**Figure 2.4e**). Strikingly, blocking RyR with tetracaine (200 μM) robustly reduced the frequency, spatial area, and duration of Ca^{2+} transients in mid-capillary pericyte processes and soma (**Figure 2.4g-j, Tables 2.1, 2.2**), as well as resting Ca^{2+} levels (**Figure 2.S4**). We additionally confirmed the reversibility of the tetracaine effect on transient frequency in five cells (200 - 500 μM tetracaine = 30.33% ± 8.610%, washout = 108.2% ± 25.01% (% baseline frequency, mean ± SEM); $p = 0.0305$, two-tailed paired Students' t-test). Consistent with a functional role of RyRs in mid-capillary pericytes, application of caffeine

(10 mM), a RyR potentiator, elevated mid-capillary pericyte Ca^{2+} (**Figure 2.4f**). Altogether, these results point to a mechanism whereby constitutive Ca^{2+} entry through SOCE channels is required to maintain spontaneous Ca^{2+} release through RyRs and IP_3Rs, which in turn lead to store depletion and activation of Orai channels.

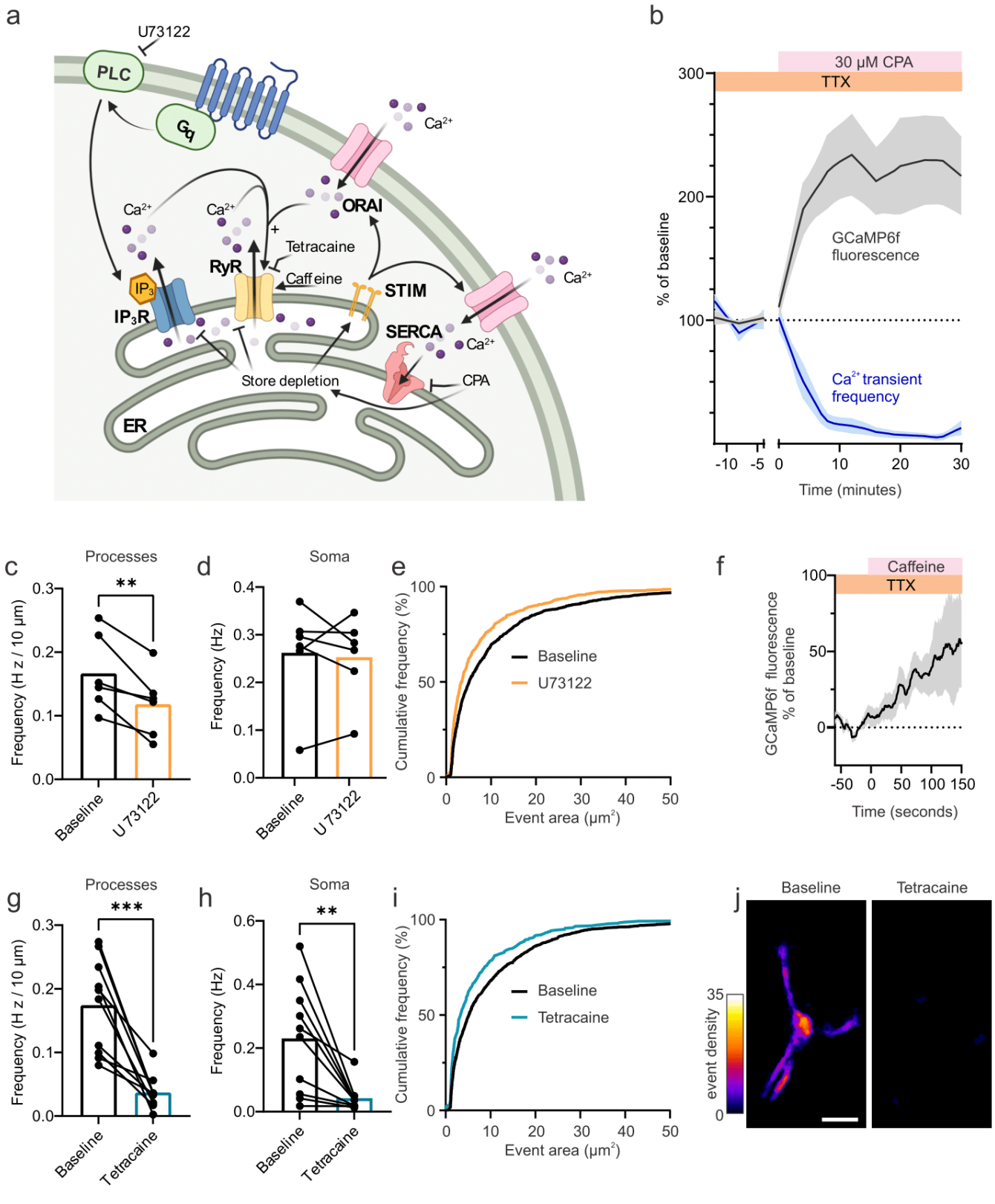
a
U73122
PLC
Gq
Ca2+
ORAI
Tetracaine
RyR
Caffeine
STIM
IP3
IP3R
SERCA
Store depletion
CPA
ER
b
30 µM CPA
TTX
% of baseline
GCaMP6f fluorescence
Ca2+ transient frequency
Time (minutes)
c
Processes
Frequency (H z / 10 µm)
Baseline
U 73122
d
Soma
Frequency (Hz)
e
Cumulative frequency (%)
Baseline
U73122
Event area (µm2)
f
Caffeine
TTX
GCaMP6f fluorescence % of baseline
Time (seconds)
g
Processes
Tetracaine
h
Soma
i
Baseline
Tetracaine
j
event density

Figure 2.4: Mid-capillary pericyte Ca^{2+} transients are mediated by RyR and IP_3R store release pathways.
(a) Schematic of experimental plan and pharmacology. Created with biorender.com
(b) Perfusion of cyclopiazonic acid (CPA 30 μM) to block SERCA pump and deplete intracellular stores, reduces the frequency of mid-capillary pericyte Ca^{2+} transients (blue trace), while elevating cytosolic Ca^{2+} (black trace). N = 4, n = 9.
(c, d) Effect of phospholipase C inhibition with U 73122 (25 μM) on mid-capillary pericyte Ca^{2+} transient frequency measured in the processes (**c**, N = 2, n = 6) and soma (**d**, N = 2, n = 6). Analysis was conducted 10-20 minutes after drugs reached the bath.
(e) Cumulative frequency plot showing reduction in event area in the presence of U 73122.
(f) Caffeine (10 mM) increases cytosolic Ca^{2+} in mid-capillary pericytes (GCaMP6f fluorescence measured in the soma). N = 4, n = 9.
(g, h) Effect of RyR inhibition with tetracaine (200 μM) on mid-capillary pericyte Ca^{2+} transient frequency measured in the processes (**g**, N = 3, n = 10) and soma (**h**, N = 3, n = 10). Analysis was conducted 10-20 minutes after drugs reached the bath.
(i) Cumulative frequency plot showing reduction in event area in the presence of tetracaine (200 μM).
(j) Heat map of event density in a mid-capillary pericyte before and after application of tetracaine (200 μM). Scale bar, 10 μm.
All experiments performed in 500 nM TTX. Shaded area **(b, f)** represents SEM. Time 0 represents the start of the first acquisition in the presence of the new bathing solution (when the solution is estimated to have reached the slice chamber). For statistical comparisons *$p < 0.05$, ** $p< 0.01$, *** $p< 0.001$.

To confirm that the Ca^{2+} influx through Orai channels was indeed store-operated, we tested whether Ca^{2+} entry to maximal store depletion was also sensitive to Orai channel antagonists, by adapting a protocol commonly used to maximally activate SOCE in expression systems and cell culture (Bird et al., 2008). First, we applied CPA (30 μM) for 20 minutes in Ca^{2+}-free ACSF to deplete ER stores and maximally activate "store-operated" channels. Then, we reintroduced 1.2 mM $[Ca^{2+}]_{ex}$ to the bathing solution while imaging a mid-capillary pericyte (**Figure 2.5a, b**), triggering a large influx of Ca^{2+} through the open transmembrane channels. As expected, a large increase in mid-capillary pericyte Ca^{2+} was measured upon reintroduction of $[Ca^{2+}]_{ex}$, indicative of functional store-operated Ca^{2+} channels (**Figure 2.5a-c**). As with the Ca^{2+} transients, this store depletion-induced Ca^{2+} influx was also sensitive to the Orai channel blockers, 2-APB and GSK-7975A, in mid-capillary pericytes (**Figure 2.5a, c)**. However, this experiment alone does not prove that store Ca^{2+} levels dictate the opening of the plasma membrane Orai channels, as the increase in cytoplasmic Ca^{2+} upon reintroduction of $[Ca^{2+}]_{ex}$ could simply be occurring through store independent channels that are constitutively open. Therefore, we performed an experiment in which the brain slice was exposed to Ca^{2+}-free solution for the same duration as in the CPA experiments outlined above, but in the presence of tetracaine and U73122 to block store release via RyRs and IP3Rs. If plasma membrane Ca^{2+} influx is truly controlled by ER store Ca^{2+} levels in mid-capillary pericytes, then the increase in $[Ca^{2+}]_i$ upon reintroduction of $[Ca^{2+}]_{ex}$ should be smaller than when stores are depleted and SOCE is activated. Indeed, in slices perfused with 200 μM tetracaine and 25 μM U73122, re-introduction of $[Ca^{2+}]_{ex}$ resulted in a minute increase in Ca^{2+} entry that was not significantly different than when stores were depleted in the presence of Orai inhibitors (**Figure 2.5a, c**). These results confirm that plasma membrane Ca^{2+} influx in mid-capillary pericytes is driven by ER store depletion.

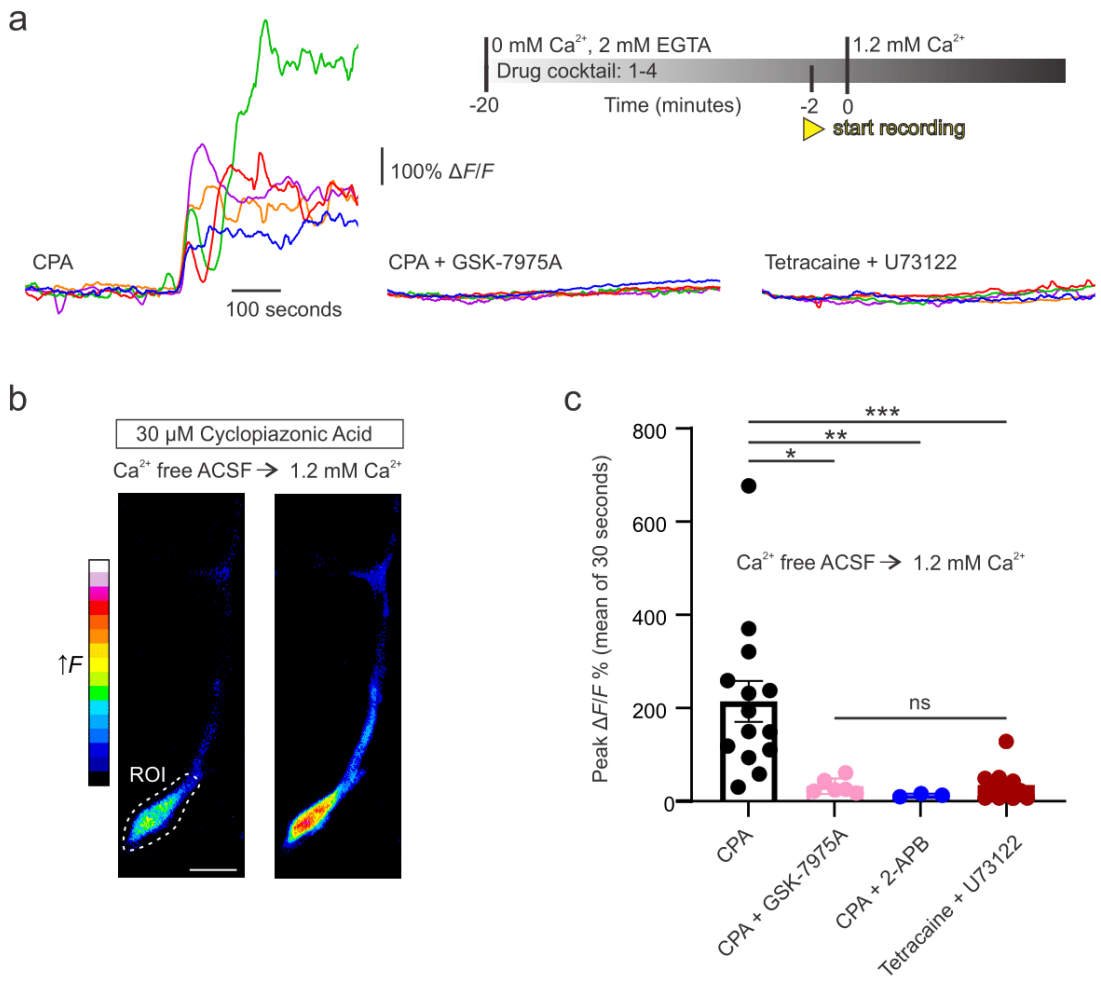

Figure 2.5: Mid-capillary pericytes express functional SOCE that is blocked with Orai inhibitors.

(a) Inset (top right), shows timing of experimental protocol. 5 overlayed representative traces in different colours are shown in 3 different experimental conditions (left to right) from example cells in which 1.2 mM $[Ca^{2+}]_{ex}$ is washed back on the brain slice. Left, in 30 μM cyclopiazonic acid (CPA) to deplete ER stores and quantify the magnitude of Ca^{2+} entry via store operated channels. Middle, same as left, but in the presence of the Orai inhibitor 40 μM GSK-7975A. Right, wash back of Ca^{2+} in condition where store depletion is prevented by blocking RyR and IP_3R release pathways with tetracaine (200 μM) and U73122 (25 μM), respectively.

(b) Example image showing increase in pericyte GCaMP6f fluorescence when extracellular ACSF is switched from Ca^{2+} free to 1.2 mM $[Ca^{2+}]_{ex}$ in conditions where endoplasmic reticulum stores are depleted with 30 μM CPA. An ROI around soma is used for quantification in (**a**) and (**c**). Scale bar, 10 μM.

(c) Summarized data showing effect of ACSF (N = 8, n = 14), 40 μM GSK-7975A (N = 2, n = 6), and 100 μM 2-APB (N = 1, n = 3) on SOCE, following transition from 0 mM to 1.2 mM Ca^{2+} ACSF in the presence of 30 μM CPA, and the dependence on store depletion as it is prevented when $[Ca^{2+}]_{ex}$ is reintroduced when store depletion is prevented by 200 μM tetracaine and 25 μM U 73122 (N = 2, n = 11). Statistics were calculated with a Kruskal-Wallis test followed by Dunn's multiple comparisons test. Error bars represent SEM. For statistical comparisons *p < 0.05, ** p< 0.01, *** p< 0.001.

The above evidence supporting SOCE channels in mid-capillary pericytes raised the intriguing possibility that Orai channels may be required to amplify and sustain GPCR mediated Ca^{2+} elevations, following robust release of Ca^{2+} from internal stores, as has been reported in other cell types (e.g., Jairaman et al., 2022). Therefore, we harnessed the potent vasoconstrictor ET-1, which has been previously shown to induce large elevations in mid-capillary pericyte Ca^{2+} (Glück et al., 2021). Indeed, in 1.2 mM $[Ca^{2+}]_{ex}$, ET-1 triggered a robust and sustained, but highly variable, Ca^{2+} elevation in mid-capillary pericytes (**Figure 2.6a, b**). In contrast to the previously described role of the Ca^{2+} activated chloride channel, TMEM16A, and VGCCs, which are required to amplify ET-1 mediated Ca^{2+} elevations in ensheathing type pericytes (1^{st}-3^{rd} branch orders) (Korte et al., 2022), in mid-capillary pericytes, blocking VGCCs (20 μM nifedipine and 2 μM Z944) or TMEM16A (2 uM Ani9) for 20 minutes had no significant effect on the magnitude of the ET-1 mediated Ca^{2+} elevation (**Figure 2.6a, b**). However, when Orai channels were blocked with GSK-7975A for 20 minutes prior to ET-1 application, the magnitude of this elevation in $[Ca^{2+}]_i$ was strongly reduced (**Figure 2.6a, b**), and as in Ca^{2+}-free ACSF (**Figure 2.S2**), ET-1 evoked a transient increase in event frequency rather than a sustained elevation (**Figure 2.6c, d**). Importantly, these Ca^{2+} elevations were prevented by preincubation with U73122 (25 μM, 20 minutes), confirming that ET-1 induced signals are initiated by the Gq-GPCR-PLC pathway (**Figure 2.6a, b**). These results suggest that Orai mediated SOCE amplifies Gq-GPCR mediated Ca^{2+} elevations and may contribute to sustained increases in mid-capillary pericyte Ca^{2+} following the release of vasoconstrictive agents.

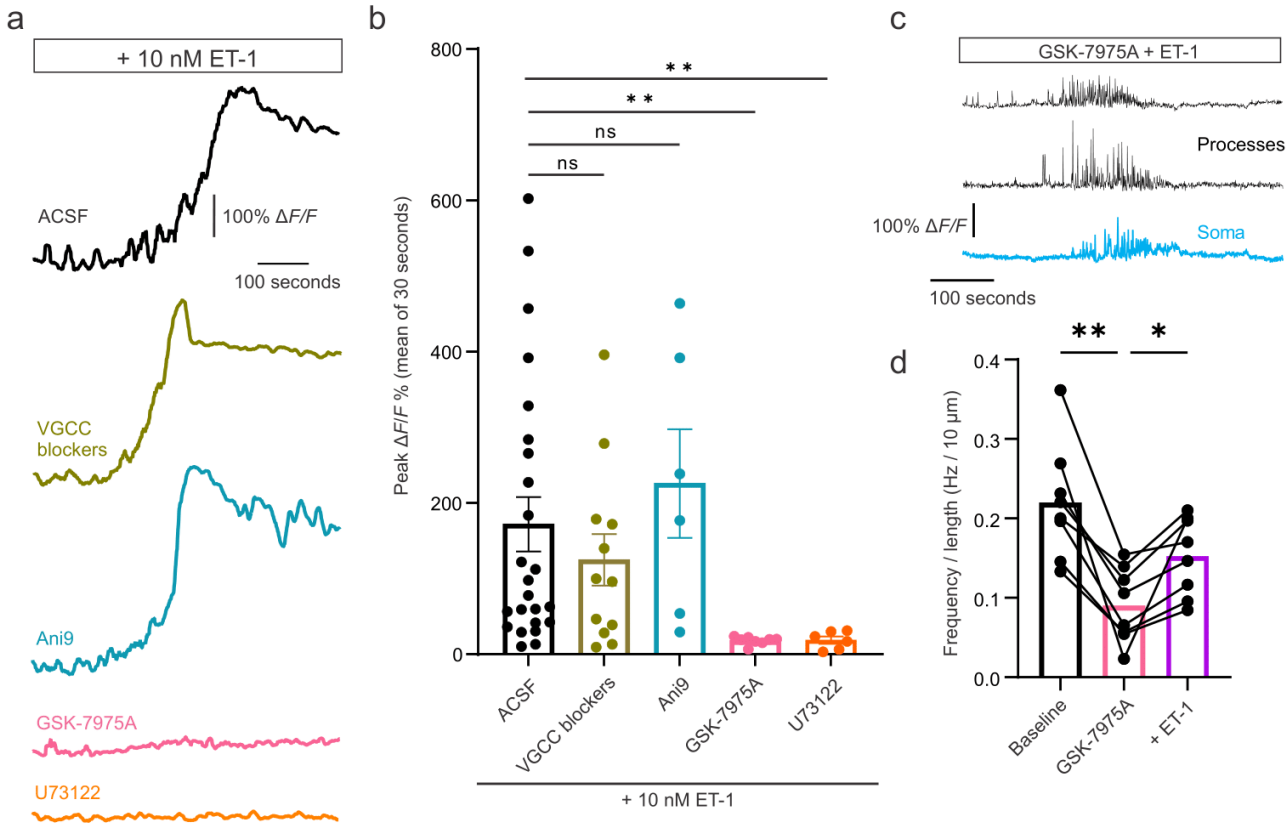

Figure 2.6: Ca^{2+} influx via Orai SOCE influx is required to sustain and amplify endothelin-1 $[Ca^{2+}]_i$ elevations.

(**a, b**) Example traces (**a**) and summarized data (**b**) in different experimental conditions showing ET-1 evokes large amplitude and sustained Ca^{2+} elevations when applied alone (N = 10, n = 24), and which is not dependent on VGCC channels (blocked with 20 µM nifedipine + 2 µM Z944; N = 3, n = 12) or the Ca^{2+} activated Cl^- channel, TMEM16A (blocked with 2 µM Ani9; N = 3, n = 6). Blocking Orai Ca^{2+} channels with 40 µM GSK-7975A reduces the ET-1 evoked rise in intracellular Ca^{2+} (N = 3, n = 8). Blocking phospholipase C with 25 µM U73122 prevents ET-1 induced Ca^{2+} elevation (N = 2, n = 6), confirming it is dependent on GqGPCR-PLC pathway. Traces in (**a**) are temporally filtered with a 5 second running average.

(c) Example trace showing that ET-1 induces a temporary increase in transient frequency when Orai channels are blocked with GSK-7975A (example is from the pericyte with the largest observed change in frequency).

(d) Summarized data showing Ca^{2+} transient frequency increased (over a ~3-minute window), when ET-1 is added in the presence of GSK-7975A. Statistics were calculated with a Kruskal-Wallis test followed by Dunn's multiple comparisons test.

All experiments performed in 500 nM TTX. Error bars represent SEM. For statistical comparisons *p < 0.05, ** p< 0.01, *** p< 0.001.

2.5 Discussion

Here we demonstrate that spontaneous Ca^{2+} transients in mid-capillary brain pericytes are mediated by an interplay between plasma membrane SOCE channels and ER store release through RyRs and IP_3Rs. Our results are suggestive of bidirectional coupling, whereby Orai transmembrane Ca^{2+} influx is required to sustain spontaneous Ca^{2+} release through RyRs and IP_3Rs, which in turn lead to store depletion and activation of Orai SOCE. These mechanisms are difficult to study in isolation: SOCE is dependent on store depletion, while store release is dependent on ER luminal Ca^{2+} load and intracellular Ca^{2+} levels, which are both heavily dictated by SOCE channels. Nevertheless, our pharmacological evidence, in conjunction with the short duration (~1 – 3 seconds) and spatially propagating nature of the observed Ca^{2+} transients, are consistent with a model in which spontaneous store release through RyRs and IP_3Rs is maintained by constitutive SOCE (Dupont et al., 2011; Yoast et al., 2020). Orai channels are ideally suited due to their high Ca^{2+} selectivity and tight coupling with luminal $[Ca^{2+}]$ in the ER via STIM proteins. Orai Ca^{2+} influx may additionally be critical for RyR activation by recruiting the intracellular Ca^{2+} required for calcium-induced-calcium-release (CICR) (e.g., Thakur et al., 2012), a mechanism which classically depends on L-type VGCCs in cardiac muscle (Näbuer et al., 1989) and in smooth muscle (Collier et al., 2000).

Our study adds to a growing body of evidence that the mural cells of the cerebral vasculature represent a continuum, with morphological, molecular, and functional heterogeneity along the arterio-venous axis. Our work is largely in agreement with a previous study which found that Ca^{2+} transients in mid-capillary pericyte processes were independent of L-type VGCCs at rest. However, in slight contrast to our results with 20 μM nifedipine, a minimal decrease in Ca^{2+} transient frequency within the soma was reported with 100 μM nimodipine (Glück et al., 2021).

Here we extend on these results and further show that these transients are not increased by depolarization and are likewise also independent of low-voltage-activated T-type calcium channels ($Ca_V3.2$), which pericytes robustly express (Vanlandewijck et al., 2018). These findings contrast with our initial hypothesis that these transients would require VGCC activity, which was based on our previous finding that $[Ca^{2+}]_i$ and Ca^{2+} transient frequency decreases in mid-capillary olfactory bulb pericytes following local increases in neuronal activity, although on a slower time scale than upstream ensheathing pericytes and SMCs (Rungta et al., 2018). While we show that VGCCs are not required for mid-capillary pericyte Ca^{2+} transients, they highly express both L- and T-type VGCCs (Vanlandewijck et al., 2018) and it is possible that these channels become inactivated at ~-20 mV when exposed to 60 mM $[K^+]_{ex}$. Therefore, we cannot conclude that these channels are entirely functionally absent, but rather that Ca^{2+} signaling in mid-capillary pericytes is dominated by other mechanisms, which we report here. Intriguingly, a concurrent study has reported that distal retinal pericytes do show nifedipine-sensitive Ca^{2+} elevations in response to 60 mM $[K^+]_{ex}$ (Klug et al., 2023). However, in contrast to SMCs and ensheathing pericytes, L-type VGCCs were not required for the Ca^{2+} elevation in retinal mid-capillary pericytes following increased intraluminal pressure (Klug et al., 2023), consistent with our results exhibiting that Ca^{2+} transients in different subtypes of pericytes exhibit a differential dependence on VGCCs.

Our results in ensheathing pericytes are largely consistent with recent reports that have uncovered prominent roles of depolarization, L-type VGCCs, and Gq-GPCR-IP_3R signaling in mediating their Ca^{2+} transients and $[Ca^{2+}]_i$ (Gonzales et al., 2020; Korte et al., 2022). Elucidating the molecular and functional differences between pericyte subtypes, including in the Ca^{2+} signaling mechanisms described here, remains an important task. While SOCE is universal across cell types, it is more prominent in non-excitable cells, perhaps due, in part, to the inhibition of VGCCs by the

essential SOCE proteins STIM1 and STIM2 (Park et al., 2010; Wang et al., 2010), raising the possibility that elevated STIM-plasma membrane interactions could have inhibitory effects on mid-capillary pericyte VGCCs. Another interesting possibility is differential inhibition by endogenous polyamines, such as spermine, which has been previously suggested to underlie the decreased functional expression of VGCCs in distal capillary pericytes of the retina (Matsushita et al., 2010). How these signaling differences translate into functional differences remains another key point of future study.

Although, our data suggests Ca^{2+} influx in mid-capillary pericytes occurs primarily via non-voltage gated channels, this does not exclude a role for pericyte hyperpolarization in functional hyperemia. Several reports on pericyte membrane potential have been made in various preparations from different regions of the CNS, reporting mean resting membrane potentials of between -35 mV and -50 mV (Li et al., 2011; Hall et al., 2014; Hariharan et al., 2022; Korte et al., 2022; Sancho et al., 2022; Klug et al., 2023). In pressurized intact retina preparations, pericytes across the vascular arbor are found more depolarized than smooth muscle cells at low pressure (-43 mV vs. -64 mV) (Klug et al., 2023), suggesting pericytes have lower K^+ permeability at rest. Opening of K_{ATP} channels increases K^+ permeability of mid-capillary pericytes, and therefore causes a robust hyperpolarization (Li and Puro, 2001; Hariharan et al., 2022; Sancho et al., 2022), which can then be propagated to upstream mural and endothelial cells (Li and Puro, 2001; Hariharan et al., 2022; Sancho et al., 2022). Retrograde hyperpolarization is a robust phenomenon in the microvasculature which rapidly closes VGCCs on upstream SMCs and ensheathing pericytes, thereby decreasing intracellular Ca^{2+} and dilating these contractile cells to increase local cerebral blood flow (Iadecola et al., 1997; Chen et al., 2014; Longden et al., 2017; Rungta et al., 2018; Gonzales et al., 2020). Interestingly, we found that blocking K_{ATP} channels with

glibenclamide led to a decrease in the frequency of Ca^{2+} transients, consistent with a decreased driving force for Orai mediated Ca^{2+} influx. This result suggests that K_{ATP} channels may be open at rest in pericytes from our brain slices, potentially due to increased adenosine tone which can open K_{ATP} channels via A_{2A} receptors (Li et al., 2001; Sancho et al., 2022). Although modest increases in $[K^+]_{ex}$ to 10 mM were previously suggested to decrease Ca^{2+} transient frequency via K_{ATP} dependent hyperpolarization (Glück et al., 2021), unlike $K_{ir}2.x$ channels, K_{ATP} channels are not known to be activated by $[K^+]_{ex}$. If K_{ATP} channels were indeed open at rest, as appears to be the case in our study, even modest increases in K^+ would depolarize pericytes via these open K^+ channels. Therefore, an alternative interpretation of these results could be that blocking K_{ATP} channels in their experiments blocked K^+ induced depolarization rather than hyperpolarization, and thereby reduced driving force for Ca^{2+} entry via non-voltage-gated channels, consistent with our findings. Recordings of mid-capillary pericyte membrane potential changes in response to modest changes in K^+ concentration are therefore needed to properly interpret these differences.

During neurovascular coupling, ensheathing pericytes of the capillary-arteriole transition zone (which robustly express α-SMA) dilate rapidly, whereas the pericytes of the mid-capillary bed (low or negative for α-SMA) increase their diameter more slowly (Rungta et al., 2018; Rungta et al., 2021). Whereas ensheathing type pericytes dilate actively and independently from the arteriole (Hall et al., 2014), it remains to be determined whether the mid-capillary diameter increase is a purely passive process or has an active component mediated by mid-capillary pericytes. Interestingly, under pathological conditions such as Alzheimer's disease and stroke, even mid-capillary pericytes are found to be constricted (Nortley et al., 2019; Korte et al., 2022), and prolonged optogenetic activation of ChR2 on cortical mid-capillary pericytes has been shown to locally constrict the capillaries that they contact on a slow timescale (Nelson et al., 2020;

Hartmann et al., 2021). Likewise, increases in intraluminal pressure lead to mid-capillary pericyte depolarization in the retina, and are followed by a delayed constriction (Klug et al., 2023). Although these studies suggest that mid-capillary pericyte membrane depolarization is correlated with increased rigidity and tone of the capillary bed, a causal relationship is lacking. Given that our data suggests that mid-capillary pericyte Ca^{2+} influx is dominated by voltage-independent channels, depolarization would be expected to reduce this Ca^{2+} influx and subsequent store filling, due to a decrease in driving force, as in other non-excitable cells. This is consistent with a recent report showing that hyperpolarization of mid-capillary pericytes by application of pinacidil increased pressure-induced Ca^{2+} influx (Klug et al., 2023).

Finally, we show here that SOCE is required to amplify the mid-capillary pericyte Ca^{2+} elevation mediated by the vasoconstrictor ET-1. The magnitude of the ET-1-induced Ca^{2+} responses when applied in normal ACSF were highly variable, which could reflect heterogeneous expression of the endothelin-A receptor and/or SOCE proteins in mid-capillary pericytes. ET-1 is a central molecule to pericyte pathology, which is released in ischemia (Lampl et al., 1997), and which is elevated downstream of Amyloid-β oligomers to constrict pericytes in Alzheimer's disease (Nortley et al., 2019). In ensheathing pericytes (1-3rd branch order), the ET-1 evoked $[Ca^{2+}]_i$ increase was also recently shown to require an amplification step, but via Ca^{2+} activated Cl^- channel mediated depolarization and L-type VGCC activation (Korte et al., 2022). Our results indicate a similar amplification process in mid-capillary pericytes, but with a clear molecular divergence in the mechanisms mediating ET-1 evoked Ca^{2+} influx. As Ca^{2+} is a ubiquitous signal transduction molecule throughout biology, mediating an array of cellular functions, including gene transcription and contraction, SOCE channels may therefore play an important role in numerous pericyte functions and contribute to their dysfunction in disease.

2.5.1 Study Limitations

Genetic tools will ultimately be required to uncover the precise molecular identities underlying mid-capillary pericyte Ca^{2+} signaling. Our pharmacological modulation of SOCE with non-selective (SKF-96365 and 2-APB) and relatively selective (GSK-7975A and IA65) compounds is consistent with the highly Ca^{2+} selective family of Orai channels (namely, Orai1 and Orai3) as the molecular identities underlying pericyte SOCE. However, TRPC channels have been shown to interact with and contribute to SOCE in certain conditions (Molnár et al., 2016; Ong et al., 2016), although this concept is heavily debated (DeHaven et al., 2009). While our results show that TRPC3/6 are not major contributors, we cannot completely rule out participation of the TRPC1/4/5 subfamily to pericyte SOCE.

The molecular identities of the IP_3R and RyR channels in mid-capillary pericytes will similarly require genetic tools to elucidate. While the IP_3Rs are broadly dispersed throughout cell types, the distribution of RyR isoforms is more segregated, with RyR2 constituting the dominant variant in smooth muscle cells (Westcott et al., 2012), making it the most likely variant to be functional in pericytes. Interestingly, RyRs have been classified as functionally absent in most (Burdyga and Borysova, 2018) (but not all (Zhang et al., 2008; Hashitani et al., 2015)) pericytes of different tissues, including ensheathing type pericytes in the retinal CNS vasculature (Gonzales et al., 2020). It remains to be determined whether the functional expression of RyRs in cortical CNS mid-capillary pericytes represents a difference across brain regions and/or between pericyte subtypes.

Our study was conducted solely in the brain slice preparation, which is a highly useful tool for probing cellular signaling mechanisms, as pharmacological compounds can be delivered at a controlled concentration and cellular architecture is kept largely intact. However, there are

important limitations when compared to *in vivo* settings: there is no blood pressure and myogenic tone, arterioles and capillaries are collapsed, oxygen concentration (95%) is supraphysiological, and the slice surface has undergone mechanical damage. Translation of this work to *in vivo* experimentation is an important future direction.

2.6 Appendix

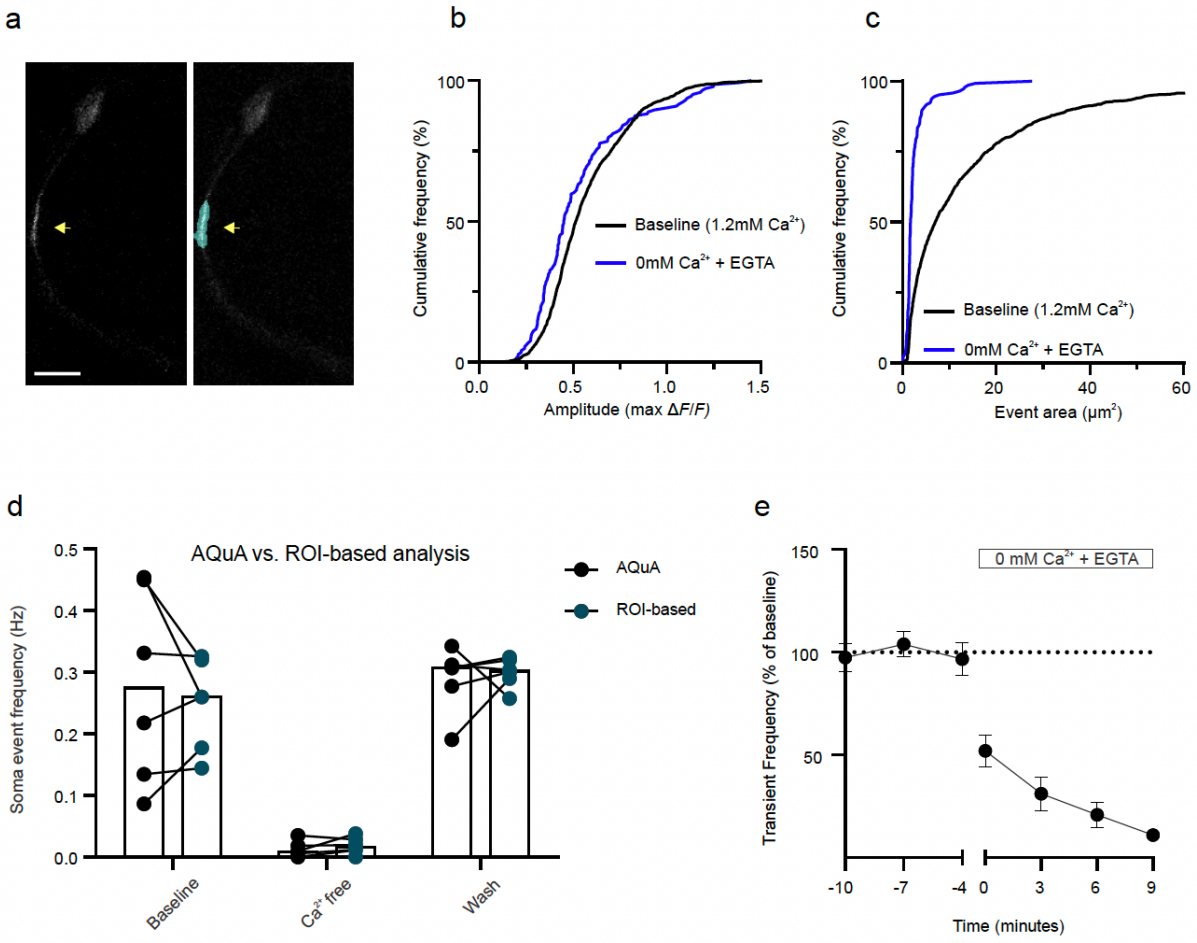
a
b
c
Cumulative frequency (%)
Baseline (1.2mM Ca2+)
0mM Ca2+ + EGTA
Amplitude (max ΔF/F)
Event area (μm2)
d
AQuA vs. ROI-based analysis
AQuA
ROI-based
Soma event frequency (Hz)
Baseline
Ca2+ free
Wash
e
0 mM Ca2+ + EGTA
Transient Frequency (% of baseline)
Time (minutes)

Figure 2.S1: Related to Figure. 2.1, Imaging of mid-capillary pericyte microdomain Ca^{2+} signals and their dependence on extracellular Ca^{2+}

(a) An example of an AQuA detected event in a mid-capillary pericyte process, taken from **Movie S1**. Scale bar = 10 μm.

(b, c) Cumulative histograms of event amplitude **(b)** and event area **(c)** at baseline (black) and following wash out of extracellular Ca^{2+} (blue), for 4-13 minutes. 1572 events (baseline), 153 events (0 mM Ca^{2+}), n = 6 cells.

(d) Comparison of event frequency measured in the soma using the AQuA event-based detection method to an ROI based analysis (> 3 standard deviations from baseline). Same cells analyzed in **Fig. 1e**.

(e) Time course of the effect of $[Ca^{2+}]_{ex}$ removal on the transient frequency in mid-capillary pericytes (processes + soma). n = 11 cells analyzed from **Fig. 1f-g** in which 50 second videos were taken every 3 minutes, x-axis represents measurements over a duration of 50 seconds starting at time, t. Time 0 represents time at which solution was calculated to reach the bath based on the flow rate, which was calculated to vary by +/- 30 seconds over the course of an experimental day.

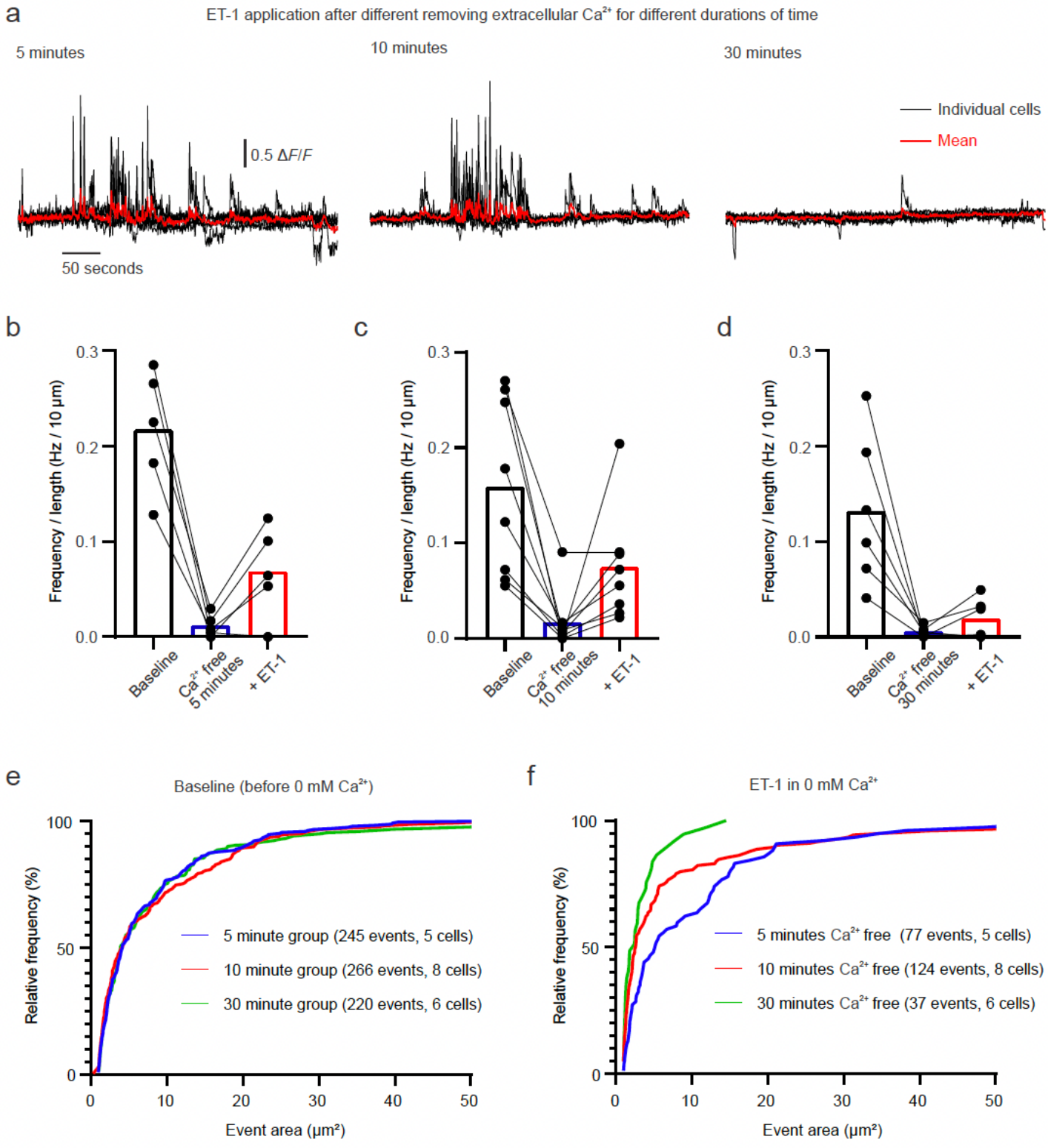
a
ET-1 application after different removing extracellular Ca2+ for different durations of time
5 minutes
10 minutes
30 minutes
Individual cells
Mean
0.5 ΔF/F
50 seconds
b
c
d
Frequency / length (Hz / 10 µm)
0.3
0.2
0.1
0.0
Baseline
Ca2+ free 5 minutes
Ca2+ free 10 minutes
Ca2+ free 30 minutes
+ ET-1
e
Baseline (before 0 mM Ca2+)
Relative frequency (%)
100
50
0
0
10
20
30
40
50
Event area (µm²)
5 minute group (245 events, 5 cells)
10 minute group (266 events, 8 cells)
30 minute group (220 events, 6 cells)
f
ET-1 in 0 mM Ca2+
5 minutes Ca2+ free (77 events, 5 cells)
10 minutes Ca2+ free (124 events, 8 cells)
30 minutes Ca2+ free (37 events, 6 cells)

Figure 2.S2: Related to Figure 2.1, Effect of ET-1 at different time points following extracellular Ca^{2+} removal.

(a) Example traces of GCaMP6f fluorescence in the soma of mid-capillary pericyte when ET-1 was applied either 5 minutes (left), 10 minutes (middle), or 30 minutes following perfusion of ACSF containing 0 mM $[Ca^{2+}]$, 2 mM EGTA. Black traces represent overlaid traces from 5 individual cells in each condition, red trace represents the mean of the 5 traces

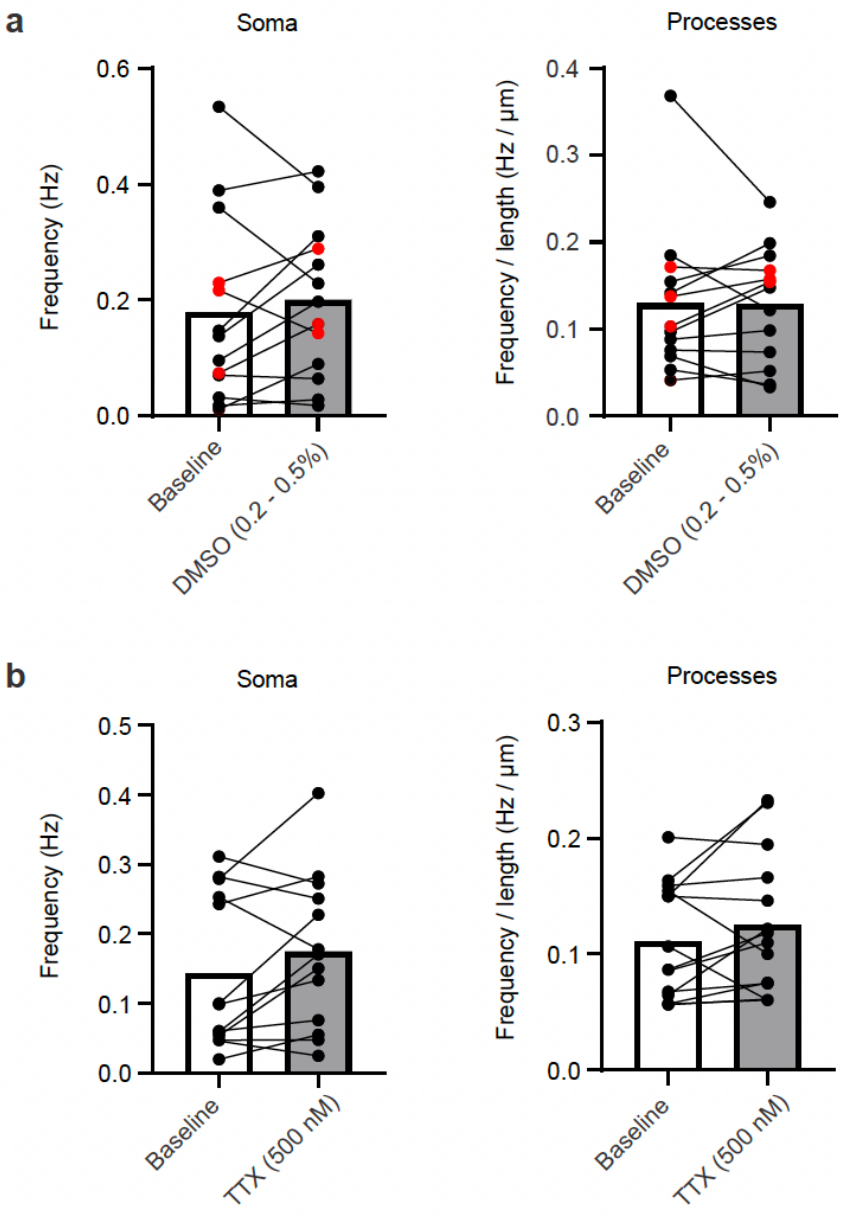

Figure 2.S3: Related to Figure 2.2, Analysis of Ca^{2+} transient frequency in response to DMSO and 500 nM TTX.

(a) Vehicle control showing that 0.2% (black circles) - 0.5% (red circles) dimethyl sulfoxide (DMSO) used in this study does not significantly alter mid-capillary pericyte Ca^{2+} transient frequency in either the soma (left; N = 3, n = 13) or processes (right; N = 3, n = 13).

(b) Perfusion of 500 nM tetrodotoxin (TTX) onto brain slices to block neuronal action potentials did not significantly alter mid-capillary pericyte Ca^{2+} transient frequency in either the soma (left; N = 6, n = 13) or processes (right; N = 6, n = 14).

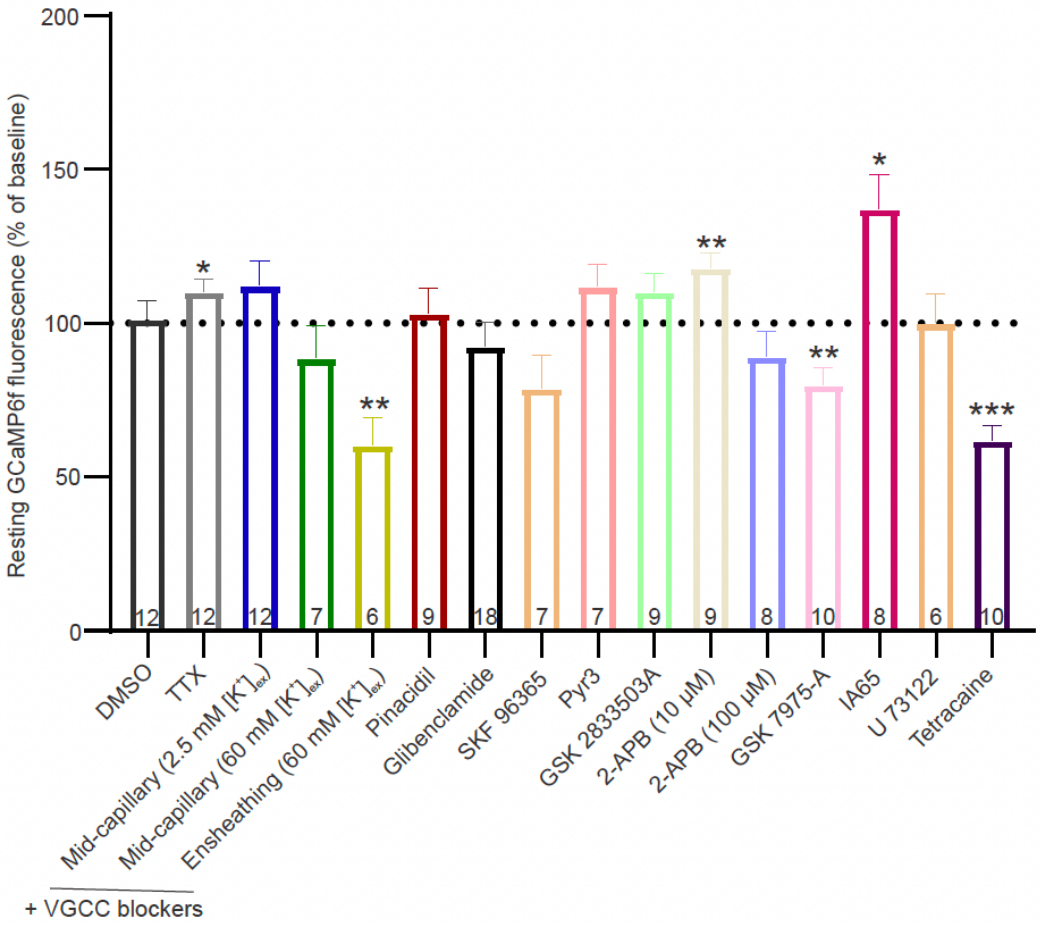

Figure 2.S4: Related to Figures 2.2-2.4, Effects of pharmacological compounds on resting Ca^{2+}. Analysis of changes in resting GCaMP6f fluorescence compared to baseline of various drugs used in the study. Measurements made in the soma (10-20 minutes after drug application). Numbers at bottom of bars represent n values (cells), Error bars represent SEM.

Table 2.1: Summarized data and statistics for all pharmacological treatments on pericyte processes

Drug	Mice (N)	Cells (n)	Frequency (Hz / 10 µm)		
			Baseline	Drug	p-value
DMSO (0.2 - 0.5%)	3	13	0.1296 (± 0.02354)	0.1286 (± 0.01840)	0.9418
TTX (500 nM)	6	14	0.1114 (± 0.01330)	0.1252 (± 0.01626)	0.2028
Nifedipine (20 µM) and Z944 (2 µM)	2	16	0.153 (± 0.02303)	0.1646 (± 0.03816)	0.5926
Nifedipine (20 µM) and Z944 (2 µM) in 60mM K+ (mid-capillary)	4	8	0.1775 (± 0.02488)	0.1581 (± 0.02499)	0.1385
Nifedipine (20 µM) and Z944 (2 µM) in 60mM K+ (ensheathing)	5	9	0.1389 (± 0.01308)	0.05067 (± 0.01009)	**0.0019**
Pinacidil (10 µM)	2	11	0.1102 (± 0.02124)	0.09687 (± 0.01881)	0.2079
Glibenclamide (20 µM)	3	20	0.08559 (± 0.01257)	0.05062 (± 0.009259)	**0.0003**
SKF 963365 (100 µM)	3	8	0.1614 (± 0.03523)	0.04428 (± 0.01427)	**0.0133**
Pyr3 (20 µM)	3	7	0.1323 (± 0.02181)	0.1258 (± 0.01808)	0.6291
GSK 2833503A (10 µM)	2	9	0.191 (± 0.01208)	0.1703 (± 0.01043)	0.1183
2-APB (10 µM)	3	9	0.1279 (± 0.02547)	0.1591 (± 0.01953)	**0.0384**
2-APB (100 µM)	3	9	0.09411 (± 0.01592)	0.01759 (± 0.009440)	**0.0001**
GSK 7975A (40 µM)	2	10	0.1488 (± 0.02143)	0.06693 (± 0.01065)	**0.0001**
IA65 (10 µM)	2	8	0.1431 (± 0.03229)	0.1215 (± 0.03076)	0.1168
U 73122 (25 µM)	2	6	0.1667 (± 0.02476)	0.1180 (± 0.02093)	**0.0093**
Tetracaine (200 µM)	3	10	0.1741 (± 0.02332)	0.03721 (± 0.008163)	**0.0004**
60 mM K^+ (mid-capillary): *Processes plus soma analyzed (Fig. 2d)*	2	8	0.1989 (± 0.03499)	0.1449 (± 0.02388)	0.1715
60 mM K^+ (ensheathing): *Processes plus soma analyzed (Fig. 2d)*	2	21	0.04909 (± 0.009518)	0.1155 (± 0.01700)	**0.0001**

Drug	Mice (N)	Cells (n)	Area (µm^2)		
			Baseline	Drug	p-value
DMSO (0.2 - 0.5%)	3	13	9.213 (± 0.7387)	8.316 (± 0.6403)	0.1647
TTX (500 nM)	6	14	10.75 (± 1.039)	9.573 (± 0.7749)	0.3454
Nifedipine (20 µM) and Z944 (2 µM)	2	16	4.914 (± 0.5680)	4.286 (± 0.6428)	0.3258
Nifedipine (20 µM) and Z944 (2 µM) in 60mM K+ (mid-capillary)	4	8	14.07 (± 3.532)	11.83 (± 2.747)	0.1705
Nifedipine (20 µM) and Z944 (2 µM) in 60mM K+ (ensheathing)	5	9	14.18 (± 2.748)	10.02 (± 2.570)	**0.0081**
Pinacidil (10 µM)	2	11	4.994 (± 0.6130)	4.496 (± 0.5458)	0.2143
Glibenclamide (20 µM)	3	20	4.611 (± 0.7727)	3.244 (± 0.3403)	**0.0375**
SKF 963365 (100 µM)	3	8	14.84 (± 2.363)	5.190 (± 1.118)	**0.011**
Pyr3 (20 µM)	3	7	9.572 (± 0.9827)	9.040 (± 0.8545)	0.2371
GSK 2833503A (10 µM)	2	9	9.813 (± 1.588)	8.732 (± 1.456)	0.0815
2-APB (10 µM)	3	9	10.79 (± 1.151)	10.44 (± 0.9508)	0.6511
2-APB (100 µM)	3	9	9.418 (± 2.199)	3.761 (± 0.5282)	**0.0377**
GSK 7975A (40 µM)	2	10	9.672 (± 1.097)	7.393 (± 1.542)	**0.0328**
IA65 (10 µM)	2	8	12.54 (± 1.524)	7.835 (± 1.419)	**0.0221**
U 73122 (25 µM)	2	6	11.48 (± 2.409)	8.881 (± 1.543)	0.1232
Tetracaine (200 µM)	3	10	10.61 (± 1.055)	6.027 (± 1.017)	**0.0001**
60 mM K^+ (mid-capillary): *Processes plus soma analyzed (Fig. 2d)*	2	8	13.40 (± 2.943)	9.987 (± 1.097)	0.272
60 mM K^+ (ensheathing): *Processes plus soma analyzed (Fig. 2d)*	2	21	8.053 (± 1.692)	7.795 (± 1.344)	0.8197

Drug	Mice (N)	Cells (n)	Amplitude (dF/F)		
			Baseline	Drug	p-value
DMSO (0.2 - 0.5%)	3	13	1.362 (± 0.06796)	1.299 (± 0.05628)	0.0559
TTX (500 nM)	6	14	1.275 (± 0.07252)	1.217 (± 0.07313)	0.2886
Nifedipine (20 µM) and Z944 (2 µM)	2	16	1.26 (± 0.06352)	1.401 (± 0.1762)	0.4526
Nifedipine (20 µM) and Z944 (2 µM) in 60mM K+ (mid-capillary)	4	8	1.314 (± 0.09787)	1.242 (± 0.06909)	0.2448
Nifedipine (20 µM) and Z944 (2 µM) in 60mM K+ (ensheathing)	5	9	1.136 (± 0.06587)	2.640 (± 1.459)	0.3378
Pinacidil (10 µM)	2	11	1.452 (± 0.1140)	1.407 (± 0.1032)	0.1515
Glibenclamide (20 µM)	3	20	1.424 (± 0.05288)	1.531 (± 0.07824)	0.1615
SKF 963365 (100 µM)	3	8	1.554 (± 0.1869)	1.419 (± 0.1046)	0.262
Pyr3 (20 µM)	3	7	1.468 (± 0.06324)	1.41 (± 0.02775)	0.2821
GSK 2833503A (10 µM)	2	9	1.147 (± 0.08309)	1.108 (± 0.07834)	0.1069
2-APB (10 µM)	3	9	1.319 (± 0.07848)	1.158 (± 0.05173)	**0.0018**
2-APB (100 µM)	3	9	1.309 (± 0.1818)	1.288 (± 0.1376)	0.9244
GSK 7975A (40 µM)	2	10	1.156 (± 0.07688)	1.191 (± 0.05333)	0.3832
IA65 (10 µM)	2	8	1.253 (± 0.07170)	1.204 (± 0.06083)	0.2333
U 73122 (25 µM)	2	6	1.314 (± 0.08654)	1.426 (± 0.1775)	0.511
Tetracaine (200 µM)	3	10	1.196 (± 0.0627)	1.574 (± 0.1147)	**0.014**
60 mM K^+ (mid-capillary): *Processes plus soma analyzed (Fig. 2d)*	2	8	1.154 (± 0.1302)	1.316 (± 0.03653)	0.2116
60 mM K^+ (ensheathing): *Processes plus soma analyzed (Fig. 2d)*	2	21	1.047 (± 0.07867)	1.382 (± 0.3249)	0.3132

Drug	Mice (N)	Cells (n)	Duration (s)		
			Baseline	Drug	p-value
DMSO (0.2 - 0.5%)	3	13	1.537 (± 0.06649)	1.489 (± 0.08689)	0.3724
TTX (500 nM)	6	14	1.725 (± 0.05649)	1.696 (± 0.05343)	0.5653
Nifedipine (20 µM) and Z944 (2 µM)	2	16	1.416 (± 0.06997)	1.483 (± 0.1627)	0.6518
Nifedipine (20 µM) and Z944 (2 µM) in 60mM K+ (mid-capillary)	4	8	1.439 (± 0.04916)	1.339 (± 0.05710)	0.084
Nifedipine (20 µM) and Z944 (2 µM) in 60mM K+ (ensheathing)	5	9	1.699 (± 0.08994)	1.827 (± 0.4185)	0.7927
Pinacidil (10 µM)	2	11	1.372 (± 0.07622)	1.234 (± 0.05032)	0.0796
Glibenclamide (20 µM)	3	20	1.147 (± 0.04976)	1.099 (± 0.03433)	0.3368
SKF 963365 (100 µM)	3	8	1.925 (± 0.2676)	1.404 (± 0.2933)	**0.0314**
Pyr3 (20 µM)	3	7	1.613 (± 0.07212)	1.582 (± 0.06962)	0.6469
GSK 2833503A (10 µM)	2	9	1.65 (± 0.06381)	1.547 (± 0.04660)	0.1074
2-APB (10 µM)	3	9	1.538 (± 0.05469)	1.548 (± 0.03383)	0.7812
2-APB (100 µM)	3	9	1.654 (± 0.1066)	1.289 (± 0.1475)	0.1332
GSK 7975A (40 µM)	2	10	1.787 (± 0.04214)	1.451 (± 0.07618)	**0.0004**
IA65 (10 µM)	2	8	1.573 (± 0.0429)	1.640 (± 0.05330)	0.2181
U 73122 (25 µM)	2	6	1.575 (± 0.09196)	1.675 (± 0.1132)	0.1901
Tetracaine (200 µM)	3	10	1.453 (± 0.06113)	1.172 (± 0.05666)	**0.0038**
60 mM K^+ (mid-capillary): *Processes plus soma analyzed (Fig. 2d)*	2	8	1.400 (± 0.06776)	1.572 (± 0.06427)	0.1018
60 mM K^+ (ensheathing): *Processes plus soma analyzed (Fig. 2d)*	2	21	1.351 (± 0.05639)	1.870 (± 0.1144)	**0.0002**

Table 2.2: Summarized data and statistics for all pharmacological treatments on pericyte soma

Drug	Mice (N)	Cells (n)	Frequency (Hz)		
			Baseline	Drug	p-value
DMSO (0.2 - 0.5%)	3	13	0.1781 (± 0.04495)	0.2004 (± 0.03673)	0.4084
TTX (500 nM)	6	13	0.1427 (± 0.03076)	0.1749 (± 0.03067)	0.1047
Nifedipine (20 µM) and Z944 (2 µM)	2	16	0.3039 (± 0.03947)	0.3517 (± 0.04741)	0.0593
Nifedipine (20 µM) and Z944 (2 µM) in 60mM K+ (mid-capillary)	4	8	0.4284 (± 0.05747)	0.4196 (± 0.08973)	0.8977
Nifedipine (20 µM) and Z944 (2 µM) in 60mM K+ (ensheathing)	5	6	0.3068 (± 0.04269)	0.09877 (± 0.03751)	**0.0158**
Pinacidil (10 µM)	2	11	0.171 (± 0.05009)	0.1723 (± 0.05375)	0.9387
Glibenclamide (20 µM)	3	15	0.1624 (± 0.03490)	0.1305 (± 0.03253)	0.3809
SKF 963365 (100 µM)	3	8	0.1951 (± 0.05209)	0.06131 (± 0.02653)	**0.0291**
Pyr3 (20 µM)	3	7	0.1922 (± 0.02889)	0.1965 (± 0.03481)	0.9179
GSK 2833503A (10 µM)	2	9	0.3298 (± 0.03407)	0.2852 (± 0.04663)	0.1583
2-APB (10 µM)	3	9	0.1643 (± 0.03763)	0.2565 (± 0.03821)	**0.0069**
2-APB (100 µM)	3	8	0.1406 (± 0.04465)	0.03530 (± 0.009946)	**0.0344**
GSK 7975A (40 µM)	2	10	0.2499 (± 0.02938)	0.1321 (± 0.02374)	**0.0011**
IA65 (10 µM)	2	7	0.2260 (± 0.06223)	0.2051 (± 0.03479)	0.685
U 73122 (25 µM)	2	6	0.2622 (± 0.04338)	0.2529 (± 0.03615)	0.7216
Tetracaine (200 µM)	3	10	0.2302 (± 0.05449)	0.04226 (± 0.01326)	**0.0054**

Resting Ca2+ (% of baseline GCaMP6f fluoresence)	
Mean	p-value
101.5 (± 5.946)	0.8057
110.4 (± 3.853)	**0.0194**
112.44 (± 8.032)	0.1511
88.79 (± 10.62)	0.3318
60.56 (± 8.675)	**0.0061**
103.3 (± 8.077)	0.6971
92.54 (± 7.665)	0.3441
78.89 (± 10.85)	0.0997
112 (± 7.099)	0.1414
110.3 (± 5.760)	0.1106
118.2 (± 4.591)	**0.0042**
89.25 (± 7.937)	0.2176
80.09 (± 5.310)	**0.0046**
137.3 (± 10.97)	**0.0114**
100.3 (± 9.128)	0.9786
62.08 (± 4.770)	**0.0001**

Drug	Mice (N)	Cells (n)	Area (µm^2)		
			Baseline	Drug	p-value
DMSO (0.2 - 0.5%)	3	13	13.12 (± 2.250)	11.76 (± 1.592)	0.5178
TTX (500 nM)	6	13	13.31 (± 2.112)	14.00 (± 2.713)	0.7843
Nifedipine (20 µM) and Z944 (2 µM)	2	16	5.81 (± 0.7784)	7.436 (± 1.444)	0.0683
Nifedipine (20 µM) and Z944 (2 µM) in 60mM K+ (mid-capillary)	4	8	27.83 (± 7.515)	21.25 (± 5.037)	0.1618
Nifedipine (20 µM) and Z944 (2 µM) in 60mM K+ (ensheathing)	5	6	28.51 (± 4.200)	9.546 (± 3.793)	**0.0032**
Pinacidil (10 µM)	2	11	5.84 (± 1.262)	5.161 (± 1.084)	0.3919
Glibenclamide (20 µM)	3	15	3.845 (± 0.6481)	2.740 (± 0.3747)	0.102
SKF 963365 (100 µM)	3	8	19.29 (± 5.849)	4.230 (± 1.210)	**0.0438**
Pyr3 (20 µM)	3	7	11.79 (± 2.204)	10.78 (± 2.546)	0.5794
GSK 2833503A (10 µM)	2	9	16.81 (± 3.626)	15.15 (± 3.835)	0.468
2-APB (10 µM)	3	9	17.89 (± 3.149)	14.8 (± 1.193)	0.2821
2-APB (100 µM)	3	8	12.7 (± 1.677)	2.841 (± 0.7122)	**0.0023**
GSK 7975A (40 µM)	2	10	14.65 (± 1.635)	12.23 (± 2.111)	0.1935
IA65 (10 µM)	2	7	17.42 (± 4.010)	11.54 (± 3.348)	0.0696
U 73122 (25 µM)	2	6	18.28 (± 3.822)	9.084 (± 1.315)	**0.0265**
Tetracaine (200 µM)	3	10	16.04 (± 3.815)	3.525 (± 0.9906)	**0.0078**

Drug	Mice (N)	Cells (n)	Amplitude (dF/F)		
			Baseline	Drug	p-value
DMSO (0.2 - 0.5%)	3	13	1.227 (± 0.07934)	1.196 (± 0.07938)	0.7455
TTX (500 nM)	6	13	1.235 (± 0.09715)	1.133 (± 0.08491)	0.3214
Nifedipine (20 µM) and Z944 (2 µM)	2	16	1.016 (± 0.05588)	1.203 (± 0.2211)	0.4032
Nifedipine (20 µM) and Z944 (2 µM) in 60mM K+ (mid-capillary)	4	8	1.211 (± 0.1599)	1.063 (± 0.1085)	0.2052
Nifedipine (20 µM) and Z944 (2 µM) in 60mM K+ (ensheathing)	5	6	1.059 (± 0.08104)	1.066 (± 0.1306)	0.9537
Pinacidil (10 µM)	2	11	1.297 (± 0.1370)	1.039 (± 0.07270)	0.1108
Glibenclamide (20 µM)	3	15	1.098 (± 0.08155)	1.009 (± 0.08089)	0.0891
SKF 963365 (100 µM)	3	8	1.687 (± 0.3553)	1.116 (± 0.1398)	0.1283
Pyr3 (20 µM)	3	7	1.332 (± 0.1250)	1.219 (± 0.08436)	0.1697
GSK 2833503A (10 µM)	2	9	1.042 (± 0.1199)	0.9326 (± 0.1037)	0.2648
2-APB (10 µM)	3	9	1.294 (± 0.1663)	1.017 (± 0.07862)	**0.0421**
2-APB (100 µM)	3	8	1.205 (± 0.1632)	0.7631 (± 0.04756)	**0.036**
GSK 7975A (40 µM)	2	10	1.079 (± 0.1129)	1.153 (± 0.1282)	0.2615
IA65 (10 µM)	2	7	1.051 (± 0.1301)	0.9300 (± 0.06816)	0.3818
U 73122 (25 µM)	2	6	1.079 (± 0.0843)	0.9697 (± 0.03612)	0.1801
Tetracaine (200 µM)	3	10	0.9379 (± 0.06413)	1.160 (± 0.1243)	0.2096

Drug	Mice (N)	Cells (n)	Duration (s)		
			Baseline	Drug	p-value
DMSO (0.2 - 0.5%)	3	13	1.680 (± 0.2046)	1.679 (± 0.1288)	0.9981
TTX (500 nM)	6	13	1.812 (± 0.1669)	1.838 (± 0.09642)	0.8933
Nifedipine (20 µM) and Z944 (2 µM)	2	16	1.562 (± 0.07127)	1.652 (± 0.1180)	0.4504
Nifedipine (20 µM) and Z944 (2 µM) in 60mM K+ (mid-capillary)	4	8	1.678 (± 0.06614)	1.505 (± 0.08723)	0.1315
Nifedipine (20 µM) and Z944 (2 µM) in 60mM K+ (ensheathing)	5	6	1.843 (± 0.07871)	1.299 (± 0.2078)	**0.0223**
Pinacidil (10 µM)	2	11	1.408 (± 0.1344)	1.339 (± 0.09024)	0.589
Glibenclamide (20 µM)	3	15	1.346 (± 0.09424)	1.155 (± 0.07388)	0.0538
SKF 963365 (100 µM)	3	8	1.925 (± 0.2676)	1.404 (± 0.2933)	**0.0314**
Pyr3 (20 µM)	3	7	1.778 (± 0.09761)	1.525 (± 0.1765)	0.0806
GSK 2833503A (10 µM)	2	9	1.887 (± 0.1064)	1.853 (± 0.09920)	0.8186
2-APB (10 µM)	3	9	1.820 (± 0.1660)	1.747 (± 0.07129)	0.6283
2-APB (100 µM)	3	8	2.073 (± 0.3742)	1.587 (± 0.3125)	0.1266
GSK 7975A (40 µM)	2	10	2.094 (± 0.1152)	2.033 (± 0.1019)	0.7195
IA65 (10 µM)	2	7	1.848 (± 0.2062)	2.015 (± 0.1478)	0.167
U 73122 (25 µM)	2	6	1.829 (± 0.1461)	1.776 (± 0.1065)	0.7665
Tetracaine (200 µM)	3	10	1.607 (± 0.1644)	1.256 (± 0.1302)	0.1018

Table 2.3: Information on pharmacological agents and vehicles used

Drug	Supplier	Identifier	Vehicle (concentration in solution)
TO-PRO-3	Thermo Scientific	T3605	DMSO (0.1%)
EGTA	Sigma-Aldrich	E3889	N/A
U46619	Tocris	Cat. No. 1932	H_2O (0.01%)
Endothelin-1	Millipore Sigma	05-23-3800	H_2O (0.1%)
Tetrodotoxin citrate	Abcam	ab120055	H_2O (0.05%)
Nifedipine	Sigma-Aldrich	N7634	DMSO (0.1%)
Z944	Dr. Terrance Snutch, University of British Columbia		DMSO (0.02%)
Pinacidil monohydrate	Sigma-Aldrich	P154	DMSO (0.1%)
Glibenclamide	Tocris	Cat. No. 0911	DMSO (0.1%)
SKF 96365 hydrochloride	Tocris	Cat. No. 1147	H_2O (0.5%)
Pyr3	Tocris	Cat. No. 3751	DMSO (0.1%)
GSK 2833503A	Tocris	Cat. No. 6497	DMSO (0.1%)
2-APB	Millipore Sigma	100065	DMSO (0.02% or 0.2%)
GSK-7975A	AdooQ BioScience	A16931-10	DMSO (0.1%)
Cyclopiazonic acid	Tocris	Cat. No. 1235	DMSO (0.1%)
IA65	Dr. Mohamed Trebak, University of Pittsburgh		DMSO (0.02%)
U 73122	Tocris	Cat. No. 1268	DMSO (0.5%)
Tetracaine hydrochloride	Sigma-Aldrich	T7508	H_2O (0.2%)
Caffeine	Sigma-Aldrich	C0750	N/A

Chapter 3: General Discussion

3.1 Summary of Research Findings

We show that spontaneous Ca^{2+} signaling in mid-capillary pericytes is dependent on both extracellular Ca^{2+} and Ca^{2+} uptake into the ER. Our results with pharmacological compounds presently known to be specific to their targets indicate that the spontaneous Ca^{2+} transients arise from IP_3R and RyR mediated store-release pathways, but that Ca^{2+} influx through the Orai family of SOCE channels is required to maintain this regenerative signaling. In agreement with previous results, we show that ensheathing pericytes possess minimal Ca^{2+} signaling at rest, perhaps due to the lack of intraluminal pressure in *ex vivo* preparations (Gonzales et al., 2020; Glück et al., 2021). We further affirmed results from the retina, whereby high K^+ solution robustly induced Ca^{2+} transients in proximal pericytes, which were then largely inhibited by VGCCs blockers (Gonzales et al., 2020), in cortical ensheathing pericytes. Furthermore, we exhibit that mid-capillary pericytes respond to the potent vasoconstrictor ET-1 with a substantial increase in $[Ca^{2+}]_i$, which we confirm is initiated by the G_q-GPCR pathway. In contrast to ensheathing pericytes, in which $[Ca^{2+}]_i$ increases in response to ET-1 are dependent on Ca^{2+}-activated- Cl^- channel activation, depolarization, and Ca^{2+} influx through VGCCs(Korte et al., 2022), we show that mid-capillary pericyte $[Ca^{2+}]_i$ increases in response to ET-1 dependent on store depletion and activation of Orai channels.

3.2 Expanded Discussion of Research Findings

Relation to recent and concurrent research into brain pericyte Ca^{2+} signaling

This work adds to the growing body of research concerning the molecular and functional heterogeneity of morphologically distinct pericytes. Firstly, our findings that mid-capillary pericyte Ca2+ transients are independent of VGCCs are in agreement with previous results from the retina, which show there is a substantial reduction in VGCC current in mural cells as one progresses deeper into the vascular bed (Matsushita et al., 2010; Klug et al., 2023), and previous results from the cortex, in which mid-capillary pericytes Ca^{2+} transients were largely insensitive to the L-type VGCC blocker nimodipine (Glück et al., 2021). Studies of pericyte contraction have concurrently found a greater role for store release and store filling pathways in pericytes of the mid-capillary bed. In the retina, distal pericytes contract in response to U46619 and dilate with removal of extracellular Ca^{2+}, albeit with smaller magnitude and after a longer timescale than proximal pericytes (Gonzales et al., 2020). Interestingly, although they did not directly test effects of 60 mM K^+ on distal pericyte Ca^{2+}, Gonzales et al., also found no influence of high K^+ on distal pericyte contraction, in stark contrast to proximal pericytes. A follow-up study from the Nelson lab has shown that all mural cells constrict in response to intraluminal pressure, and thereby appear to contribute to the myogenic response (Klug et al., 2023). However, constriction of distal pericytes was insensitive to nifedipine, blocked by SKF-96365 as well as YM-254890 (an inhibitor of G_q-coupled signaling), and enhanced by hyperpolarizing these cells with pinacidil (Klug et al., 2023). It remains to be directly tested whether these contractions are dependent on SOCE or

highlight a function of non-selective cation channels such as TRPC3, which we did not find a role for in spontaneous Ca^{2+} signaling, but which are also activated downstream of G_q-GPCR signaling.

Potential functions of L-type VGCCs in brain mid-capillary pericytes

Although we did not identify a contribution of L-type VGCCs to spontaneous Ca^{2+} signaling of mid-capillary pericytes, others have found functional expression of these channels in distal pericytes of the retina. The Puro and Nelson labs have both observed $[Ca^{2+}]_i$ increases in distal pericytes following stimulation with high K^+ (Matsushita et al., 2010; Klug et al., 2023), although the magnitude of these increases substantially differed between these studies, with the latter showing increases equivalent to those in proximal pericytes and SMCs. Indeed, functional L-type channels are commonly found in pericytes of other organs, such as the kidney and ureter (Zhang et al., 2002; Borysova et al., 2013). However, in agreement with a study of the retina (Gonzales et al., 2020) both find that changes in pericyte $[Ca^{2+}]$i and contractility following application of high K^+ are substantially lower than those evoked by G_q-GPCR stimulation (Zhang et al., 2002; Borysova et al., 2013). Nevertheless, genetic knockout of Cacna1c, the gene encoding the L-type channel Cav1.2, is protective against pathological increases in retinal mid-capillary pericyte Ca^{2+} found in ocular hypertension, a mouse model of glaucoma (Alarcon-Martinez et al., 2022). NVC responses (constrictions and dilations) correlated with changes in Ca^{2+} transient frequency (increases and decreases, respectively) as well as intercellular Ca^{2+} waves between IP-TNT connected pericytes (Alarcon-Martinez et al., 2020; Alarcon-Martinez et al., 2022). Importantly, these NVC responses were preserved in Cacna1c$^{-/-}$ mice, although a slight increase in basal capillary diameter was observed (Alarcon-Martinez et al., 2022). Although a causative

relationship between Ca^{2+} transients and contractility in these cells requires further examination, this suggests that L-type VGCCs influx is primarily pathological and that homeostatic Ca^{2+} signaling is mediated by a distinct mechanism. Given that the observed transients propagate within and between cells, and that IP-TNTs are organelle-rich (including with ER) (Alarcon-Martinez et al., 2020), a likely hypothesis is that homeostatic signals in retinal distal pericytes are likewise mediated by CICR activation of IP_3Rs and/or RyRs. Interestingly, we have shown that Orai channel mediated Ca^{2+} influx is required for sustaining and amplifying $[Ca^{2+}]_i$ elevations in response to prolonged stimulation with ET-1. Therefore, further experimentation is required to elucidate the relative contributions of L-type VGCCs and Orai channels to pathological increases in cortical mid-capillary pericyte Ca^{2+}, as seen in middle cerebral artery occlusion (Yemisci et al., 2009), and following application of amyloid β, which increases autocrine ET-1 signaling in pericytes across the vascular bed (Nortley et al., 2019).

Transcriptome insight into potential mid-capillary pericyte Ca^{2+} signaling mechanisms

It is also interesting to consider our results in the context of a recent transcriptomics analysis of brain mural cells, which found that mid-capillary pericytes are a distinct population with substantial molecular differences to upstream mural cells (Vanlandewijck et al., 2018). A specific examination of ion channels and transporters from this dataset identified transcripts involved in voltage-gated Ca^{2+} entry as relatively upregulated in SMC-like cells (Cacna2d1, Cacna1g), while transcripts involved in non-selective cation entry (Trpc3), store-operated Ca^{2+} entry (Stim2), and Ca^{2+} store release (Itpr2) were identified as upregulated in mid-capillary pericytes (Vanlandewijck et al., 2018). STIM2 is a particularly interesting protein, as it is known

to mediate SOCE after sub-maximal store depletion (Brandman et al., 2007), positioning it as a likely candidate underlying the putative constitutive SOCE of mid-capillary pericytes that may be absent from upstream mural cells. Although most investigations of SOCE have used maximal depletion protocols, this only captures an extreme end of the cellular Ca^{2+} signaling repertoire (Yoast et al., 2020; Yoast et al., 2021). Similarly, Orai2 and Orai3, which conduct less current than Orai1, are sufficient to maintain ER store levels and regenerative Ca^{2+} oscillations in HEK293 cells (Yoast et al., 2021). Studies are only beginning to recognize the contributions of these proteins to physiological Ca^{2+} signaling (Emrich et al., 2021; Yoast et al., 2021), and their roles in mid-capillary pericytes represent an exciting avenue for future exploration.

Potential functions of the SOCE and store release pathways in brain mid-capillary pericytes

Our work still begs the question as to why mid-capillary pericytes presumably commit precious cellular energy into maintaining spontaneous Ca^{2+} signaling. Given the tight coupling between store release and SOCE, it is likely that a major function of these Ca^{2+} transients is to maintain cytosolic Ca^{2+} levels. Indeed, we find extracellular Ca^{2+} is required to maintain mid-capillary pericyte $[Ca^{2+}]_i$ and that inhibiting store release profoundly limits Ca^{2+} influx. The most compelling uses for this $[Ca^{2+}]_i$ are contractility and gene expression. For example, if Ca^{2+} is required for a slow mid-capillary pericyte contractile function that contributes a basal tone to the vasculature, as is currently hypothesized (Berthiaume et al., 2018; Hartmann et al., 2021; Hartmann et al., 2022), then spontaneous Ca^{2+} release from the ER and subsequent SOCE activation could provide a method for mid-capillary pericytes to couple agonist signaling to adjustments in tone. The properties of Ca^{2+} transients may also be important for gene transcription

pathways, as many transcription factors, including the NFAT isoforms and NF-κB, are differentially regulated by the frequency, amplitude, and duration of Ca^{2+} signals (Dolmetsch et al., 1997; Yoast et al., 2021). In this manner, spontaneous Ca^{2+} transients through RyRs, maintained through a feedforward mechanism, may sustain some essential transcription pathways, which can then be modulated by agonist induced IP_3R signaling. However, within *in vivo* settings, there may be greater fluctuations of circulating agonists in vivo due to the less homogeneous environment and greater tissue health in comparison to *ex vivo* preparations. Therefore, it is possible that IP_3Rs take on a more active role *in vivo* to adjust mid-capillary pericyte basal tone and/or transcription pathways in response to changing extracellular signals.

Still, our results suggest that at least a portion of mid-capillary pericyte Ca^{2+} signals are intrinsically generated. Store depletion by RyRs and IP_3Rs appears to be the primary driver of Ca^{2+} influx at rest in these cells, and Ca^{2+} influx is the primary method of activating RyRs (through both cytosolic and luminal Ca^{2+}-binding domains). Although coupling between SOCE channels and RyRs is understudied compared to RyR-VGCC or IP_3R-SOCE coupling, there is evidence of this bidirectional signaling in other cell types, including T lymphocytes (Thakur et al., 2012) and skeletal myocytes (Pearce et al., 2022). An open question remains as to if mid-capillary pericytes possess functional BK_{Ca} channels like their SMC counterparts. If so, it is plausible that these channels are activated by spontaneous Ca^{2+} release from RyRs, which subsequently generate hyperpolarizing spontaneous transient outward currents (STOCs) to maintain the driving force for Ca^{2+} entry through SOCE channels, further amplifying this positive feedback mechanism.

In summary, our results align with recent work in the neurovascular field that have uncovered a decreasing reliance on VGCCs and an increase in Ca^{2+} store release activity in mural cells residing deeper in the vascular bed. Furthermore, we have introduced the novel concept of

mid-capillary pericyte Ca^{2+} being largely regulated by SOCE channels, which to the best of our knowledge, has not been previously investigated. We anticipate that this work will assist researchers in developing new hypotheses into the unique functional properties of mid-capillary pericytes, with a particular focus on contractile mechanisms.

3.3 Future Directions

While pharmacology and the brain slice preparation are excellent tools to decipher general cellular signaling mechanisms, their applications are limited. Although our results largely depend on selective compounds, evidence obtained with genetic knockdown models are increasingly used as a complimentary tool due to their perceived target specificity (however, there are known issues with the Cre-lox system, see Song and Palmiter, 2018). Furthermore, pharmacological modulators of Orai, RyR, and IP_3R are limited in their ability to differentiate between isoforms. Transgenic mice with loxP sites flanking coding regions of Orai1 and Orai3 have been developed (Emrich et al., 2023) and constitute ideal avenues to explore the specific contributions of these channels. Given the overlap in function, and the uncertainty on whether Orai channels form homomers or heteromers in vivo, a combined knockout approach will also be useful (Emrich et al., 2023). This knockout approach will alleviate the reliance on pharmacology while simultaneously allowing us to study the effects of modulating pericyte Ca^{2+} channels on *in vivo* functions – critically, blood vessel diameter and measurements of blood flow and velocity. Genetic manipulation of RyRs and IP_3Rs could also provide valuable clues, but a higher through-put method of genetic knockdown would be preferrable, as the variants functional in pericytes are largely unknown based off pharmacology. Likewise, given their ubiquitous expression and overlapping function, it is uncertain whether any effect of genetic targeting a single IP3R isoform could be expected.

Perhaps one of our most surprising results is the substantial contribution of RyRs to store release in mid-capillary pericytes. RyRs were not found to be functionally expressed in a study of proximal pericytes in the mouse retina; distal pericytes were not tested (Gonzales et al., 2020). Similarly, our study did not investigate the function of RyRs in cortical ensheathing pericytes. Therefore, it remains an open question whether this difference is due to heterogeneity within brain regions (cortex vs. retina) or if RyR function is lost in all CNS lower-order mural cells but regained in higher-order pericytes. Future work should expand the pharmacological profile of both pericyte subtypes within the cortical brain slice and retinal mount preparations.

While any conclusive proof would have to be translated in vivo (Grutzendler and Nedergaard, 2019), a tantalizing future direction is to observe changes in capillary diameter following direct modulation of pericyte Ca^{2+} levels. The brain slice would be a useful tool to investigate correlated changes in pericyte Ca^{2+} in response to substances such as ET-1 or caffeine with changes in capillary constrictions. There are commercially available lectins which can be used to label the basal membrane, allowing for *ex vivo* measurements of blood vessel diameter changes (Mishra et al., 2014). Likewise, mouse lines encoding fluorescent proteins indicators in pericytes (such as NG2:dsRed mice) are widely used and could be crossed with our PDGFRβ-Cre::GCaMP6f mice to simultaneously image changes to pericyte shape and $[Ca^{2+}]_i$. ET-1 has also been applied topically *in vivo* to mimic focal ischemia (Windle et al., 2006). Therefore, although ET-1 could act on other neurovascular cells, this approach could be used alongside transgenic mice lacking Orai1 and/or Orai3 in pericytes to investigate SOCE contributions to mid-capillary pericyte contractility *in vivo*.

References

Adachi T, Weisbrod RM, Pimentel DR, Ying J, Sharov VS, Schöneich C, Cohen RA (2004) S-Glutathiolation by peroxynitrite activates SERCA during arterial relaxation by nitric oxide. Nature medicine 10:1200-1207.

Adams PJ, Garcia E, David LS, Mulatz KJ, Spacey SD, Snutch TP (2009) CaV2. 1 P/Q-type calcium channel alternative splicing affects the functional impact of familial hemiplegic migraine mutations: implications for calcium channelopathies. Channels 3:110-121.

Ahmmed GU, Mehta D, Vogel S, Holinstat M, Paria BC, Tiruppathi C, Malik AB (2004) Protein kinase Cα phosphorylates the TRPC1 channel and regulates store-operated Ca2+ entry in endothelial cells. Journal of Biological Chemistry 279:20941-20949.

Alarcon-Martinez L, Shiga Y, Villafranca-Baughman D, Belforte N, Quintero H, Dotigny F, Cueva Vargas JL, Di Polo A (2022) Pericyte dysfunction and loss of interpericyte tunneling nanotubes promote neurovascular deficits in glaucoma. Proceedings of the National Academy of Sciences 119:e2110329119.

Alarcon-Martinez L, Villafranca-Baughman D, Quintero H, Kacerovsky JB, Dotigny F, Murai KK, Prat A, Drapeau P, Di Polo A (2020) Interpericyte tunnelling nanotubes regulate neurovascular coupling. Nature 585:91-95.

Alarcon-Martinez L, Yilmaz-Ozcan S, Yemisci M, Schallek J, Kılıç K, Can A, Di Polo A, Dalkara T (2018) Capillary pericytes express α-smooth muscle actin, which requires prevention of filamentous-actin depolymerization for detection. elife 7:e34861.

Armstrong C, Bezanilla F, Horowicz P (1972) Twitches in the presence of ethylene glycol bis (β-aminoethyl ether)-N, N′-tetraacetic acid. Biochimica et Biophysica Acta (BBA)-Bioenergetics 267:605-608.

Armulik A, Genové G, Betsholtz C (2011) Pericytes: developmental, physiological, and pathological perspectives, problems, and promises. Developmental cell 21:193-215.

Armulik A, Genové G, Mäe M, Nisancioglu MH, Wallgard E, Niaudet C, He L, Norlin J, Lindblom P, Strittmatter K (2010) Pericytes regulate the blood–brain barrier. Nature 468:557-561.

Attwell D, Mishra A, Hall CN, O'Farrell FM, Dalkara T (2016) What is a pericyte? Journal of Cerebral Blood Flow & Metabolism 36:451-455.

Azimi I, Stevenson RJ, Zhang X, Meizoso-Huesca A, Xin P, Johnson M, Flanagan JU, Chalmers SB, Yoast RE, Kapure JS (2020) A new selective pharmacological enhancer of the Orai1 Ca2+ channel reveals roles for Orai1 in smooth and skeletal muscle functions. ACS pharmacology & translational science 3:135-147.

Balabanov R, Beaumont T, Dore-Duffy P (1999) Role of central nervous system microvascular pericytes in activation of antigen-primed splenic T-lymphocytes. Journal of neuroscience research 55:578-587.

Balabanov R, Washington R, Wagnerova J, Dore-Duffy P (1996) CNS microvascular pericytes express macrophage-like function, cell surface integrin αM, and macrophage marker ED-2. Microvascular research 52:127-142.

Bánsághi S, Golenár T, Madesh M, Csordás G, RamachandraRao S, Sharma K, Yule DI, Joseph SK, Hajnóczky G (2014) Isoform-and species-specific control of inositol 1, 4, 5-trisphosphate (IP3) receptors by reactive oxygen species. Journal of Biological Chemistry 289:8170-8181.

Bayguinov O, Hagen B, Bonev AD, Nelson MT, Sanders KM (2000) Intracellular calcium events activated by ATP in murine colonic myocytes. American Journal of Physiology-Cell Physiology 279:C126-C135.

Bell RD, Winkler EA, Sagare AP, Singh I, LaRue B, Deane R, Zlokovic BV (2010) Pericytes control key neurovascular functions and neuronal phenotype in the adult brain and during brain aging. Neuron 68:409-427.
Berthiaume A-A, Hartmann DA, Majesky MW, Bhat NR, Shih AY (2018) Pericyte structural remodeling in cerebrovascular health and homeostasis. Frontiers in aging neuroscience 10:210.
Bird GS, DeHaven WI, Smyth JT, Putney Jr JW (2008) Methods for studying store-operated calcium entry. Methods 46:204-212.
Boado R, Pardridge W (1994) Differential expression of α-actin mRNA and immunoreactive protein in brain microvascular pericytes and smooth muscle cells. Journal of neuroscience research 39:430-435.
Bogeski I, Kummerow C, Al-Ansary D, Schwarz EC, Koehler R, Kozai D, Takahashi N, Peinelt C, Griesemer D, Bozem M (2010) Differential redox regulation of ORAI ion channels: a mechanism to tune cellular calcium signaling. Science signaling 3:ra24-ra24.
Borysova L, Wray S, Eisner DA, Burdyga T (2013) How calcium signals in myocytes and pericytes are integrated across in situ microvascular networks and control microvascular tone. Cell Calcium 54:163-174.
Brandman O, Liou J, Park WS, Meyer T (2007) STIM2 is a feedback regulator that stabilizes basal cytosolic and endoplasmic reticulum Ca2+ levels. Cell 131:1327-1339.
Burdyga T, Borysova L (2018) Ca 2+ signalling in pericytes. Pericyte Biology-Novel Concepts:95-109.
Cai C, Fordsmann JC, Jensen SH, Gesslein B, Lønstrup M, Hald BO, Zambach SA, Brodin B, Lauritzen MJ (2018) Stimulation-induced increases in cerebral blood flow and local capillary vasoconstriction depend on conducted vascular responses. Proceedings of the National Academy of Sciences 115:E5796-E5804.
Catterall WA (2011) Voltage-gated calcium channels. Cold Spring Harbor perspectives in biology 3:a003947.
Chen BR, Kozberg MG, Bouchard MB, Shaik MA, Hillman EM (2014) A critical role for the vascular endothelium in functional neurovascular coupling in the brain. Journal of the American Heart Association 3:e000787.
Cheong E, Shin H-S (2013) T-type Ca2+ channels in normal and abnormal brain functions. Physiological reviews 93:961-992.
Clapham DE (2003) TRP channels as cellular sensors. Nature 426:517-524.
Clapham DE (2007) Calcium signaling. Cell 131:1047-1058.
Clarke DD (1999) Circulation and energy metabolism of the brain. Basic neurochemistry: Molecular, cellular, and medical aspects.
Collier M, Ji G, Wang Y-X, Kotlikoff M (2000) Calcium-induced calcium release in smooth muscle: loose coupling between the action potential and calcium release. The Journal of general physiology 115:653-662.
Crisan M, Yap S, Casteilla L, Chen C-W, Corselli M, Park TS, Andriolo G, Sun B, Zheng B, Zhang L (2008) A perivascular origin for mesenchymal stem cells in multiple human organs. Cell stem cell 3:301-313.
Cuttler AS, LeClair RJ, Stohn JP, Wang Q, Sorenson CM, Liaw L, Lindner V (2011) Characterization of Pdgfrb-Cre transgenic mice reveals reduction of ROSA26 reporter activity in remodeling arteries. Genesis 49:673-680.
Dabertrand F, Nelson MT, Brayden JE (2012) Acidosis dilates brain parenchymal arterioles by conversion of calcium waves to sparks to activate BK channels. Circulation research 110:285-294.

Daneman R, Zhou L, Kebede AA, Barres BA (2010) Pericytes are required for blood–brain barrier integrity during embryogenesis. Nature 468:562-566.
DeHaven WI, Jones BF, Petranka JG, Smyth JT, Tomita T, Bird GS, Putney Jr JW (2009) TRPC channels function independently of STIM1 and Orai1. The Journal of physiology 587:2275-2298.
Dehouck M-P, Vigne P, Torpier G, Breittmayer JP, Cecchelli R, Frelin C (1997) Endothelin-1 as a mediator of endothelial cell–pericyte interactions in bovine brain capillaries. Journal of Cerebral Blood Flow & Metabolism 17:464-469.
Dias DO, Göritz C (2018) Fibrotic scarring following lesions to the central nervous system. Matrix Biology 68:561-570.
Dias DO, Kalkitsas J, Kelahmetoglu Y, Estrada CP, Tatarishvili J, Holl D, Jansson L, Banitalebi S, Amiry-Moghaddam M, Ernst A (2021) Pericyte-derived fibrotic scarring is conserved across diverse central nervous system lesions. Nature communications 12:5501.
Diercks B-P, Werner R, Weidemüller P, Czarniak F, Hernandez L, Lehmann C, Rosche A, Krüger A, Kaufmann U, Vaeth M (2018) ORAI1, STIM1/2, and RYR1 shape subsecond Ca2+ microdomains upon T cell activation. Science signaling 11:eaat0358.
Dodge AB, Hechtman HB, Shepro D (1991) Microvascular endothelial-derived autacoids regulate pericyte contractility. Cell motility and the cytoskeleton 18:180-188.
Dolmetsch RE, Lewis RS, Goodnow CC, Healy JI (1997) Differential activation of transcription factors induced by Ca2+ response amplitude and duration. Nature 386:855-858.
Dore-Duffy P, Katychev A, Wang X, Van Buren E (2006) CNS microvascular pericytes exhibit multipotential stem cell activity. Journal of Cerebral Blood Flow & Metabolism 26:613-624.
Dorn Gd, Becker MW (1993) Thromboxane A2 stimulated signal transduction in vascular smooth muscle. Journal of Pharmacology and Experimental Therapeutics 265:447-456.
Drew PJ, Shih AY, Kleinfeld D (2011) Fluctuating and sensory-induced vasodynamics in rodent cortex extend arteriole capacity. Proceedings of the National Academy of Sciences 108:8473-8478.
Duan L, Zhang X-D, Miao W-Y, Sun Y-J, Xiong G, Wu Q, Li G, Yang P, Yu H, Li H (2018) PDGFRβ cells rapidly relay inflammatory signal from the circulatory system to neurons via chemokine CCL2. Neuron 100:183-200. e188.
Dupont G, Combettes L, Bird GS, Putney JW (2011) Calcium oscillations. Cold Spring Harbor perspectives in biology 3:a004226.
Earley S, Waldron BJ, Brayden JE (2004) Critical role for transient receptor potential channel TRPM4 in myogenic constriction of cerebral arteries. Circulation research 95:922-929.
Emrich SM, Yoast RE, Xin P, Arige V, Wagner LE, Hempel N, Gill DL, Sneyd J, Yule DI, Trebak M (2021) Omnitemporal choreographies of all five STIM/Orai and IP3Rs underlie the complexity of mammalian Ca2+ signaling. Cell reports 34:108760.
Emrich SM, Yoast RE, Zhang X, Fike AJ, Wang Y-H, Bricker KN, Tao AY, Xin P, Walter V, Johnson MT (2023) Orai3 and Orai1 mediate CRAC channel function and metabolic reprogramming in B cells. Elife 12:e84708.
Fabiato A (1983) Calcium-induced release of calcium from the cardiac sarcoplasmic reticulum. American Journal of Physiology-Cell Physiology 245:C1-C14.
Fernández-Klett F, Offenhauser N, Dirnagl U, Priller J, Lindauer U (2010) Pericytes in capillaries are contractile in vivo, but arterioles mediate functional hyperemia in the mouse brain. Proceedings of the National Academy of Sciences 107:22290-22295.

Feske S, Gwack Y, Prakriya M, Srikanth S, Puppel S-H, Tanasa B, Hogan PG, Lewis RS, Daly M, Rao A (2006) A mutation in Orai1 causes immune deficiency by abrogating CRAC channel function. Nature 441:179-185.

Fill M, Copello JA (2002) Ryanodine receptor calcium release channels. Physiological reviews 82:893-922.

Fomina AF (2021) Neglected wardens: T lymphocyte ryanodine receptors. The Journal of Physiology 599:4415-4426.

Gerhardt H, Betsholtz C (2003) Endothelial-pericyte interactions in angiogenesis. Cell and tissue research 314:15-23.

Glück C, Ferrari KD, Binini N, Keller A, Saab AS, Stobart JL, Weber B (2021) Distinct signatures of calcium activity in brain mural cells. Elife 10:e70591.

Gonzales AL, Garcia ZI, Amberg GC, Earley S (2010) Pharmacological inhibition of TRPM4 hyperpolarizes vascular smooth muscle. American Journal of Physiology-Cell Physiology 299:C1195-C1202.

Gonzales AL, Klug NR, Moshkforoush A, Lee JC, Lee FK, Shui B, Tsoukias NM, Kotlikoff MI, Hill-Eubanks D, Nelson MT (2020) Contractile pericytes determine the direction of blood flow at capillary junctions. Proceedings of the National Academy of Sciences 117:27022-27033.

Gonzales AL, Yang Y, Sullivan MN, Sanders L, Dabertrand F, Hill-Eubanks DC, Nelson MT, Earley S (2014) A PLCγ1-dependent, force-sensitive signaling network in the myogenic constriction of cerebral arteries. Science Signaling 7:ra49-ra49.

Göritz C, Dias DO, Tomilin N, Barbacid M, Shupliakov O, Frisén J (2011) A pericyte origin of spinal cord scar tissue. Science 333:238-242.

Grant RI, Hartmann DA, Underly RG, Berthiaume A-A, Bhat NR, Shih AY (2019) Organizational hierarchy and structural diversity of microvascular pericytes in adult mouse cortex. Journal of Cerebral Blood Flow & Metabolism 39:411-425.

Grubb S, Cai C, Hald BO, Khennouf L, Murmu RP, Jensen AG, Fordsmann J, Zambach S, Lauritzen M (2020) Precapillary sphincters maintain perfusion in the cerebral cortex. Nature communications 11:395.

Grubb S, Lauritzen M, Aalkjær C (2021) Brain capillary pericytes and neurovascular coupling. Comparative Biochemistry and Physiology Part A: Molecular & Integrative Physiology 254:110893.

Grutzendler J, Nedergaard M (2019) Cellular control of brain capillary blood flow: in vivo imaging veritas. Trends in neurosciences 42:528-536.

Guijarro-Muñoz I, Compte M, Álvarez-Cienfuegos A, Álvarez-Vallina L, Sanz L (2014) Lipopolysaccharide activates Toll-like receptor 4 (TLR4)-mediated NF-κB signaling pathway and proinflammatory response in human pericytes. Journal of Biological Chemistry 289:2457-2468.

Guimaraes-Camboa N, Cattaneo P, Sun Y, Moore-Morris T, Gu Y, Dalton ND, Rockenstein E, Masliah E, Peterson KL, Stallcup WB (2017) Pericytes of multiple organs do not behave as mesenchymal stem cells in vivo. Cell stem cell 20:345-359. e345.

Gwack Y, Feske S, Srikanth S, Hogan PG, Rao A (2007) Signalling to transcription: store-operated Ca2+ entry and NFAT activation in lymphocytes. Cell calcium 42:145-156.

Hall CN, Reynell C, Gesslein B, Hamilton NB, Mishra A, Sutherland BA, O'Farrell FM, Buchan AM, Lauritzen M, Attwell D (2014) Capillary pericytes regulate cerebral blood flow in health and disease. Nature 508:55-60.

Halliday MR, Rege SV, Ma Q, Zhao Z, Miller CA, Winkler EA, Zlokovic BV (2016) Accelerated pericyte degeneration and blood–brain barrier breakdown in apolipoprotein E4 carriers with Alzheimer's disease. Journal of Cerebral Blood Flow & Metabolism 36:216-227.
Hariharan A, Weir N, Robertson C, He L, Betsholtz C, Longden TA (2020) The ion channel and GPCR toolkit of brain capillary pericytes. Frontiers in Cellular Neuroscience 14:601324.
Harraz OF, Abd El-Rahman RR, Bigdely-Shamloo K, Wilson SM, Brett SE, Romero M, Gonzales AL, Earley S, Vigmond EJ, Nygren A (2014) CaV3. 2 channels and the induction of negative feedback in cerebral arteries. Circulation research 115:650-661.
Hartmann DA, Berthiaume A-A, Grant RI, Harrill SA, Koski T, Tieu T, McDowell KP, Faino AV, Kelly AL, Shih AY (2021) Brain capillary pericytes exert a substantial but slow influence on blood flow. Nature neuroscience 24:633-645.
Hartmann DA, Coelho-Santos V, Shih AY (2022) Pericyte control of blood flow across microvascular zones in the central nervous system. Annual review of physiology 84:331-354.
Hashimoto T, Kihara M, Sato K, Imai N, Tanaka Y, Sakai M, Tamura K, Hirawa N, Toya Y, Kitamura H (2005) Heparin recovers AT1 receptor and its intracellular signal transduction in cultured vascular smooth muscle cells. FEBS letters 579:281-284.
Hashitani H, Mitsui R, Masaki S, Van Helden DF (2015) Pacemaker role of pericytes in generating synchronized spontaneous Ca2+ transients in the myenteric microvasculature of the guinea-pig gastric antrum. Cell Calcium 58:442-456.
Heppner TJ, Bonev AD, Santana LF, Nelson MT (2002) Alkaline pH shifts Ca2+ sparks to Ca2+ waves in smooth muscle cells of pressurized cerebral arteries. American Journal of Physiology-Heart and Circulatory Physiology 283:H2169-H2176.
Hill RA, Tong L, Yuan P, Murikinati S, Gupta S, Grutzendler J (2015) Regional blood flow in the normal and ischemic brain is controlled by arteriolar smooth muscle cell contractility and not by capillary pericytes. Neuron 87:95-110.
Hill-Eubanks DC, Werner ME, Heppner TJ, Nelson MT (2011) Calcium signaling in smooth muscle. Cold Spring Harbor perspectives in biology 3:a004549.
Hofmann T, Obukhov AG, Schaefer M, Harteneck C, Gudermann T, Schultz G (1999) Direct activation of human TRPC6 and TRPC3 channels by diacylglycerol. Nature 397:259-263.
Hørlyck S, Cai C, Helms HCC, Lauritzen M, Brodin B (2021) ATP induces contraction of cultured brain capillary pericytes via activation of P2Y-type purinergic receptors. American Journal of Physiology-Heart and Circulatory Physiology 320:H699-H712.
Hoth M, Niemeyer BA (2013) The neglected CRAC proteins: Orai2, Orai3, and STIM2. Current topics in membranes 71:237-271.
Hoth M, Penner R (1992) Depletion of intracellular calcium stores activates a calcium current in mast cells. Nature 355:353-356.
Hoth M, Penner R (1993) Calcium release-activated calcium current in rat mast cells. The Journal of physiology 465:359-386.
Iadecola C (2017) The neurovascular unit coming of age: a journey through neurovascular coupling in health and disease. Neuron 96:17-42.
Iadecola C, Yang G, Ebner TJ, Chen G (1997) Local and propagated vascular responses evoked by focal synaptic activity in cerebellar cortex. Journal of neurophysiology 78:651-659.
Inoue R, Jensen LJ, Jian Z, Shi J, Hai L, Lurie AI, Henriksen FH, Salomonsson M, Morita H, Kawarabayashi Y (2009) Synergistic activation of vascular TRPC6 channel by receptor and mechanical stimulation via phospholipase C/diacylglycerol and phospholipase A2/ω-hydroxylase/20-HETE pathways. Circulation research 104:1399-1409.

Jaggar JH, Nelson MT (2000) Differential regulation of Ca2+ sparks and Ca2+ waves by UTP in rat cerebral artery smooth muscle cells. American Journal of Physiology-Cell Physiology 279:C1528-C1539.
Jaggar JH, Porter VA, Lederer WJ, Nelson MT (2000) Calcium sparks in smooth muscle. American Journal of Physiology-Cell Physiology 278:C235-C256.
Jairaman A, McQuade A, Granzotto A, Kang YJ, Chadarevian JP, Gandhi S, Parker I, Smith I, Cho H, Sensi SL (2022) TREM2 regulates purinergic receptor-mediated calcium signaling and motility in human iPSC-derived microglia. Elife 11:e73021.
Kamouchi M, Kitazono T, Ago T, Wakisaka M, Ooboshi H, Ibayashi S, Iida M (2004) Calcium influx pathways in rat CNS pericytes. Molecular brain research 126:114-120.
Keef KD, Hume JR, Zhong J (2001) Regulation of cardiac and smooth muscle Ca2+ channels (CaV1. 2a, b) by protein kinases. American Journal of Physiology-Cell Physiology 281:C1743-C1756.
Kim D, Song I, Keum S, Lee T, Jeong M-J, Kim S-S, McEnery MW, Shin H-S (2001) Lack of the burst firing of thalamocortical relay neurons and resistance to absence seizures in mice lacking α1G T-type Ca2+ channels. Neuron 31:35-45.
Klug NR, Sancho M, Gonzales AL, Heppner TJ, O'Brien RIC, Hill-Eubanks D, Nelson MT (2023) Intraluminal pressure elevates intracellular calcium and contracts CNS pericytes: Role of voltage-dependent calcium channels. Proceedings of the National Academy of Sciences 120:e2216421120.
Knot HJ, Nelson MT (1998) Regulation of arterial diameter and wall [Ca2+] in cerebral arteries of rat by membrane potential and intravascular pressure. The Journal of physiology 508:199-209.
Korte N, Ilkan Z, Pearson CL, Pfeiffer T, Singhal P, Rock JR, Sethi H, Gill D, Attwell D, Tammaro P (2022) The Ca 2+-gated channel TMEM16A amplifies capillary pericyte contraction and reduces cerebral blood flow after ischemia. The Journal of Clinical Investigation 132.
Korte N, James G, You H, Hirunpattarasilp C, Christie I, Sethi H, Attwell D (2023) Noradrenaline released from locus coeruleus axons contracts cerebral capillary pericytes via α 2 adrenergic receptors. Journal of Cerebral Blood Flow & Metabolism:0271678X231152549.
Kovac A, Erickson MA, Banks WA (2011) Brain microvascular pericytes are immunoactive in culture: cytokine, chemokine, nitric oxide, and LRP-1 expression in response to lipopolysaccharide. Journal of neuroinflammation 8:1-9.
Krueger M, Bechmann I (2010) CNS pericytes: concepts, misconceptions, and a way out. Glia 58:1-10.
Lampl Y, Fleminger G, Gilad R, Galron R, Sarova-Pinhas I, Sokolovsky M (1997) Endothelin in cerebrospinal fluid and plasma of patients in the early stage of ischemic stroke. Stroke 28:1951-1955.
Langwieser N, Christel CJ, Kleppisch T, Hofmann F, Wotjak CT, Moosmang S (2010) Homeostatic switch in hebbian plasticity and fear learning after sustained loss of Cav1. 2 calcium channels. Journal of Neuroscience 30:8367-8375.
Latini S, Bordoni F, Pedata F, Corradetti R (1999) Extracellular adenosine concentrations during in vitro ischaemia in rat hippocampal slices. British journal of pharmacology 127:729-739.
Leblanc N, Ledoux J, Saleh S, Sanguinetti A, Angermann J, O'Driscoll K, Britton F, Perrino BA, Greenwood IA (2005) Regulation of calcium-activated chloride channels in smooth muscle cells: a complex picture is emerging. Canadian journal of physiology and pharmacology 83:541-556.
Li Q, Puro DG (2001) Adenosine activates ATP-sensitive K+ currents in pericytes of rat retinal microvessels: role of A1 and A2a receptors. Brain research 907:93-99.
Li Y, Camacho P (2004) Ca2+-dependent redox modulation of SERCA 2b by ERp57. The Journal of cell biology 164:35-46.

Lia A, Sansevero G, Chiavegato A, Sbrissa M, Pendin D, Mariotti L, Pozzan T, Berardi N, Carmignoto G, Fasolato C (2023) Rescue of astrocyte activity by the calcium sensor STIM1 restores long-term synaptic plasticity in female mice modelling Alzheimer's disease. Nature Communications 14:1590.
Lin Q, Zhao G, Fang X, Peng X, Tang H, Wang H, Jing R, Liu J, Lederer WJ, Chen J (2016) IP3 receptors regulate vascular smooth muscle contractility and hypertension. JCI insight 1.
Liou J, Kim ML, Do Heo W, Jones JT, Myers JW, Ferrell JE, Meyer T (2005) STIM is a Ca2+ sensor essential for Ca2+-store-depletion-triggered Ca2+ influx. Current biology 15:1235-1241.
Liu D, Yang D, He H, Chen X, Cao T, Feng X, Ma L, Luo Z, Wang L, Yan Z (2009) Increased transient receptor potential canonical type 3 channels in vasculature from hypertensive rats. Hypertension 53:70-76.
Longden TA, Dabertrand F, Koide M, Gonzales AL, Tykocki NR, Brayden JE, Hill-Eubanks D, Nelson MT (2017) Capillary K+-sensing initiates retrograde hyperpolarization to increase local cerebral blood flow. Nature neuroscience 20:717-726.
Mai-Morente SP, Marset VM, Blanco F, Isasi EE, Abudara V (2021) A nuclear fluorescent dye identifies pericytes at the neurovascular unit. Journal of Neurochemistry 157:1377-1391.
Maneshi MM, Toth AB, Ishii T, Hori K, Tsujikawa S, Shum AK, Shrestha N, Yamashita M, Miller RJ, Radulovic J (2020) Orai1 channels are essential for amplification of glutamate-evoked Ca2+ signals in dendritic spines to regulate working and associative memory. Cell reports 33:108464.
Mangoni ME, Couette B, Marger L, Bourinet E, Striessnig J, Nargeot J (2006) Voltage-dependent calcium channels and cardiac pacemaker activity: from ionic currents to genes. Progress in biophysics and molecular biology 90:38-63.
Matsugi T, Chen Q, Anderson DR (1997) Contractile responses of cultured bovine retinal pericytes to angiotensin II. Archives of ophthalmology 115:1281-1285.
Matsushita K, Fukumoto M, Kobayashi T, Kobayashi M, Ishizaki E, Minami M, Katsumura K, Liao SD, Wu DM, Zhang T (2010) Diabetes-induced inhibition of voltage-dependent calcium channels in the retinal microvasculature: role of spermine. Investigative ophthalmology & visual science 51:5979-5990.
Meissner G (1984) Adenine nucleotide stimulation of Ca2+-induced Ca2+ release in sarcoplasmic reticulum. Journal of Biological Chemistry 259:2365-2374.
Michaelis M, Nieswandt B, Stegner D, Eilers J, Kraft R (2015) STIM1, STIM2, and Orai1 regulate store-operated calcium entry and purinergic activation of microglia. Glia 63:652-663.
Miners JS, Schulz I, Love S (2018) Differing associations between Aβ accumulation, hypoperfusion, blood–brain barrier dysfunction and loss of PDGFRB pericyte marker in the precuneus and parietal white matter in Alzheimer's disease. Journal of Cerebral Blood Flow & Metabolism 38:103-115.
Mishra A, O'farrell FM, Reynell C, Hamilton NB, Hall CN, Attwell D (2014) Imaging pericytes and capillary diameter in brain slices and isolated retinae. Nature protocols 9:323-336.
Mishra A, Reynolds JP, Chen Y, Gourine AV, Rusakov DA, Attwell D (2016) Astrocytes mediate neurovascular signaling to capillary pericytes but not to arterioles. Nature Neuroscience 19:1619-1627.
Missiaen L, Taylor CW, Berridge MJ (1991) Spontaneous calcium release from inositol trisphosphate-sensitive calcium stores. Nature 352:241-244.
Molnár T, Yarishkin O, Iuso A, Barabas P, Jones B, Marc RE, Phuong TT, Križaj D (2016) Store-operated calcium entry in Müller glia is controlled by synergistic activation of TRPC and Orai channels. Journal of Neuroscience 36:3184-3198.

Montagne A, Nikolakopoulou AM, Zhao Z, Sagare AP, Si G, Lazic D, Barnes SR, Daianu M, Ramanathan A, Go A, Lawson EJ, Wang Y, Mack WJ, Thompson PM, Schneider JA, Varkey J, Langen R, Mullins E, Jacobs RE, Zlokovic BV (2018) Pericyte degeneration causes white matter dysfunction in the mouse central nervous system. Nature Medicine 24:326-337.

Montagne A et al. (2020) APOE4 leads to blood–brain barrier dysfunction predicting cognitive decline. Nature 581:71-76.

Moosmang S, Haider N, Klugbauer N, Adelsberger H, Langwieser N, Müller J, Stiess M, Marais E, Schulla V, Lacinova L (2005) Role of hippocampal Cav1. 2 Ca2+ channels in NMDA receptor-independent synaptic plasticity and spatial memory. Journal of Neuroscience 25:9883-9892.

Moosmang S, Schulla V, Welling A, Feil R, Feil S, Wegener JW, Hofmann F, Klugbauer N (2003) Dominant role of smooth muscle L-type calcium channel Cav1. 2 for blood pressure regulation. The EMBO journal 22:6027-6034.

Näbauer M, Callewaert G, Cleemann L, Morad M (1989) Regulation of calcium release is gated by calcium current, not gating charge, in cardiac myocytes. Science 244:800-803.

Nakagomi T, Kubo S, Nakano-Doi A, Sakuma R, Lu S, Narita A, Kawahara M, Taguchi A, Matsuyama T (2015) Brain vascular pericytes following ischemia have multipotential stem cell activity to differentiate into neural and vascular lineage cells. Stem cells 33:1962-1974.

Nehls V, Drenckhahn D (1991) Heterogeneity of microvascular pericytes for smooth muscle type alpha-actin. The Journal of cell biology 113:147-154.

Nelson AR, Sagare MA, Wang Y, Kisler K, Zhao Z, Zlokovic BV (2020) Channelrhodopsin excitation contracts brain pericytes and reduces blood flow in the aging mouse brain in vivo. Frontiers in aging neuroscience 12:108.

Nelson M, Cheng H, Rubart M, Santana L, Bonev A, Knot H, Lederer W (1995) Relaxation of arterial smooth muscle by calcium sparks. Science 270:633-637.

Nikolakopoulou AM, Montagne A, Kisler K, Dai Z, Wang Y, Huuskonen MT, Sagare AP, Lazic D, Sweeney MD, Kong P, Wang M, Owens NC, Lawson EJ, Xie X, Zhao Z, Zlokovic BV (2019) Pericyte loss leads to circulatory failure and pleiotrophin depletion causing neuron loss. Nature Neuroscience 22:1089-1098.

Nilius B, Hess P, Lansman J, Tsien R (1985) A novel type of cardiac calcium channel in ventricular cells. Nature 316:443-446.

Nilius B, Prenen J, Tang J, Wang C, Owsianik G, Janssens A, Voets T, Zhu MX (2005) Regulation of the Ca2+ sensitivity of the nonselective cation channel TRPM4. Journal of biological chemistry 280:6423-6433.

Nortley R, Korte N, Izquierdo P, Hirunpattarasilp C, Mishra A, Jaunmuktane Z, Kyrargyri V, Pfeiffer T, Khennouf L, Madry C (2019) Amyloid β oligomers constrict human capillaries in Alzheimer's disease via signaling to pericytes. Science 365:eaav9518.

Numazaki M, Tominaga T, Toyooka H, Tominaga M (2002) Direct phosphorylation of capsaicin receptor VR1 by protein kinase Cε and identification of two target serine residues. Journal of Biological Chemistry 277:13375-13378.

Okubo Y, Iino M, Hirose K (2020) Store-operated Ca2+ entry-dependent Ca2+ refilling in the endoplasmic reticulum in astrocytes. Biochemical and Biophysical Research Communications 522:1003-1008.

Ong HL, de Souza LB, Ambudkar IS (2016) Role of TRPC channels in store-operated calcium entry. Calcium entry pathways in non-excitable cells:87-109.

Palade P, Mitchell RD, Fleischer S (1983) Spontaneous calcium release from sarcoplasmic reticulum. General description and effects of calcium. Journal of Biological Chemistry 258:8098-8107.

Park CY, Shcheglovitov A, Dolmetsch R (2010) The CRAC channel activator STIM1 binds and inhibits L-type voltage-gated calcium channels. Science 330:101-105.
Pearce L, Meizoso-Huesca A, Seng C, Lamboley CR, Singh DP, Launikonis BS (2022) Ryanodine receptor activity and store-operated Ca2+ entry: Critical regulators of Ca2+ content and function in skeletal muscle. The Journal of Physiology.
Peppiatt CM, Howarth C, Mobbs P, Attwell D (2006) Bidirectional control of CNS capillary diameter by pericytes. Nature 443:700-704.
Peppiatt-Wildman C, Albert A, Saleh S, Large W (2007) Endothelin-1 activates a Ca2+-permeable cation channel with TRPC3 and TRPC7 properties in rabbit coronary artery myocytes. The Journal of physiology 580:755-764.
Pérez GJ, Bonev AD, Patlak JB, Nelson MT (1999) Functional coupling of ryanodine receptors to KCa channels in smooth muscle cells from rat cerebral arteries. The Journal of general physiology 113:229-238.
Perez-Reyes E (2003) Molecular physiology of low-voltage-activated t-type calcium channels. Physiological reviews 83:117-161.
Pietrobon D (2010) Ca V 2.1 channelopathies. Pflügers Archiv-European Journal of Physiology 460:375-393.
Potier M, Gonzalez JC, Motiani RK, Abdullaev IF, Bisaillon JM, Singer HA, Trebak M (2009) Evidence for STIM1-and Orai1-dependent store-operated calcium influx through ICRAC in vascular smooth muscle cells: role in proliferation and migration. The FASEB Journal 23:2425.
Prakriya M, Lewis RS (2001) Potentiation and inhibition of Ca2+ release-activated Ca2+ channels by 2-aminoethyldiphenyl borate (2-APB) occurs independently of IP3 receptors. The Journal of physiology 536:3.
Proebstl D, Voisin M-B, Woodfin A, Whiteford J, D'Acquisto F, Jones GE, Rowe D, Nourshargh S (2012) Pericytes support neutrophil subendothelial cell crawling and breaching of venular walls in vivo. Journal of Experimental Medicine 209:1219-1234.
Putney Jr JW (1986) A model for receptor-regulated calcium entry. Cell calcium 7:1-12.
Ratelade J, Klug NR, Lombardi D, Angelim MKSC, Dabertrand F, Domenga-Denier V, Salman RA-S, Smith C, Gerbeau J-F, Nelson MT (2020) Reducing hypermuscularization of the transitional segment between arterioles and capillaries protects against spontaneous intracerebral hemorrhage. Circulation 141:2078-2094.
Reading SA, Earley S, Waldron B, Welsh D, Brayden J (2005) TRPC3 mediates pyrimidine receptor-induced depolarization of cerebral arteries. American Journal of Physiology-Heart and Circulatory Physiology 288:H2055-H2061.
Roos J, DiGregorio PJ, Yeromin AV, Ohlsen K, Lioudyno M, Zhang S, Safrina O, Kozak JA, Wagner SL, Cahalan MD (2005) STIM1, an essential and conserved component of store-operated Ca2+ channel function. The Journal of cell biology 169:435-445.
Rosenbaum DM, Rasmussen SG, Kobilka BK (2009) The structure and function of G-protein-coupled receptors. Nature 459:356-363.
Roth S, Park SS, Sikorski CW, Osinski J, Chan R, Loomis K (1997) Concentrations of adenosine and its metabolites in the rat retina/choroid during reperfusion after ischemia. Current eye research 16:875-885.
Rungta RL, Chaigneau E, Osmanski B-F, Charpak S (2018) Vascular compartmentalization of functional hyperemia from the synapse to the pia. Neuron 99:362-375. e364.

Rungta RL, Zuend M, Aydin A-K, Martineau É, Boido D, Weber B, Charpak S (2021) Diversity of neurovascular coupling dynamics along vascular arbors in layer II/III somatosensory cortex. Communications Biology 4:855.
Rustenhoven J, Aalderink M, Scotter EL, Oldfield RL, Bergin PS, Mee EW, Graham ES, Faull RL, Curtis MA, Park TI (2016) TGF-beta1 regulates human brain pericyte inflammatory processes involved in neurovasculature function. Journal of neuroinflammation 13:1-15.
Rustenhoven J, Jansson D, Smyth LC, Dragunow M (2017) Brain pericytes as mediators of neuroinflammation. Trends in pharmacological sciences 38:291-304.
Sakuma R, Kawahara M, Nakano-Doi A, Takahashi A, Tanaka Y, Narita A, Kuwahara-Otani S, Hayakawa T, Yagi H, Matsuyama T (2016) Brain pericytes serve as microglia-generating multipotent vascular stem cells following ischemic stroke. Journal of neuroinflammation 13:1-13.
Sakuragi S, Niwa F, Oda Y, Mikoshiba K, Bannai H (2017) Astroglial Ca2+ signaling is generated by the coordination of IP3R and store-operated Ca2+ channels. Biochemical and biophysical research communications 486:879-885.
Sancho M, Klug NR, Mughal A, Koide M, Huerta de la Cruz S, Heppner TJ, Bonev AD, Hill-Eubanks D, Nelson MT (2022) Adenosine signaling activates ATP-sensitive K+ channels in endothelial cells and pericytes in CNS capillaries. Science signaling 15:eabl5405.
Sekiguchi Y, Takuwa H, Kawaguchi H, Kikuchi T, Okada E, Kanno I, Ito H, Tomita Y, Itoh Y, Suzuki N (2014) Pial arteries respond earlier than penetrating arterioles to neural activation in the somatosensory cortex in awake mice exposed to chronic hypoxia: an additional mechanism to proximal integration signaling? Journal of Cerebral Blood Flow & Metabolism 34:1761-1770.
Sims DE (1986) The pericyte—a review. Tissue and Cell 18:153-174.
Singh A, Hildebrand M, Garcia E, Snutch T (2010) The transient receptor potential channel antagonist SKF96365 is a potent blocker of low-voltage-activated T-type calcium channels. British journal of pharmacology 160:1464-1475.
Soderblom C, Luo X, Blumenthal E, Bray E, Lyapichev K, Ramos J, Krishnan V, Lai-Hsu C, Park KK, Tsoulfas P (2013) Perivascular fibroblasts form the fibrotic scar after contusive spinal cord injury. Journal of Neuroscience 33:13882-13887.
Somasundaram A, Shum AK, McBride HJ, Kessler JA, Feske S, Miller RJ, Prakriya M (2014) Store-operated CRAC channels regulate gene expression and proliferation in neural progenitor cells. Journal of Neuroscience 34:9107-9123.
Song AJ, Palmiter RD (2018) Detecting and Avoiding Problems When Using the Cre–lox System. Trends in Genetics 34:333-340.
Sonkusare SK, Bonev AD, Ledoux J, Liedtke W, Kotlikoff MI, Heppner TJ, Hill-Eubanks DC, Nelson MT (2012) Elementary Ca2+ signals through endothelial TRPV4 channels regulate vascular function. Science 336:597-601.
Stegner D, Hofmann S, Schuhmann MK, Kraft P, Herrmann AM, Popp S, Höhn M, Popp M, Klaus V, Post A (2019) Loss of Orai2-mediated capacitative Ca2+ entry is neuroprotective in acute ischemic stroke. Stroke 50:3238-3245.
Sweeney MD, Ayyadurai S, Zlokovic BV (2016) Pericytes of the neurovascular unit: key functions and signaling pathways. Nature neuroscience 19:771-783.
Takemura H, Hughes A, Thastrup O, Putney J (1989) Activation of calcium entry by the tumor promoter thapsigargin in parotid acinar cells: evidence that an intracellular calcium pool, and not an inositol phosphate, regulates calcium fluxes at the plasma membrane. Journal of Biological Chemistry 264:12266-12271.

Tanabe T, Beam KG, Adams BA, Niidome T, Numa S (1990) Regions of the skeletal muscle dihydropyridine receptor critical for excitation–contraction coupling. Nature 346:567-569.
Taylor CW, Tovey SC (2010) IP3 receptors: toward understanding their activation. Cold Spring Harbor perspectives in biology 2:a004010.
Thakur P, Dadsetan S, Fomina AF (2012) Bidirectional coupling between ryanodine receptors and Ca2+ release-activated Ca2+ (CRAC) channel machinery sustains store-operated Ca2+ entry in human T lymphocytes. Journal of Biological Chemistry 287:37233-37244.
Török O, Schreiner B, Schaffenrath J, Tsai H-C, Maheshwari U, Stifter SA, Welsh C, Amorim A, Sridhar S, Utz SG (2021) Pericytes regulate vascular immune homeostasis in the CNS. Proceedings of the National Academy of Sciences 118:e2016587118.
Toth AB, Hori K, Novakovic MM, Bernstein NG, Lambot L, Prakriya M (2019) CRAC channels regulate astrocyte Ca2+ signaling and gliotransmitter release to modulate hippocampal GABAergic transmission. Science signaling 12:eaaw5450.
Tringham E, Powell KL, Cain SM, Kuplast K, Mezeyova J, Weerapura M, Eduljee C, Jiang X, Smith P, Morrison J-L (2012) T-type calcium channel blockers that attenuate thalamic burst firing and suppress absence seizures. Science translational medicine 4:121ra119-121ra119.
Tsujikawa S, DeMeulenaere KE, Centeno MV, Ghazisaeidi S, Martin ME, Tapies MR, Maneshi MM, Yamashita M, Stauderman KA, Apkarian AV (2023) Regulation of neuropathic pain by microglial Orai1 channels. Science Advances 9:eade7002.
Vanlandewijck M, He L, Mäe MA, Andrae J, Ando K, Del Gaudio F, Nahar K, Lebouvier T, Laviña B, Gouveia L (2018) A molecular atlas of cell types and zonation in the brain vasculature. Nature 554:475-480.
Várnai P, Hunyady L, Balla T (2009) STIM and Orai: the long-awaited constituents of store-operated calcium entry. Trends in pharmacological sciences 30:118-128.
Verbeek MM, Otte-Höller I, Wesseling P, Ruiter DJ, De Waal R (1994) Induction of alpha-smooth muscle actin expression in cultured human brain pericytes by transforming growth factor-beta 1. The American journal of pathology 144:372.
Vig M, Beck A, Billingsley JM, Lis A, Parvez S, Peinelt C, Koomoa DL, Soboloff J, Gill DL, Fleig A (2006) CRACM1 multimers form the ion-selective pore of the CRAC channel. Current Biology 16:2073-2079.
Wang Y, DelRosso NV, Vaidyanathan TV, Cahill MK, Reitman ME, Pittolo S, Mi X, Yu G, Poskanzer KE (2019) Accurate quantification of astrocyte and neurotransmitter fluorescence dynamics for single-cell and population-level physiology. Nature neuroscience 22:1936-1944.
Wang Y, Deng X, Mancarella S, Hendron E, Eguchi S, Soboloff J, Tang XD, Gill DL (2010) The calcium store sensor, STIM1, reciprocally controls Orai and CaV1. 2 channels. Science 330:105-109.
Welsh DG, Morielli AD, Nelson MT, Brayden JE (2002) Transient receptor potential channels regulate myogenic tone of resistance arteries. Circulation research 90:248-250.
Westcott EB, Goodwin EL, Segal SS, Jackson WF (2012) Function and expression of ryanodine receptors and inositol 1, 4, 5-trisphosphate receptors in smooth muscle cells of murine feed arteries and arterioles. The Journal of physiology 590:1849-1869.
Westenbroek RE, Hell JW, Warner C, Dubel SJ, Snutch TP, Catterall WA (1992) Biochemical properties and subcellular distribution of an N-type calcium hannel α1 subunit. Neuron 9:1099-1115.
Wheeler DB, Randall A, Tsien RW (1994) Roles of N-type and Q-type Ca2+ channels in supporting hippocampal synaptic transmission. Science 264:107-111.

Wheeler DG, Groth RD, Ma H, Barrett CF, Owen SF, Safa P, Tsien RW (2012) CaV1 and CaV2 channels engage distinct modes of Ca2+ signaling to control CREB-dependent gene expression. Cell 149:1112-1124.
Windle V, Szymanska A, Granter-Button S, White C, Buist R, Peeling J, Corbett D (2006) An analysis of four different methods of producing focal cerebral ischemia with endothelin-1 in the rat. Experimental neurology 201:324-334.
Woll KA, Van Petegem F (2022) Calcium-release channels: Structure and function of IP3 receptors and ryanodine receptors. Physiological Reviews 102:209-268.
Xu L, Mann G, Meissner G (1996) Regulation of cardiac Ca2+ release channel (ryanodine receptor) by Ca2+, H+, Mg2+, and adenine nucleotides under normal and simulated ischemic conditions. Circulation research 79:1100-1109.
Xu W, Lipscombe D (2001) Neuronal CaV1. 3α1 L-type channels activate at relatively hyperpolarized membrane potentials and are incompletely inhibited by dihydropyridines. Journal of Neuroscience 21:5944-5951.
Yahn SL, Li J, Goo I, Gao H, Brambilla R, Lee JK (2020) Fibrotic scar after experimental autoimmune encephalomyelitis inhibits oligodendrocyte differentiation. Neurobiology of disease 134:104674.
Yanagisawa M, Kurihara H, Kimura S, Tomobe Y, Kobayashi M, Mitsui Y, Yazaki Y, Goto K, Masaki T (1988) A novel potent vasoconstrictor peptide produced by vascular endothelial cells. nature 332:411-415.
Yang AC, Vest RT, Kern F, Lee DP, Agam M, Maat CA, Losada PM, Chen MB, Schaum N, Khoury N (2022) A human brain vascular atlas reveals diverse mediators of Alzheimer's risk. Nature 603:885-892.
Yang L, Liu G, Zakharov SI, Morrow JP, Rybin VO, Steinberg SF, Marx SO (2005) Ser1928 is a common site for Cav1. 2 phosphorylation by protein kinase C isoforms. Journal of Biological Chemistry 280:207-214.
Yao X, Garland CJ (2005) Recent developments in vascular endothelial cell transient receptor potential channels. Circulation research 97:853-863.
Yemisci M, Gursoy-Ozdemir Y, Vural A, Can A, Topalkara K, Dalkara T (2009) Pericyte contraction induced by oxidative-nitrative stress impairs capillary reflow despite successful opening of an occluded cerebral artery. Nature medicine 15:1031-1037.
Yoast RE, Emrich SM, Trebak M (2020) The anatomy of native CRAC channel (s). Current opinion in physiology 17:89-95.
Yoast RE, Emrich SM, Zhang X, Xin P, Johnson MT, Fike AJ, Walter V, Hempel N, Yule DI, Sneyd J (2020) The native ORAI channel trio underlies the diversity of Ca2+ signaling events. Nature communications 11:2444.
Zambach SA, Cai C, Helms HCC, Hald BO, Dong Y, Fordsmann JC, Nielsen RM, Hu J, Lønstrup M, Brodin B (2021) Precapillary sphincters and pericytes at first-order capillaries as key regulators for brain capillary perfusion. Proceedings of the National Academy of Sciences 118:e2023749118.
Zhang Q, Cao C, Zhang Z, Wier WG, Edwards A, Pallone TL (2008) Membrane current oscillations in descending vasa recta pericytes. American Journal of Physiology-Renal Physiology 294:F656-F666.
Zhang SL, Yeromin AV, Zhang XH-F, Yu Y, Safrina O, Penna A, Roos J, Stauderman KA, Cahalan MD (2006) Genome-wide RNAi screen of Ca2+ influx identifies genes that regulate Ca2+ release-activated Ca2+ channel activity. Proceedings of the National Academy of Sciences 103:9357-9362.

Zhang X, Xin P, Yoast RE, Emrich SM, Johnson MT, Pathak T, Benson JC, Azimi I, Gill DL, Monteith GR (2020) Distinct pharmacological profiles of ORAI1, ORAI2, and ORAI3 channels. Cell calcium 91:102281.

Zhang Y, Chen K, Sloan SA, Bennett ML, Scholze AR, O'Keeffe S, Phatnani HP, Guarnieri P, Caneda C, Ruderisch N (2014) An RNA-sequencing transcriptome and splicing database of glia, neurons, and vascular cells of the cerebral cortex. Journal of Neuroscience 34:11929-11947.

Zhang Z, Rhinehart K, Pallone TL (2002) Membrane potential controls calcium entry into descending vasa recta pericytes. American Journal of Physiology-Regulatory, Integrative and Comparative Physiology 283:R949-R957.

Zweifach A, Lewis RS (1993) Mitogen-regulated Ca2+ current of T lymphocytes is activated by depletion of intracellular Ca2+ stores. Proceedings of the National Academy of Sciences 90:6295-6299.